

BÜLENT ECEVİT UNIVERSITY
GRADUATE SCHOOL OF NATURAL AND APPLIED SCIENCES

**HIGH-ORDER IONOSPHERIC EFFECTS ON GPS TROPOSPHERIC AND
COORDINATE ESTIMATIONS**



DEPARTMENT OF GEOMATICS ENGINEERING

MASTER OF SCIENCE THESIS

VOLKAN AKGÜL

DECEMBER 2017

BÜLENT ECEVİT UNIVERSITY
GRADUATE SCHOOL OF NATURAL AND APPLIED SCIENCES

**HIGH-ORDER IONOSPHERIC EFFECTS ON GPS TROPOSPHERIC AND
COORDINATE ESTIMATIONS**

DEPARTMENT OF GEOMATICS ENGINEERING

MASTER OF SCIENCE THESIS

Volkan AKGÜL

ADVISOR: Prof. SHUANGGEN JIN

ZONGULDAK

December 2017

APPROVAL OF THE THESIS:

The thesis entitled “High-Order Ionospheric Effects on GPS Tropospheric and Coordinate Estimations” and submitted by Volkan AKGÜL has been examined and accepted by the jury as a Master of Science thesis in Department of Geomatics Engineering, Graduate School of Natural and Applied Sciences, Bülent Ecevit University. 18/12/2017

Advisor: Prof. Shuanggen JIN

Bülent Ecevit University, Faculty of Engineering, Department of Geomatics

Member: Prof. Şenol Hakan KUTOĞLU

Bülent Ecevit University, Faculty of Engineering, Department of Geomatics

Member: Prof. Bahadır AKTUĞ

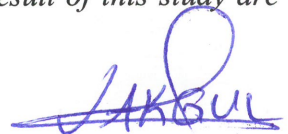
Ankara University, Faculty of Engineering, Department of Geophysics

Approved by the Graduate School of Natural and Applied Sciences.

.../.../2017


Assoc. Prof. Ahmet ÖZARSLAN
Director

“With this thesis it is declared that all the information in this thesis is obtained and presented according to academic rules and ethical principles. Also as required by academic rules and ethical principles all works that are not result of this study are cited properly.”



Volkan AKGÜL

ABSTRACT

Master of Science Thesis

HIGH-ORDER IONOSPHERIC EFFECTS ON GPS TROPOSPHERIC AND COORDINATE ESTIMATIONS

Volkan AKGÜL

Bülent Ecevit University

Graduate School of Natural and Applied Sciences

Department of Geomatics Engineering

Thesis Advisor: Prof. Shuanggen JIN

December 2017, 71 pages

The tropospheric delay and gradient can be estimated from dual-frequency GPS observations with removing the ionospheric delay, which has been widely used for atmospheric study and weather forecasting. However, high-order ionospheric (HOI) effects are generally ignored in tropospheric and coordinate estimation. In this study, high-order ionospheric effects on GPS-estimated tropospheric delay, gradients and coordinates have been investigated for the first time from 30 days of GPS data in June 2011 at 8 GPS stations in Turkey. Firstly, the second and third-order effects on GPS data are corrected in RINEX using IGRF11 (International Geomagnetic Reference Field: 11th generation) model, and then tropospheric delay and gradient values are obtained from raw and corrected RINEX data using the GAMIT software. Results show that high-order ionospheric effects are up to 6 mm on zenith tropospheric delay (ZTD), 4 mm on North-South (NS) gradient and 12 mm on East-West (EW) gradient during this period, but can reach over 30 mm in slant tropospheric delay. Furthermore, the high-order

ABSTRACT (continued)

effects on tropospheric delay and gradient are larger in the day time than in the night time. Also, solar activity effects on high-order ionospheric delay corrections are further investigated. The high-order ionospheric effects on GPS estimated tropospheric delay and gradient in high solar activity days are much larger than those in low solar activity days. While RMS values are 0.40 mm, 0.86 mm, 0.69 mm in low solar activity days, in peak solar activity days they can increase up to 0.81 mm, 2.74 mm, 2.20 mm on ZTD, North-South, and East-West gradients, respectively.

Global Positioning System (GPS) gives a chance for users to obtain high precision positioning information with the real time applications. Precise positioning components can be obtained using observation files evaluated on academic GAMIT/GlobK software with post processing applications. When the same GPS data in June 2011 has been used for precise positioning before and after HOI corrections, results show that, 10, 7 and 24 mm changes occurred in order of north, east and up components. When the data during the peak solar activity day observation files are used for same stations in 2011, it is observed that, high-order ionospheric effects on north, east and up components can be reached in order of 18, 11 and 43 mm change.

Keywords: GPS, High-order ionospheric delay, Tropospheric delay, Gradients, Coordinates

Science Code: 616.03.00

ÖZET

Yüksek Lisans Tezi

GPS İLE TROPOSFER VE KOORDİNAT KESTİRİMLERİ ÜZERİNDEKİ YÜKSEK DERECELİ İYONOSFERİK ETKİLER

Volkan AKGÜL

Bülent Ecevit Üniversitesi

Fen Bilimleri Enstitüsü

Geomatik Mühendisliği Anabilim Dalı

Tez Danışmanı: Prof. Dr. Shuanggen JIN

Aralık 2017, 71 sayfa

Atmosferik çalışmalar ve hava durumu tahminlerinde yaygın olarak kullanılan troposferik gecikme ve gradyent, çift frekanslı GPS gözlemleri ile iyonosferik gecikme ortadan kaldırılarak kestirilebilmektedir. Bununla birlikte, troposferik ve koordinat kestirimlerinde yüksek dereceli iyonosferik (HOI) etkiler genellikle göz ardı edilmektedir. Bu çalışmada, GPS ile kestirilen troposferik gecikme, gradyent ve koordinatlar üzerindeki yüksek dereceli iyonosferik etkiler, 8 GPS istasyonuna ait 30 günlük Haziran 2011 verileri ile Türkiye’de ilk kez araştırılmıştır. İlk olarak, GPS verileri üzerindeki ikinci ve üçüncü dereceli etkiler, IGRF11 (International Geomagnetic Reference Field: 11th generation) modeli kullanılarak RINEX dosyası içerisinde düzeltilip, ardından troposferik gecikme ve gradyent değerleri, ham ve düzeltilmiş RINEX verilerinin GAMIT yazılımında değerlendirilmesi ile elde edilmiştir. Değerlendirme aralığında yüksek dereceli iyonosferik etkilerin, zenit troposferik gecikmesi (ZTD) üzerinde 6 mm, Kuzey-Güney (NS) gradyentinde 4 mm ve Doğu-Batı (EW) gradyentinde 12 mm'ye kadar olduğu ve eğik troposferik gecikmede yaklaşık 30 mm kadar ulaştığı görülmüştür. Dahası,

ÖZET (devam ediyor)

troposferik gecikme ve gradyent üzerindeki yüksek dereceli iyonosferik etkiler, gündüz saatlerinde gece saatlerinden daha yüksektir. Ayrıca, solar aktivitenin yüksek dereceli iyonosferik gecikme düzeltmeleri üzerindeki etkileri de araştırılmıştır. GPS ile kestirilen troposferik gecikme ve gradyent üzerindeki yüksek dereceli iyonosferik etkiler solar aktivitenin yüksek olduğu günlerde solar aktivitenin düşük olduğu günlere göre daha yüksektir. Karesel ortalama hata değerleri düşük solar aktivite günlerinde 0.40 mm, 0.86 mm, 0.69 mm iken, solar aktivitenin yüksek olduğu günlerde ZTD, Kuzey-Güney ve Doğu-Batı gradyentlerinde sırasıyla 0.81 mm, 2.74 mm ve 2.20 mm'ye kadar artabilmektedir.

Küresel Konumlama Sistemi (GPS), kullanıcıların gerçek zamanlı uygulamalarla yüksek hassasiyetli konum bilgisi elde etmelerine olanak tanır. Hassas konum bileşenleri, akademik ileri işleme uygulamaları ile GAMIT / GlobK yazılımında değerlendirilen gözlem dosyaları kullanılarak elde edilebilmektedir. Haziran 2011'de aynı GPS verileri HOI etkilerinin düzeltme öncesi ve sonrası için hassas konum belirlemede kullanıldığında, sonuçlar, yukarı, sağa ve yükseklik bileşenlerinde sırasıyla 10, 7 ve 24 mm'lik değişikliklerin gerçekleştiğini göstermektedir. 2011 yılında solar aktivitenin yüksek olduğu günlerin gözlem dosyaları kullanıldığında ise, yukarı, sağa ve yükseklik bileşenlerinde yüksek dereceli iyonosferik etkiler, 18, 11 ve 43 mm'lik değişimlere kadar ulaşabileceği görülmektedir.

Anahtar Kelimeler: GPS, Yüksek dereceli iyonosferik gecikme, Troposferik gecikme, Gradyent, Koordinat

Bilim Kodu: 616.03.00

ACKNOWLEDGEMENTS

Above all, I would like to express my gratitude to have experienced the privilege of working with Prof. Shuanggen JIN. All my studies were under the control of him, and he forced me to study every time. I am also grateful from him to give me a vision and change my point of view. Secondly, I would like to thank our unifying force Prof. Hakan KUTOĞLU, who provided us working environment, who defused the when we got stressed. And, I would like to thank head of our department Prof. Çetin MEKİK for trusting me while giving every responsibility.

I am grateful to Prof. Kazimierz BECEK, who asks questions about my work and tries to find solutions when it is needed, who listens to my troubles in a friendly way and who is enlightening me with his knowledge.

After Prof. Rahmi Nurhan ÇELİK my favourite academician from ITU, I admired to Prof. Bahadır AKTUĞ who is a valuable person giving speech to make people encouraged since I met him.

Thank you to my esteemed housemate, Assoc. Prof. Weibing DU, who entered to my life with different food, faith and culture for a while. And also, I am grateful to Assist. Prof. K. Sedar GÖRMÜŞ and Assist. Prof. Eray KÖKSAL for their contribution and friendships like my elder brother.

I especially like to thank my colleague and roommate Gökhan GÜRBÜZ who forced me to study hard and who contributed my academic work as an advisor. I would also like to thank Alihsan ŞEKERTEKİN a distinguished personality that I appreciate in my department and whom I have consulted about the various issues.

Another thanks to my dear friends Ali CAM and Oya Burcu BAKİOĞLU. It was not easy to spare time for you during this period, but I could aware of life with your favour.

ACKNOWLEDGEMENTS (continued)

I am also grateful to the BEU Geomatics Family, which makes an international world in small Zonguldak and forces me to speak English as much as I have never experienced before.

Finally, I want to express my gratefulness to my family who supported my decisions in every conditions. I believe that I have an honourable life with the contributions of them.



TABLE OF CONTENTS

| | <u>Page</u> |
|--|-------------|
| APPROVAL OF THE THESIS: | ii |
| ABSTRACT | iii |
| ÖZET | iv |
| ACKNOWLEDGEMENTS | viii |
| TABLE OF CONTENTS | x |
| LIST OF FIGURES | xi |
| LIST OF TABLES | xv |
| LIST OF SYMBOLS AND ABBREVIATIONS | xvii |
| | |
| CHAPTER 1 INTRODUCTION | 1 |
| | |
| 1.1 BACKGROUND | 1 |
| 1.2 ATMOSPHERIC DELAY | 3 |
| 1.2.1 Ionospheric Delay | 5 |
| 1.2.1.1 First-Order Ionospheric Effects | 7 |
| 1.2.1.2 Second-Order Ionospheric Effects | 9 |
| 1.2.1.3 Third-Order Ionospheric Effects | 10 |
| 1.2.2 Tropospheric Delay | 11 |
| 1.2.2.1 Saastamoinen Model | 13 |
| 1.2.2.2 Vienna Mapping Function Model | 14 |
| 1.2.2.3 Tropospheric delay gradient | 15 |
| 1.2.2.4 Precipitable water vapor | 16 |
| 1.3 CONTENTS | 17 |
| | |
| CHAPTER 2 THEORY AND METHODS | 19 |
| | |
| 2.1 GPS THEORY | 19 |
| 2.2 HOI EFFECTS CORRECTION | 20 |

TABLE OF CONTENTS (continued)

| | <u>Page</u> |
|---|-------------|
| 2.3 RINEX HO | 22 |
| 2.3.1 Compiling for Windows | 24 |
| 2.3.2 Compiling for Linux | 25 |
| 2.4 GEOMAGNETIC AND SOLAR CONDITIONS..... | 26 |
| 2.4.1 Geomagnetic Field Model..... | 26 |
| 2.4.2 Solar Activity | 28 |
| 2.4.3 F10.7 Flux | 29 |
| | |
| CHAPTER 3 HIGH-ORDER IONOSPHERIC EFFECTS ON TROPOSPHERIC PARAMETERS | 31 |
| | |
| 3.1 HOI EFFECTS ON GPS ESTIMATED ZTD | 31 |
| 3.1.1 HOI effects on GPS estimated ZTD during the day and night time | 36 |
| 3.1.2 HOI effects on GPS estimated ZTD during the high and low solar activities | 37 |
| 3.1.3 HOI effects on slant tropospheric delay | 39 |
| 3.2 HOI EFFECTS ON GPS GRADIENTS..... | 40 |
| 3.2.1 HOI effects on North-South Gradients With Solar Activities | 44 |
| 3.2.2 HOI effects on East-West Gradients With Solar Activities | 45 |
| 3.3 HOI EFFECTS ON GPS ESTIMATED PWV | 45 |
| 3.3.1 HOI Effects on GPS PWV During the High and Low Solar Activities..... | 49 |
| 3.3.2 Radiosonde and GPS PWV Comparison | 50 |
| | |
| CHAPTER 4 HIGH-ORDER IONOSPHERIC EFFECTS ON COORDINATES..... | 55 |
| | |
| 4.1 COORDINATE CHANGES ON LOW SOLAR ACTIVITY DAYS..... | 59 |
| 4.2 COORDINATE CHANGES ON HIGH SOLAR ACTIVITY DAYS..... | 60 |
| | |
| CHAPTER 5 CONCLUSION | 63 |
| | |
| REFERENCES..... | 65 |
| CURRICULUM VITAE | 71 |

LIST OF FIGURES

| <u>No</u> | | <u>Page</u> |
|-------------|---|-------------|
| Figure 1.1 | Parts of atmospheric delay | 5 |
| Figure 1.2 | Ionospheric effect on different frequency GPS signals | 6 |
| Figure 1.3 | Ionospheric propagation delay | 8 |
| Figure 1.4 | Geomagnetic local system. Adapted from Odijk (2002) | 10 |
| Figure 1.5 | Tropospheric delay on GPS signals | 12 |
| Figure 2.1 | Positioning with GPS receiver | 19 |
| Figure 2.2 | HOI Effects Correction | 26 |
| Figure 2.3 | Solar Radiation | 28 |
| Figure 2.4 | Solar index F10.7 cm | 30 |
| Figure 3.1 | GPS and Radiosonde Stations..... | 32 |
| Figure 3.2 | ADAN Station GPS ZTD Time Series and Residuals | 33 |
| Figure 3.3 | ANRK Station GPS ZTD Time Series and Residuals | 33 |
| Figure 3.4 | DIYB Station GPS ZTD Time Series and Residuals..... | 34 |
| Figure 3.5 | ERZR Station GPS ZTD Time Series and Residuals | 34 |
| Figure 3.6 | ISPT Station GPS ZTD Time Series and Residuals | 34 |
| Figure 3.7 | ISTN Station GPS ZTD Time Series and Residuals..... | 35 |
| Figure 3.8 | IZMI Station GPS ZTD Time Series and Residuals..... | 35 |
| Figure 3.9 | SAMN Station GPS ZTD Time Series and Residuals | 35 |
| Figure 3.10 | GPS Stations ZTD RMS | 36 |
| Figure 3.11 | ZTD differences with HOI effects at ANRK Station during the night and the day time..... | 36 |
| Figure 3.12 | Daytime and night time HOI effects on GPS ZTD On day 167, 2011 | 37 |
| Figure 3.13 | Daily averages of Solar 10.7 cm flux..... | 38 |

LIST OF FIGURES (continued)

| <u>No</u> | <u>Page</u> |
|---|-------------|
| Figure 3.14 RMS of Low and High Solar Activity Days ZTD Residuals..... | 38 |
| Figure 3.15 TEC distribution in Turkey during the days 152-181 2011 | 39 |
| Figure 3.16 GPS PRN 7 visibility on DOY 167, 2011 at ANRK station..... | 39 |
| Figure 3.17 HOI effects on GPS STD for PRN7 on Day 167 2011 at ANRK station..... | 40 |
| Figure 3.18 ADAN Station Gradient Time Series and Residuals | 41 |
| Figure 3.19 ANRK Station Gradient Time Series and Residuals | 42 |
| Figure 3.20 DIYB Station Gradient Time Series and Residuals | 42 |
| Figure 3.21 ERZR Station Gradient Time Series and Residuals | 42 |
| Figure 3.22 ISPT Station Gradient Time Series and Residuals | 43 |
| Figure 3.23 ISTN Station Gradient Time Series and Residuals..... | 43 |
| Figure 3.24 IZMI Station Gradient Time Series and Residuals | 43 |
| Figure 3.25 SAMN Station Gradient Time Series and Residuals | 44 |
| Figure 3.26 Low and High Solar Activity Days RMS of NS Gradient Residuals | 44 |
| Figure 3.27 Low and High Solar Activity Days RMS of EW Gradient Residuals | 45 |
| Figure 3.28 ADAN Station GPS PWV Time Series and Residuals..... | 46 |
| Figure 3.29 ANRK Station GPS PWV Time Series and Residuals | 46 |
| Figure 3.30 DIYB Station GPS PWV Time Series and Residuals..... | 47 |
| Figure 3.31 ERZR Station GPS PWV Time Series and Residuals | 47 |
| Figure 3.32 ISPT Station GPS PWV Time Series and Residuals | 47 |
| Figure 3.33 ISTN Station GPS PWV Time Series and Residuals..... | 48 |
| Figure 3.34 IZMI Station GPS PWV Time Series and Residuals..... | 48 |
| Figure 3.35 SAMN Station GPS PWV Time Series and Residuals..... | 48 |
| Figure 3.36 ANRK Station GPS PWV Time Series and Residuals on Solar Activity Days . | 49 |
| Figure 3.37 RMS of PWV during low and high solar activity days | 49 |
| Figure 3.38 ADAN Station PWV Time Series Comparison and Residuals..... | 50 |

LIST OF FIGURES (continued)

| <u>No</u> | | <u>Page</u> |
|-------------|--|-------------|
| Figure 3.39 | ANRK Station PWV Time Series Comparison and Residuals | 51 |
| Figure 3.40 | DIYB Station PWV Time Series Comparison and Residuals | 51 |
| Figure 3.41 | ERZR Station PWV Time Series Comparison and Residuals | 51 |
| Figure 3.42 | ISPT Station PWV Time Series Comparison and Residuals | 52 |
| Figure 3.43 | ISTN Station PWV Time Series Comparison and Residuals | 52 |
| Figure 3.45 | SAMN Station PWV Time Series Comparison and Residuals..... | 53 |
| Figure 4.1 | ADAN GPS Station Coordinate Time Series and Residuals | 56 |
| Figure 4.2 | ANRK GPS Station Coordinate Time Series and Residuals | 56 |
| Figure 4.3 | DIYB GPS Station Coordinate Time Series and Residuals..... | 57 |
| Figure 4.4 | ERZR GPS Station Coordinate Time Series and Residuals | 57 |
| Figure 4.5 | ISPT GPS Station Coordinate Time Series and Residuals | 57 |
| Figure 4.6 | ISTN GPS Station Coordinate Time Series and Residuals..... | 58 |
| Figure 4.7 | IZMI GPS Station Coordinate Time Series and Residuals..... | 58 |
| Figure 4.8 | SAMN GPS Station Coordinate Time Series and Residuals | 58 |
| Figure 4.9 | Each Stations North, East and Up Components RMS | 59 |
| Figure 4.10 | ISPT Station North, East and Up Time Series and Residuals on Low Solar Activity Days, 2011 | 59 |
| Figure 4.11 | ISPT Station North, East and Up Time Series and Residuals on High Solar Activity Days, 2011 | 60 |
| Figure 4.12 | North, East and Up Components RMS on Solar Activity Days | 60 |



LIST OF TABLES

| <u>No</u> | <u>Page</u> |
|--|-------------|
| Table 2.1 Description of Rinex_ha.inp input file..... | 23 |
| Table 2.2 Description of Rinex_ha_param.dat input file..... | 23 |
| Table 2.3 Subfolders for RINEX_HO source code..... | 24 |
| Table 2.4 Summary of IGRF generations, their intervals of validity, and related references.. | 27 |
| Table 3.1 Residuals mean differences and RMS on ZTD..... | 32 |
| Table 3.2 Residuals mean differences and RMS on Gradients..... | 41 |



LIST OF SYMBOLS AND ABBREVIATIONS

SYMBOLS

| | |
|--|--|
| L | : Carrier phase |
| P | : Pseudorange |
| i | : Frequency ($i=1, 2$) |
| s | : Satellite |
| r | : Ground-based GPS receiver |
| ρ_0 | : Geometric distance between the GPS receiver and satellite |
| d_{ion} | : Ionospheric delay |
| d_{trop} | : Tropospheric delay |
| c | : Speed of light in vacuum space |
| τ | : Satellite or receiver clock offset |
| b | : Phase delay of satellite and receiver instrument bias |
| d_k | : Code delay of satellite and receiver instrument bias |
| λ | : Carrier wavelength |
| ϕ | : Total carrier phase between the satellite and receiver |
| N | : Ambiguity of the carrier phase |
| ε | : Other residuals. |
| $c_{2,3,4,\dots}$ | : Coefficients of series expansion |
| f | : Frequency of carrier wave |
| Ne | : Electron density (electrons/m ³) |
| C | : Constant; $C = 40.3 \text{ (m}^3/\text{s}^2)$ |
| z_A^i | : Zenith angle from ground station A to satellite i |
| z_{IP}^i | : Ionospheric zenith angle from the mean ionosphere to the satellite following |
| φ_A | : Ellipsoidal latitude of receiver antenna at station A |
| λ_A | : Ellipsoidal longitude of receiver antenna at station A |
| $\Delta X_A^i \Delta Y_A^i \Delta Z_A^i$ | : Distance vector between antenna at station A and satellite i |

LIST OF SYMBOLS AND ABBREVIATIONS (continued)

| | |
|-------------------------|---|
| S_A^i | : Distance between antenna at station A and satellite i |
| Z_{IP}^i | : Zenith angle from ionospheric point IP to satellite i |
| Z_A^i | : Zenith angle from ground station A to satellite i |
| r_E | : Earth radius ($r_E = 6371$ km) |
| h_{ion} | : Mean height of ionosphere ($h_{ion} = 300 \dots 500$ km) |
| h_A | : Height of ground station A |
| $I_{dLi}^{(1)}$ | : First order ionospheric effect |
| A | : $\approx 80.6 \text{ m}^3/\text{s}^2$ |
| e | : 1.60218×10^{-19} Coulomb |
| m_e | : 9.10939×10^{-31} kg |
| $\ B\ $ | : Magnitude of the geomagnetic induction vector B |
| $I_{dLi}^{(2)}$ | : Second order ionospheric effect |
| $I_{dLi}^{(3)}$ | : Third order ionospheric effect |
| $N_{e,max}$ | : Maximum electron density |
| η | : Constant value (0.66) |
| ρ | : Total mass density of the atmosphere |
| P_w | : Partial pressure of water vapor |
| Z_w | : Compressibility factor |
| T | : Temperature in degrees Kelvin |
| r_0 | : Radius of the region being observed |
| T_0 | : Temperature in the zone |
| P_0 | : Pressure in the surface |
| M | : Molar mass of the air |
| g | : Gravitational acceleration |
| R | : Universal gas constant |
| Δ_{Saas}^{PD} | : Saastamoinen standard model for tropospheric delay |
| P, e | : Pressure in milibar |
| Z | : Zenith angle |
| T_{Wd} and T_{Dd} | : Tropospheric wet and dry delays |
| T_{ZWd} and T_{ZDd} | : Tropospheric wet and dry zenith delays |

LIST OF SYMBOLS AND ABBREVIATIONS (continued)

| | |
|-----------------------------|---|
| MF_{wet} and MF_{dry} | : Wet and dry mapping functions |
| ε | : Elevation angle of satellites |
| $A_{d(\varepsilon,\alpha)}$ | : Effects of azimuthal asymmetry in the atmospheric delay |
| α | : Azimuth |
| NS_{grad} and EW_{grad} | : Gradients on the North-South and East-West directions |
| $MF(\varepsilon)$ | : Mapping function for gradients |
| R_v | : Specific gas constant for water vapor |
| T_m | : The weighted mean temperature of the wet part of the atmosphere |
| T_s | : Function of surface temperature |
| M_w/M_d | : The ratio of molar masses of water vapor and dry air |
| k_1 and k_2 | : Physical constants |
| $\rho_{0,r_i}^{s_i}$ | : Geometric distance from satellite to receiver |
| $X^{s_i}, Y^{s_i}, Z^{s_i}$ | : Satellite coordinates |
| $X_{r_i}, Y_{r_i}, Z_{r_i}$ | : Receiver coordinates |

ABBREVIATIONS

| | |
|-------------|---|
| CGM | : Corrected Geomagnetic Model |
| DCBs | : Differential Code Biases |
| DoD | : United States Department of Defense |
| DGRF | : Definitive Geomagnetic Reference Field |
| GIM | : Global Ionosphere Maps |
| GPS | : Global Positioning System |
| HOI | : High-order Ionospheric |
| IAGA | : International Geomagnetism and Aviation Association |
| IGRF | : International Geomagnetic Reference Field |
| IPP | : Ionospheric Pierce Point |
| NGS | : National Geodetic Survey |
| NWP | : Numerical Weather Forecast |
| PIM | : Parameterized Ionospheric Model |

LIST OF SYMBOLS AND ABBREVIATIONS (continued)

| | |
|----------------------|---|
| RINEX | : Receiver Independent Exchange Format |
| RINEX_HO | : RINEX High Order |
| RMS | : Root Mean Square |
| SFU | : Solar Flux Unit |
| STD | : Slant Tropospheric Delay |
| STEC | : Slant Total Electron Content |
| TEC | : Total Electron Content |
| TECU | : Total Electron Content Unit |
| TUSAGA-Active | : Turkey National Fixed GNSS Network-Active |
| UT | : Universal Time |
| VLBI | : Very Long Baseline Interferometry |
| VTEC | : Vertical Total Electron Content |
| ZTD | : Zenith Tropospheric Delay |

CHAPTER 1

INTRODUCTION

1.1 BACKGROUND

The Global Positioning System (GPS) is designed by United States Department of Defense (DoD) for military and intelligence applications in 1960s. The system works with the logic of sending signals from the satellite described in the earth-centered inertial coordinate system to the receiver on earth. The system is allowing users to obtain positioning information from its code and phase measurements. It works with resection method and at least four satellites are needed for positioning and timing.

The Global Positioning System that started to be established in 1960, was fully operational in 1993. The system consisted of 24 satellites, which were 21 active and 3 spares. Nowadays, GPS constellation has around 30 active satellites on 6 orbits, and used for many applications like positioning, navigation, monitoring of land movements, vegetation, meteorology and climatology.

Initially, the GPS is developed for military forces to satisfy the requirements of U.S. Department of Defense. Later on, it is promoted by DoD for civilian usage with the directions of United States Congress. Following the decision of civilian usage, the production of portable GPS receivers has accelerated (Hofmann-Wellenhof et. al. 2008).

This system has capability to use at any one time in all weather conditions. The satellites launched 20200 km above the earth transmit signals constantly. After establishing this system, it is kept under control to ensure its continuity. The system has three segments which are space, user and control segments. While the space segment consists of satellite constellations, user segment consists of military or civilian users. And, the control segment consists of a master control station, worldwide monitor stations, and ground control stations to maintain the system. The satellite ephemeris errors, satellite and receiver clock errors, multipath, ionospheric and tropospheric delay are the main error sources of GPS. The selective availability was also

another error source for civilian usage, but discontinued in 2000. Accuracy of positioning and navigation is depend on these error sources.

The ionosphere is about 60-1000 km high above the Earth's surface, in fact the plasma of the upper atmosphere's ionized gas with solar radiation and high energy. The ionized electron concentrations vary according to the amount of altitude, location, time of day, season and amount of solar activity on the surface of the earth. In the past, different observation instruments have been developed and used to collect information about the ionosphere and the plasma, for example ionosonde, scatter radars (Tsunoda 1988), topside sounders on board satellites (Reinisch et. al. 2001), in situ rocket and satellite observations (Klobuchar 1991) but, they were all limited with narrow scope. Since the Global Positioning System (GPS) was fully operational in 1994, it provided unprecedented accuracy, flexibility and tremendous contribution to navigation, positioning, timing and scientific inquiries with respect to precise positioning on the earth.

The Global Positioning System (GPS) signals are transmitted to the receiver through the Earth's atmosphere on microwave (L band) carriers and naturally exposed to ionospheric effects. The signals are delayed with the reason of ionospheric refractivity. Therefore, the signal propagation way is changing and lengthening called as ionospheric delay. This delay makes errors while using the GPS for positioning and navigation applications. The error is changeable in the range of few meters to 80 meters depend on the ionospheric conditions. On the contrary, it allows users to obtain information about the ionosphere. The GPS ionospheric delay model based on realistic modelling of electrons in the ionosphere using a dipole moment approach for earth's magnetic field was introduced by Bassiri and Hajj (1993). Knowledge of the TEC is allowing to estimate significantly signal delay in the ionosphere.

The ground and space based GPS can operate in all time and weather conditions and can be used to estimate tropospheric parameters, global refraction index, TEC and electron density profiles (Rocken 1997, Syndergaard 2000). It can be used for weather analysis, weather forecasting, monitoring climate change and ionospheric events. The GPS is a low-cost and high temporal resolution (30 seconds) technique (Klobuchar 1991), so it is widely used method for investigations.

Developers of the GPS system apply two frequencies to create a linear combination of different signals that will have the least effect on ionospheric location measurements (Hofmann-Wellenhof et. al. 2008). However, the single-frequency GPS receiver does not have the ability to remove the most part of effect, but rather needs to rely on an ionospheric model such as Klobuchar model. The previous studies on ionospheric effect show that ionosphere is higher than other sources of errors and that some studies have been done to model these effects. The effect of the geomagnetic field on the anisotropic ionospheric refraction index by Elmas et. al. (2011). These concepts have been evaluated differently in order to calculate the contribution of high-order ionospheric effects to the GNSS error budget. Kim and Tinin (2007) use the perturbation theory to study the residual error of the dual-frequency ionosphere free observable; they are investigating the third-order ionospheric effect (Ion3) term associated with the ray bending effect in GNSS signals penetrating into an inhomogeneous ionosphere. Considering that the term Ion3 includes not only quadratic correction due to the refractive index but also the correction of the ray bending effect, the second-order ionosphere effect (Ion2) of the ray bending effect may dominate the error contribution. Regular large-scale and random small-scale irregularities in the ionosphere are considered that from time to time, they can create a residual error comparable or greater than the term Ion2, contributing to the residual error that can be observed in the ionosphere. While the 1st order ionospheric effect (Ion1) is having the same magnitude but opposite signs for the group and carrier phase measurements, the Ion2 and Ion3 have different magnitudes and signs for these two types of measurements. These errors are neglected in many applications but should be considered in high precision applications (Petrie et. al. 2010).

1.2 ATMOSPHERIC DELAY

In the last decades, the Global Positioning System (GPS) has been widely used in navigation, positioning and related applications. The widespread usage of GPS has brought about the need for accuracy. However, the GPS signals pass through the atmosphere and have delay while coming from satellite to receiver. It will be delayed by the atmospheric (tropospheric and ionospheric) refraction, which results in a lengthening of the geometric path of the ray, usually referred to as the tropospheric and ionospheric delays (Jin et. al. 2008a, 2008b, Jin et. al. 2009a, Jin and Luo 2009).

The Global Positioning System (GPS) contains a constellation of 30 satellites moving at a 55 inclination angle at 6 orbits with a period of about 12 hours. Each GPS satellite broadcasts a two-spectrum L-band radio signal with frequency f_1 and f_2 ($f_1=1.575$ GHz and $f_2=1.227$ GHz). Dual frequency GPS receivers can evaluate the ionospheric effect by measuring the modulations in the codes and carrier phases. The carrier phase (L) and code observations (pseudorange P) of dual frequency GPS are expressed as follows:

$$\begin{aligned} L_{i,r}^s &= \lambda_i \phi_{i,r}^s = \rho_{0,r}^s - d_{ion,i,r}^s + d_{trop,r}^s + c (\tau^s - \tau_r) - \lambda_i (b_{i,r}^s + N_{i,r}^s) \\ P_{i,r}^s &= \rho_{0,r}^s + d_{ion,i,r}^s + d_{trop,r}^s + c (\tau^s - \tau_r) + d_{k,i}^s + d_{k,i,r} + \varepsilon_r^s \end{aligned} \quad (1.1)$$

where subscript i stands for the frequency ($i=1, 2$), superscript s and subscript r represent the satellite and ground-based GPS receiver, respectively. Other parameters, ρ_0 is the geometric distance between the GPS receiver and satellite; d_{ion} and d_{trop} are the ionospheric and tropospheric delays; c is the speed of light in vacuum space; τ is the satellite or receiver clock offset; b is the phase delay of satellite and receiver instrument bias; d_k is the code delay of satellite and receiver instrument bias; λ is the carrier wavelength; ϕ is the total carrier phase between the satellite and receiver; N is the ambiguity of the carrier phase; and ε is other residuals. The atmospheric errors are the major part of GPS error sources. When the errors not including atmospheric effects considered as residual, the code and phase observation equations can be shown as below:

$$\begin{aligned} L_{i,r}^s &= \lambda_i \phi_{i,r}^s = \rho_{0,r}^s - d_{ion,i,r}^s + d_{trop,r}^s + \varepsilon_L \\ P_{i,r}^s &= \rho_{0,r}^s + d_{ion,i,r}^s + d_{trop,r}^s + \varepsilon_P \end{aligned} \quad (1.2)$$

where the ε_L and ε_P represent the other total residuals for carrier phase and code observations. Atmospheric delay is divided into two parts with the name of ionospheric and tropospheric delay. The ionospheric delay is also separated into 3 parts first, second and third-order effects. And the tropospheric delay consists of wet and dry parts.

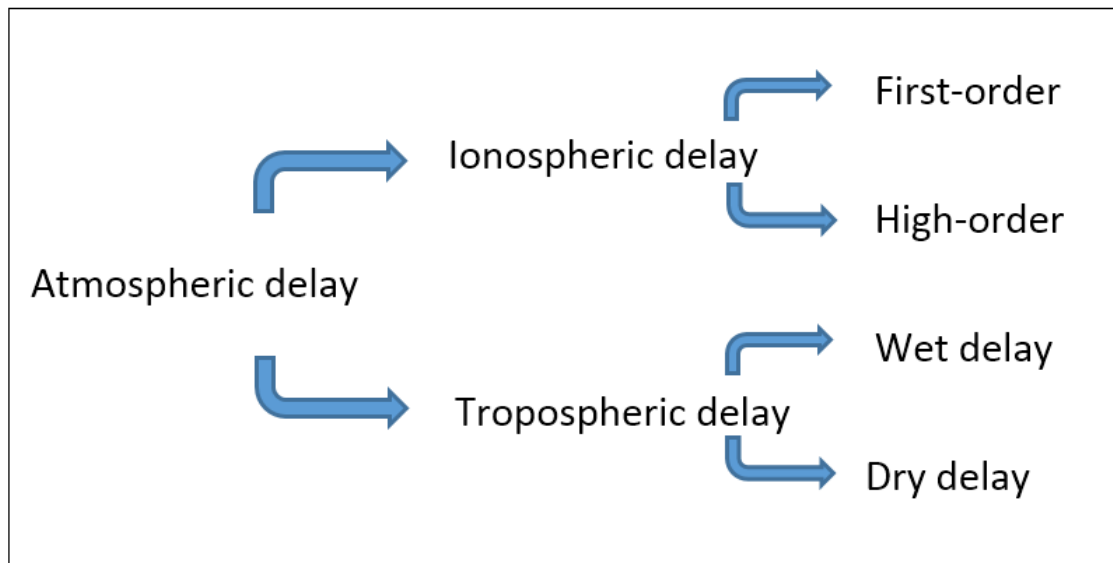


Figure 1.1 Parts of atmospheric delay

1.2.1 Ionospheric Delay

The ionosphere is the part of the atmosphere at an altitude of 60 to 1000 km above the earth and consists of ionized gas. The ionization produces free electron clouds which affect the GPS signals while passing this layer. The enlightening one part of the ionosphere by the sun is changing during the day, and ionization in the ionosphere is showing an alteration with the movements of sun. Solar activities also affect the amount of ionization in the ionosphere.

The first-order effect of the ionosphere on GPS signals is to change the speed of signal propagation relative to that of the free space. The ionosphere has opposite effect on code and carrier phase observations. While the code observations are having delay in the ionosphere, the carrier phase is advanced by the same amount. Magnitude of the error on the code and carrier phase is directly proportional with the total electron content (TEC) in a tube of 1 m^2 along the signal path.

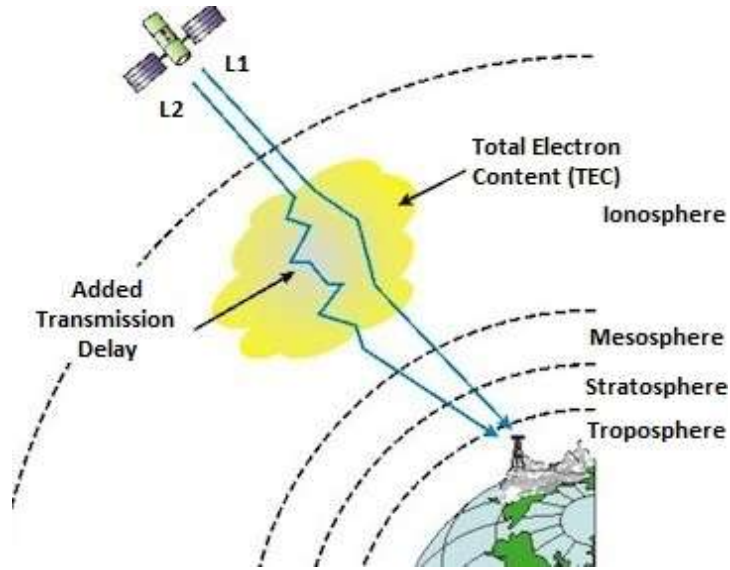


Figure 1.2 Ionospheric effect on different frequency GPS signals

Atmospheric delay is one of main GPS errors. The ionospheric effects on GPS signals contain the first and high-order effects. The first order is the major effect for the ionospheric delay at the order of $\sim 1\text{-}50\text{m}$, which can be estimated or eliminated from dual-frequency GPS observations. Higher order effects are related to the electron content along the ray-path and other parameters. For example, the second and third order terms are associated with on the order of geomagnetic field through the signal path and ray-path bending error (Hoque and Jakowski 2008).

$$L_i = \rho' - I_d^{(1)} - \frac{1}{2}I_d^{(2)} - \frac{1}{3}I_d^{(3)} + N_i + v_{L_i} \quad (1.3)$$

$$P_i = \rho' + I_d^{(1)} + I_d^{(2)} + I_d^{(3)} + v_{P_i}$$

- ρ' : is the geometric distance
- $I_d^{(1)}$: first order ionospheric effect
- $I_d^{(2)}$: second order ionospheric effect
- $I_d^{(3)}$: third-order ionospheric effect
- N_i : phase ambiguity
- v_{L_i} : unmodelled phase residuals
- v_{P_i} : pseudorange residuals

1.2.1.1 First-Order Ionospheric Effects

The first order delay is the most dominant part of the ionospheric delay so, only this term is considered in the most case studies. The total electron content in the ionosphere is sufficient to model first order term. Following Seeber (2003) the series:

$$n_{ion} = 1 + \frac{c_2}{f^2} + \frac{c_3}{f^3} + \frac{c_4}{f^4} + \dots \quad (1.4)$$

where the $c_{2,3,4,\dots}$ are coefficients of series expansion and f is the frequency of carrier wave which approximates the phase refractive index. The coefficients c_2, c_3, c_4 do not depend on frequency but on the quantity N_e denoting the number of electrons per m^3 (i.e., the electron density) along the propagation path. Using an approximation by cutting off the series expansion after the quadratic term, that is

$$n_{ion} \approx 1 + \frac{c_2}{f^2} \quad (1.5)$$

$$c_2 = C \cdot N_e ,$$

N_e : electron density (electrons/ m^3),

C : constant; $C = 40.3$ (m^3/s^2),

$$n_{ion} \approx 1 + \frac{C \cdot N_e}{f^2}$$

Now, the ionospheric propagation delay in zenith direction can be integrated using the electron density N_e . For carrier phase measurements this correction in zenith direction is

$$\delta S_{ion}^{Z=0} = \int_{h_A}^{\infty} \frac{c_2}{f^2} = \frac{C}{f^2} \cdot \int_{h_A}^{\infty} N_e(h) \cdot dh = \frac{C}{f^2} \cdot VTEC \quad (1.6)$$

VTEC : vertical total electron content (TECU)

$$1 \text{ TECU} = 10^{16} \text{ electrons}/m^2$$

In practice, the zenith ionospheric delay must be mapped into the direction of the line of sight of the particular satellite. This is done by application of a mapping function. To do so, the zenith

angle from the ground antenna at station A to satellite I is commonly corrected by taking the distance between antenna and ionosphere into account as shown in Figure 1.3:

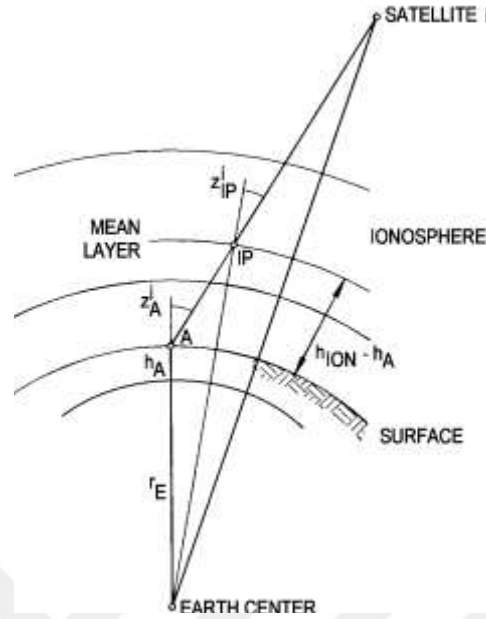


Figure 1.3 Ionospheric propagation delay

Zenith angle z_A^i from ground station A to satellite i and ionospheric zenith angle z_{IP}^i from the mean ionosphere to the satellite following Hoffmann Wellenhof (1993). The projection of the ionospheric point IP to the surface yields the horizontal coordinates needed for interpolation in TEC maps like IONEX files.

$$\cos Z_A^i = \frac{\cos \varphi_A \cdot \cos \lambda_A \cdot \Delta X_A^i + \cos \varphi_A \cdot \sin \lambda_A \cdot \Delta Y_A^i + \sin \varphi_A \cdot \Delta Z_A^i}{S_A^i} \quad (1.7)$$

φ_A : ellipsoidal latitude of receiver antenna at station A

λ_A : ellipsoidal longitude of receiver antenna at station A

$\Delta X_A^i \Delta Y_A^i \Delta Z_A^i$: components of the distance vector between antenna at station A and satellite i

S_A^i : distance between antenna at station A and satellite I

$$\sin Z_{IP}^i = \frac{r_E + h_A}{r_E + h_{ion}} \cdot \sin Z_A^i \quad (1.8)$$

Z_{IP}^i : zenith angle from ionospheric point IP to satellite i

Z_A^i : zenith angle from ground station A to satellite i

r_E : earth radius ($r_E = 6371$ km)

h_{ion} : mean height of ionosphere ($h_{ion} = 300 \dots 500$ km)

h_A : height of ground station A

where the weighted mean height of the ionosphere is normally chosen to be about 450 km. Generally speaking, heights in the range of 300 to 500 km are valid values, see Hoffmann-Wellenhof (1993). Uncertainties in h_{ion} mainly affect observations at low elevations, whereas high-elevation measurements remain more or less untouched. The slant delay now becomes

$$I_{d Li}^{(1)} = \delta S_{A(ion)}^i = m_{ion}(Z_{IP}^i) \cdot \delta S_{ion}^{Z=0} = \frac{1}{\cos Z_{IP}^i} \cdot \delta S_{ion}^{Z=0} = \frac{C}{f^2} \cdot \frac{1}{\cos Z_{IP}^i} \cdot VTEC \quad (1.9)$$

First order ionospheric effect can be expressed as:

$$I_{d Li}^{(1)} = \delta S_{A(ion)}^i = \frac{40.3}{f^2 \cdot \cos Z_{IP}^i} \cdot VTEC = \frac{40.3}{f^2} \cdot STEC \quad (1.10)$$

1.2.1.2 Second-Order Ionospheric Effects

The second order terms are associated with geomagnetic field through the signal path. The development of the equations to compute the second and third-order ionospheric effects in the GNSS observable, as well as further discussions on this matter, can be found in Bassiri and Hajj (1993), Odijk (2002), Kedar et. al. (2003) and Herná'ndez-Pajares et. al. (2007), as well as papers by other authors.

It is noticeable that the ionospheric effects are similar for phase and range, differing only by the sign and the factors 1/2 and 1/3, respectively, for the second- and third-order ionospheric effects. The second-order effects for the case of the range in the frequency f_{Li} ($i=1,2$) can be computed by (Bassiri and Hajj 1993, Odijk 2002, Kedar et. al. 2003):

$$I_{d Li}^{(2)} = \frac{eA}{f_{Li}^3 2\pi m_e} ||B|| |\cos\theta| TEC \quad (1.11)$$

$A \approx 80.6 \text{ m}^3/\text{s}^2$, $e = 1.60218 \times 10^{-19}$ Coulomb, $m_e = 9.10939 \times 10^{-31}$ kg,

$||B||$: magnitude of the geomagnetic induction vector B.

The product $\|B\| \cdot |\cos\theta|$ has to be evaluated for the computation of the second-order effect, which can be done based on the inner product of the vector B (geomagnetic induction) and the unit vector J (propagation direction of the signal) at the height of the single ionospheric layer (Fig. 1.4).

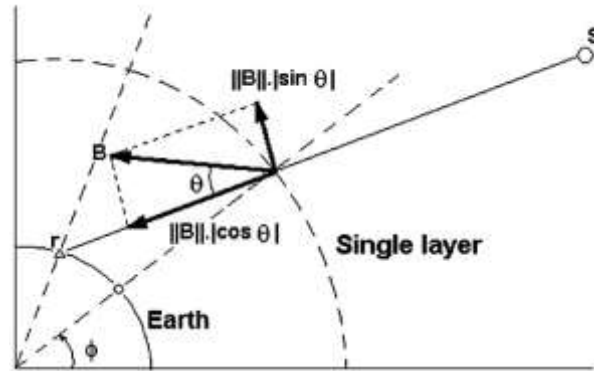


Figure 1.4 Geomagnetic local system. Adapted from Odijk (2002)

1.2.1.3 Third-Order Ionospheric Effects

The third order terms are associated with ray-path bending error and can be computed by:

$$I_{dLi}^{(3)} = \frac{3A^2}{8f_{Li}^4} \eta N_{e,max} TEC \quad (1.12)$$

$N_{e,max}$: maximum electron density

η : constant value (0.66).

The third-order ionospheric effect is very similar to the second order effect once it is given as a function of the TEC. However, it is a function of the maximum electron density $N_{e,max}$ and the factor g, which can be approximated by a constant value of 0.66 (Hartmann and Leitinger 1984). Fritsche et. al. (2005) expresses the $N_{e,max}$ as a function of TEC:

$$N_{e,max}(m^{-3}) = \frac{(20 - 6) \cdot 10^{12}}{(4.55 - 1.38) \cdot 10^{18}} TEC \quad (1.13)$$

1.2.2 Tropospheric Delay

GPS observations are subject to several sources of error, such as clock biases, multi-path delay, ionospheric and tropospheric delays. Particularly, the tropospheric delay significantly affects the GPS signals and causes errors of several meters in positioning. Since the GPS signal is sensitive to the tropospheric refractive index, which is dependent on the pressure, temperature and moisture, GPS can be used for sensing these properties in the troposphere, e.g. tropospheric water vapor (Jin and Luo 2009, Jin et. al. 2009a). Although studies have demonstrated to successfully estimate PWV from GPS within 1-2 mm of accuracy at 15 minute temporal resolution, a number of factors still affect PWV accuracies, e.g., mapping functions and Earth's tide models, (Jin et. al. 2009b).

While GPS signals passing through the troposphere, the signal is delayed caused by neutral atmosphere and optical distance from satellite to receiver becoming larger than the geometric distance. Tropospheric delay on the GPS signals can cause several centimeter errors in height even when simultaneously recorded meteorological data are used in tropospheric models (Tregoning et. al. 1998). Nowadays, the GPS is widely used to determine tropospheric delay using with mapping functions (Bevis et. al. 1994, Emaradson et. al. 1998, Jin and Park 2005, Niell 1996). Tropospheric delay on the vertical direction along neutral atmosphere can be expressed as:

$$ZTD = c\tau = 10^{-6} \int_0^{\infty} N(s) ds \quad (1.14)$$

where c represents the speed of light in a vacuum, τ represents the time and N is the neutral atmospheric refractivity. The neutral atmospheric refractivity is related with standard meteorological variables as (Davis et. al. 1985).

$$N = k_1\rho + k_2 \frac{P_w}{Z_w T} + k_3 \frac{P_w}{Z_w T^2} \quad (1.15)$$

where k_i ($i= 1, 2, 3$) is constant, ρ is the total mass density of the atmosphere, P_w is the partial pressure of water vapor, Z_w is a compressibility factor near unity accounting for the small

departures of moist air from an ideal gas, and T is the temperature in degrees Kelvin. The integral of the $k_1\rho$ is the hydrostatic component (Nh) and the integral of the $(k_2 \frac{P_w}{Z_w T} + k_3 \frac{P_w}{Z_w T^2})$ is the wet component (N_w) in the equation (1.15). Thus, ZTD consists of two parts which are dry (ZHD) and wet (ZWD) components. While dry delay is depending on dry gases, wet delay is caused by water vapor. Hydrostatic delay is related with atmospheric pressure and can be computed with natural gases law. Wet delay can be converted into precipitable water vapor (PWV), which plays an important role in affecting the numerical weather forecast (NWP) model variables directly or indirectly (Bevis et. al. 1994, Duan et. al. 1996, Tregoning et. al. 1998, Hernández-Pajares et. al. 2001).

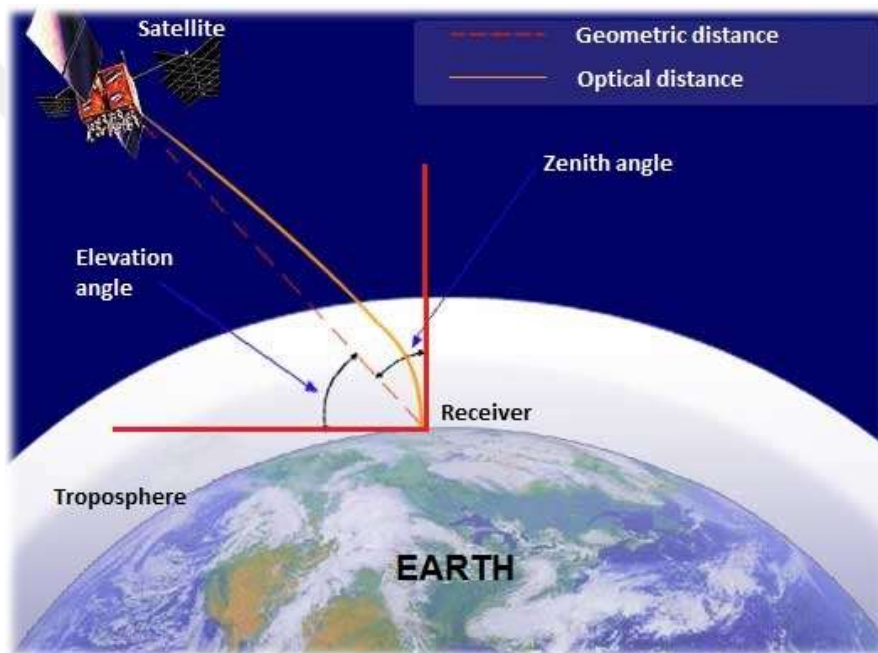


Figure 1.5 Tropospheric delay on GPS signals

Water vapor has an important role for weather forecasting and can be estimated from GPS observations. When the geometric distance between GPS station and satellite is known with negligible uncertainty, tropospheric delays on GPS signals can be estimated using with range measurement minus geometric distance. After the eliminating ionospheric and hydrostatic delay, slant wet delay can be computed. Wet delay on the zenith direction can be computed using the mapping function related to the elevation angle of each satellite. Zenith wet delay (ZWD) can be converted into the precipitable water vapor (PWV) (Rocken et. al. 1995). However, in the past time, mostly higher-order ionospheric effects were ignored. In this paper, the high-order ionospheric effects are investigated and assessed.

1.2.2.1 Saastamoinen Model

This model uses hydrostatic component definitions (Saastamoinen 1972). The Saastamoinen model uses the constant deviation rate model in the troposphere (0-10 km) for modelling hydrostatic pressure, and the isothermal model (over 10 km) in tropopause. The temperature depends on the temperature gradient is expressed as equation (1.16).

$$T = T_0 + \beta (r - r_0) \quad (1.16)$$

The resulting pressure profile is the same as (17).

$$P = P_0 \left(\frac{T}{T_0} \right)^{\frac{-Mg}{R\beta}} \quad (1.17)$$

Where r represents the radius of the earth center, r_0 is the radius of the region being observed, T_0 is the temperature in the zone, P_0 is the pressure in the surface, M is the molar mass of the air, g is the gravitational acceleration, R is the universal gas constant.

The corresponding dry refraction is the same as in Equation (1.18).

$$n - 1 = (n_0 - 1) \cdot \frac{T}{T_0} \cdot \mu \quad (1.18)$$

and $\mu = \left(\frac{-Mg}{R\beta} \right) - 1$. The pressure drops quickly from the level on the tropopause.

$$P = P_T \exp\left[\frac{-gM}{RT_T} (h - h_T) \right] \quad (1.19)$$

the subindex T used in Equation (1.19) symbolises the values on tropopause.

Saastamoinen has defined both standard model and sensitive model for tropospheric delay. The standard model for tropospheric delay is as in Equation 1.20.

$$\Delta_{Saas}^{PD} = 0.002277 \cdot \sec z \cdot \left[p + \left(\frac{1255}{T} + 0.05 \right) \cdot e - B \cdot \tan^2 z \right] + \delta R \quad (1.20)$$

where the P , e are milibar, T is Kelvin and Z symbolizes the zenith angle. The coefficient B in the equation is empirically determined coefficients based on the height of the receiver from sea level and is arranged in the form of scales. δR is given in the form of charts depending on the altitude and zenith angle of the receiver from sea level (Troller 2004).

$$\Delta_{Dry}^{PD} = 0.002277 \cdot \sec z \cdot [p - 0.155471 \cdot e - B \cdot \tan^2 z] + \delta R \quad (1.21)$$

$$\Delta_{Wet}^{PD} = 0.002277 \cdot \sec z \cdot \left(\frac{1255}{T} + 0.20547 \right) \cdot e \quad (1.22)$$

The Saastamoinen model with equations (1.21) and (1.22) can be used with standard atmospheric parameters where meteorological observations are not available in the assessment of GNSS data. In this case, station height $h = 0$ m, $p = 1013.25$ hPa, $T = 291,16$ K°, %50 humidity standards are used (Troller 2004).

If the atmosphere is in hydrostatic stability and the gravity is independent of elevation, the P/T ratio in the diffraction of humid air is reduced by the integral of the density in the zenith direction which is directly proportional to the total pressure in the surface as a result of the Saastamoinen model. Since the Saastamoinen model works with elevation angles greater than 10° , the zenith delay should be $1/\sin(\epsilon)$ for small elevation observations of 10° (Özlüdemir 2004).

1.2.2.2 Vienna Mapping Function Model

In the mapping functions developed for tropospheric modelling of GNSS and VLBI data analyses, radiosonde data is used to calculate radiation. In recent years, it has given importance to the development of mapping functions based on numerical weather model data. The principle underlying the Vienna mapping function in Equation (1.23) is to skip the intermediate steps by directly applying a ray account to the numerical weather model.

$$mf_{h,w} = \frac{1 + \frac{a}{1 + \frac{b}{1 + c}}}{\sin(e) + \frac{b}{\sin(e) + c}} \quad (1.23)$$

The continuous part formula used in wet and hydrostatic projection functions is as above. This formula has also been used in NMF and IMF models. The coefficients in the Vienna mapping function are obtained by applying a direct ray of light to the numerical weather model. The ray calculation process has hydrostatic and wet diffraction values in the diffraction contents at k-level (about 1000 hPa). These values will be used in the calculation of N Wet, N Hydrostatic, n values at (k-1) level.

1.2.2.3 Tropospheric delay gradient

Azimuthally asymmetric delays are described as troposphere gradients. Tropospheric delay gradients are continuously variable and affecting the baseline lengths and positioning (Davis et. al. 1993, Teke et. al. 2011). Here we further investigate HOI effect on tropospheric gradients. And the tropospheric delay (T_d) is expressed as:

$$T_d = T_{Wd} + T_{Dd} = T_{ZWd} MF_{wet}(\varepsilon) + T_{ZDd} MF_{dry}(\varepsilon) \quad (1.24)$$

where T_{Wd} and T_{Dd} are the tropospheric wet and dry delays, T_{ZWd} and T_{ZDd} are the wet and dry zenith delays, MF_{wet} and MF_{dry} are the wet and dry mapping functions and ε is the elevation angle of satellites. The effects of azimuthal asymmetry in the atmospheric delay $A_{d(\varepsilon, \alpha)}$ are not included in model, may be expressed as

$$A_{d(\varepsilon, \alpha)} = NS_{grad} \cos\alpha MF(\varepsilon) + EW_{grad} \sin\alpha MF(\varepsilon) \quad (1.25)$$

$$MF_\varepsilon = \frac{1}{\sin\varepsilon \tan\varepsilon + 0.0032} \quad (1.26)$$

where ε is elevation angle of satellite, α is the azimuth, NS_{grad} and EW_{grad} are the gradients on the North-South and East-West directions, and $MF(\varepsilon)$ is the mapping function for gradients.

1.2.2.4 Precipitable water vapor

When GPS signals propagate through the atmosphere, it will be delayed by the atmospheric (tropospheric and ionospheric) refraction, which results in a lengthening of the geometric path of the ray, usually referred to as the tropospheric and ionospheric delays (Jin et. al. 2008b, Jin et. al. 2009a). Atmospheric delay is one of main GPS errors. The ionospheric effects on GPS signals contain the first and high-order effects. The first order is the major effect for the ionospheric delay at the order of ~1-50m, which can be estimated or eliminated from dual-frequency GPS observations. Higher order effects are related to the electron content along the ray-path and other parameters. For example, the second and third order terms are associated with on the order of geomagnetic field through the signal path and ray-path bending error (Hoque and Jakowski 2008). Normally the higher-order ionospheric effects are generally the order of sub-millimeter to several centimeters, but they should be considered in precise GPS applications.

Water vapor has an important role for weather forecasting and can be estimated from GPS observations (Bevis et. al. 1992). When the geometric distance between GPS station and satellite is known with negligible uncertainty, tropospheric delays on GPS signals can be estimated using with range measurement minus geometric distance. After the eliminating ionospheric and hydrostatic delay, slant wet delay can be computed. Wet delay on the zenith direction can be computed using the mapping function related to the elevation angle of each satellite. Zenith wet delay (ZWD) can be converted into the precipitable water vapor (PWV) (Rocken et. al. 1995).

$$PW = \Pi \cdot ZWD \quad (1.27)$$

where the Π is a factor about 0.15 but varies with the location, elevation and season. And it can be computed as a function of surface temperature (Rocken et. al. 1995).

$$\Pi = [R_v \left(\frac{k_3}{T_m} + k'_2 \right)]^{-1} \quad (1.28)$$

where $R_v=461.495$ J/(kg·K) is the specific gas constant for water vapor. The weighted mean temperature of the wet part of the atmosphere is T_m , which can be estimated as a function of surface temperature T_s as $T_m = 70.2 + 0.72 \cdot T_s$ (Bevis et. al. 1992).

$$k'_2 = k_2 - mk_1 \quad (1.29)$$

where m is M_w/M_d , the ratio of molar masses of water vapor and dry air, k_1 and k_2 are the physical constants.

1.3 CONTENTS

In this thesis, high-order ionospheric effects on GPS tropospheric and coordinate estimation are investigated. Chapter 2 will present GPS theory and methods. This section introduces detailed information about GPS theory, high-order ionospheric corrections, RINEX-HO software and geomagnetic field model, solar activity and F10.7 flux. Chapter 3 will examine the High-order ionospheric effect on GPS estimated tropospheric parameters such as zenith tropospheric delay (ZTD), gradients and precipitable water vapor (PWV). Chapter 4 investigates the High-order ionospheric effects on coordinates and Chapter 5 includes the conclusion part which gives general interpretation of all applications done during this thesis.



CHAPTER 2

THEORY AND METHODS

2.1 GPS THEORY

Although it is widely used for GPS positioning, it is also used for many different applications. The usage of atomic clocks in the GPS allows high accuracy to be achieved. Signals transmitted from satellites that actively move on their orbit are used to determine receiver locations.

It is known that the position of each satellite and its distance from the center of the world. It is shared as broadcast ephemeris data. Knowledge of the satellite position and the distance between the satellite and the receiver allow user to determine the receiver's position. Positioning with GPS is based on the resection method and at least four satellites are needed.

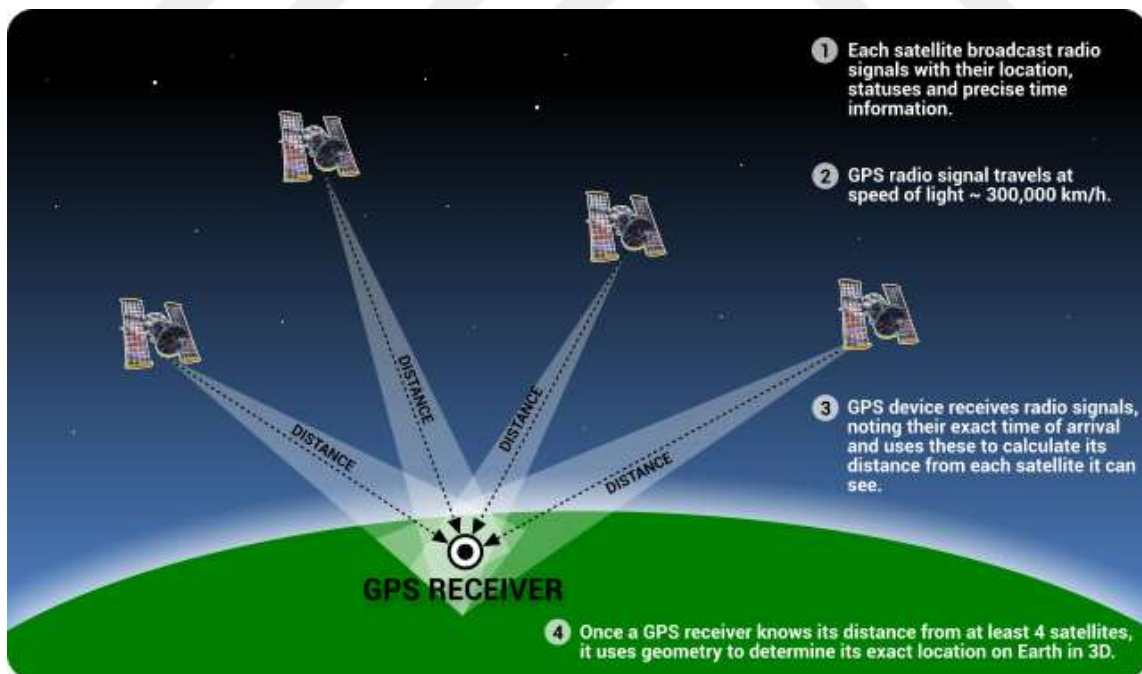


Figure 2.1 Positioning with GPS receiver

The all-weather global system is subdivided into three segments:

- The space segment consisting of active satellites which broadcast signals.
- The control segment for system and time control, and for prediction of the orbits
- The user segment including different receiver types and users.

The geometric distance between the satellite and receiver can be calculated according to the following formula

$$\rho_{0,r_i}^{s_i} = \sqrt{(X^{s_i} - X_{r_i})^2 + (Y^{s_i} - Y_{r_i})^2 + (Z^{s_i} - Z_{r_i})^2} \quad (2.1)$$

Where $\rho_{0,r_i}^{s_i}$ is the geometric distance from satellite to receiver, i represents the each satellite ($i=1, 2, \dots$), $X^{s_i}, Y^{s_i}, Z^{s_i}$ are the satellite coordinates, $X_{r_i}, Y_{r_i}, Z_{r_i}$ are the receiver coordinates. If the pseudorange is used instead of geometric distance in this equation, receiver positions can be calculated with at least four satellite observations. However, this positioning information will include all errors.

2.2 HOI EFFECTS CORRECTION

Positioning and navigation with GPS includes some errors and ionosphere is the main one of them. The ionosphere is a major source of error in GPS observations, and ionosphere based range errors can reach several tens of meters on zenith direction (Klobuchar 1996). The ionosphere has a dispersive effect for GPS signals. Most of this effect can be eliminated by linear combinations of dual frequency GPS observations. Higher-order ionospheric effects are then left behind. These errors vary depending on the elevation angle and extreme weather conditions and can reach several centimeters in low elevation angles (Klobuchar 1996). HOI effects corrections also can provide users to obtain satellite positions with in centimeter accuracy (Fritsche et. al. 2005).

The early studies worked by Brunner and Gu (1991) on the correction of high-order ionospheric effects are particularly related with second order effects and ray path bending errors. In their approach, knowledge of actual atmosphere and magnetic field components which are not easy to estimate along the ray path should be well known.

Another study has been done by Bassiri and Hajj (1993) to estimate geomagnetic field model, and they have assumed an Earth-centered tilted dipole approximation. 300 km above the earth surface is accepted as a single layer ionosphere and calculates the geomagnetic field vector at the ionospheric pierce point (IPP). Hawarey et. al. (2005), the study of very long baseline interferometry (VLBI) has included the use of more realistic geomagnetic field models in order to obtain secondary order effects. For example, the use of the international geomagnetic reference field (IGRF) model is shown instead of the dipole model.

Strangeways and Ioannides (2002) expresses a method with less than 1 cm accuracy in range correction by employing three factors which are related with ratio of the slant TEC and the ratio of their geometric path. In practice, parameter estimation at this accuracy is quite difficult.

Using the linear combination of dual frequency GPS observations first order effects can be eliminated which is known as ionosphere-free solution. The secondary and third order ionospheric effects due to the TEC difference along the frequencies f_1 and f_2 cause the ray path lengthening which cannot be eliminated in that approach.

These error sources should be determined and corrected for accurate positioning. The knowledge of total electron content in the ionosphere is enough to determine first order effects. First order ionospheric effects can be eliminated using dual frequency GPS observations, but high-order effects are generally ignored. Higher order effects are related to the electron content along the ray-path and other parameters. For example, the second and third order terms are associated with on the order of geomagnetic field through the signal path and ray-path bending error (Hoque and Jakowski 2008).

The RINEX_HO (RINEX HIGH ORDER) software has been developed by the Faculty of Science and Technology of Sao Paulo State University in Brazil to determine high-order ionospheric effects and to eliminate these effects from GPS observations. This software allows users to calculate second and third order ionospheric effects corrections using the IGRF model to obtain “corrected RINEX observation files” from the data in the “RINEX observation file”.

2.3 RINEX HO

RINEX HO software has been developed to produce corrected RINEX observation files that have been modified from raw RINEX observations files using NGS (National Geodetic Survey) classes in C ++ software. C ++ classes have been developed on the basis of calculation or interpolation of TEC values, calculation of second and third order ionospheric effects and storage of corrections in a new RINEX file. It has been used to account geomagnetic field subroutines in Fortran for Corrected Geomagnetic Model (CGM) and C subroutines for International Geomagnetic Reference Field (IGRF11).

There are three options to get TEC values which are calculated from raw pseudoranges, from pseudoranges smoothed by phase, or from Global Ionosphere Maps (GIM). When the TEC from pseudoranges smoothed by phase has been used, cycle slip detection method has been implemented following the Turbo Edit algorithm by Blewitt (1990) and the program restarts the smoothing filter when a shift cycle for a particular satellite is detected.

P1/P2 and P1/C1 satellite Differential Code Biases (DCBs) are needed to enter if pseudorange values are used in the calculation of TEC values. These files for 2011 can be reached from the CODE ftp server <ftp://ftp.unibe.ch/aiub/CODE/2011>. While the TEC values are calculated from the pseudoranges, the receiver DCBs of the used station must also be processed. When the IGS stations are used in the analysis, the receiver DCBs can be obtained from CODE ftp server. However, receiver DCBs of for other stations can be obtained by calibration procedures.

Geomagnetic field effects are the main reason of second or terms. The software supplies three options to select one of geomagnetic field model which are "Dipolar model", "CGM from PIM" and "IGRF model".

The RINEX-HO software allows second and third order ionospheric corrections to all satellite observations in the RINEX observation files, and allows the creation of corrected RINEX observation files. The files "Rinex_ha.inp" and "Rinex_ha_param.dat" are required to be included in the RINEX HO file during this correction process. Borland Builder C++ 6.0 was used to perform the evaluation on Windows and GCC/G++ software to perform on the Linux environment. The next section contains the source code for the RINEX_HO software and the compilation steps for Windows or Linux systems.

Two files named "Rinex_ha.inp" and "Rinex_ha_param.dat" are needed to compile RINEX observation files in RINEX HO software. These files are listed in Table 2.1 and Table 2.2.

Table 2.1 Description of Rinex_ha.inp input file

| Input/output files and parameters | Description of each line |
|--|--|
| adan1521.07o | Name of observation file |
| adan1521.07n | Name of navigation file |
| adan152c.07o | Name of the new observation file |
| adan152_Out | Initial name of the output files |
| X0 Y0 Z0 | Receiver coordinates (if 0.0 => Try to read coordinates from RINEX) |
| 10 | Elevation Mask (means that observables below this mask won't be corrected) |
| 1 | Save output and log files (yes=1; no=0) |
| 1 | 0 = Tec from raw pseudorange 1 = TEC from pseudorange smoothed by phase 2 = TEC from GIM |
| CODG1520.07I | Name of the CODE map: In the case before option "TEC from GIM " = 2 |
| 6.898 | DCB (P1-P2) = receiver bias in ns (nano-seconds): In the case computing TEC from pseudorange |
| P1C1_010611.DCB | DCB (P1-C1) - P1C1 bias for satellites - Found at: ftp://ftp.unibe.ch/aiub/CODE/ |
| P1P2_010611.DCB | DCB (P1-P2) - P1P2 bias for satellites - Found at: ftp://ftp.unibe.ch/aiub/CODE/ |
| 2 | 0 = Dipolar model 1 = CGM from PIM 2 = IGRF model |
| IGRF11.COF | Name of IGRF coefficient file: In the case option before = 2 |

Table 2.2 Description of Rinex_ha_param.dat input file

| Input/output files and parameters | Description of each line |
|--|--|
| 0.6 | Sigma CA (m) |
| 0.8 | Sigma P2 (m) |
| 0.006 | Sigma phase L1 (m) |
| 0.008 | Sigma phase L2 (m) |
| 450000.0 | Ionospheric layer height (m) |
| 6371000.0 | Earth Equatorial axis (m) |
| 3.12E-05 | Geomagnetic induction magnitude in the Equator (Tesla) - To be used in the Dipolar approximation |
| 3.0E12 | Maximum density of electrons - To be used in the Dipolar approximation |

The RINEX_HO software can be compiled in Windows or Linux operating systems by users. Borland C++ 6.0 software has been used to compile in Windows, then CGM source code in Fortran must be used in the format of DLL.

Source codes of RINEX HO software are compressed in a file. When this source file is ejected, the files needed for Windows and Linux systems appear. In these files, the subdirectory filed in table x will be filled. These files contain other subfolders that are listed in Table 2.3.

Table 2.3 Subfolders for RINEX_HO source code

| Folders | Content and Description |
|-----------------------|--|
| ADAN | Files example for ADAN station in the day 152 of 2011 |
| CGM_DLL_Lahey_Fujitsu | CGM subroutines in fortran 90 prepared to create the DLL in the Lahey Fujitsu |
| Class_Iono | Class to compute second and third order ionospheric effects |
| Class_TEC | Class to Read GIM and interpolate TEC, to compute TEC from raw pseudorange or from pseudorange smoothed by carrier phase |
| Cycle_Slip | Class to detect cycle slip |
| FilterCode | Class to compute Pseudorange smoothed by phase |
| Fortran_Class | Class to mix C/C++ and Fortran available at: http://arnholm.org/software/index.htm |
| IGRF11 | Class to compute geomagnetic components (X, Y, Z) from IGRF 11 model. Original source code available at: http://www.ngdc.noaa.gov/IAGA/vmod/igrf.html |
| Include | Constants and variables to be used in RINEX_HO |
| Rinex_Class | Classes for reading and writing RINEX files available at: http://www.ngs.noaa.gov/gps-toolbox/rinex.htm |

In the following steps, RINEX HO has been involved in how to compile the software on Windows and Linux operating systems.

2.3.1 Compiling for Windows

With the Lahey/Fujitsu Fortran 95 software, a DLL was created for the CGM Fortran subroutines. In this case, subroutines of Fortran must be used in the format of Fortran 90. The existing subroutines can be found in the "CGM_DLL_Lahey_Fujitsu" folder. The DLL used here is called "cgm_util.dll" and can be found with the source code in the main folder. The following command line is used to create the DLL:

Lf95 cgm_util.f90 -win -ml bc -dll

To use the "cgm_util.dll" DLL in Borland Builder C ++ as a static library, the following ".lib" file was created from the command line:

```
implib cgm_util.lib cgm_util.dll
```

where, implib tool comes with the Borland Builder C ++ 6.0 installation.

When the cgm_util.lib is used in the Borland project, it is easy to call the DLL by including the header of the fortran subroutine as:

```
extern "C" __declspec(dllimport) void _stdcall SUB_NAME (int *arg, double *arg2, etc,...);
```

where, SUB_NAME is the name of the subroutine to be called in the C++ program and must be written in capital letter.

Everything is ready for the Windows compilation and the user must only to open the project file called "rinex_ho.bpr" in the Borland C++ builder 6.0 and after compile and run the program.

2.3.2 Compiling for Linux

For Linux compilation we have used the Ubuntu Linux distribution that is free available online. In this case, the user must install the gfortran and gcc/g++ compilers. With the C++ and Fortran files inside the folder, the first step is to create the ".o" files through the two following commands:

```
gfortran -c *.f
```

```
g++ -c *.cpp
```

The second step is to link the ".o" files in the RINEX_HO program:

```
g++ -o RINEX_HO *.o -lgfortran -static
```

To mix C++ and Fortran subroutines the user must insert the header for fortran subroutine as:

```
extern "C" void sub_name_(int *arg, double *arg2, etc,...)
```

where: sub_name_ is the name of the subroutine to be called in the C++ program and must be written in lower case letter.

When the HOI effects correction is applied to the RINEX observations, the change in the observation file is shown in the following example.

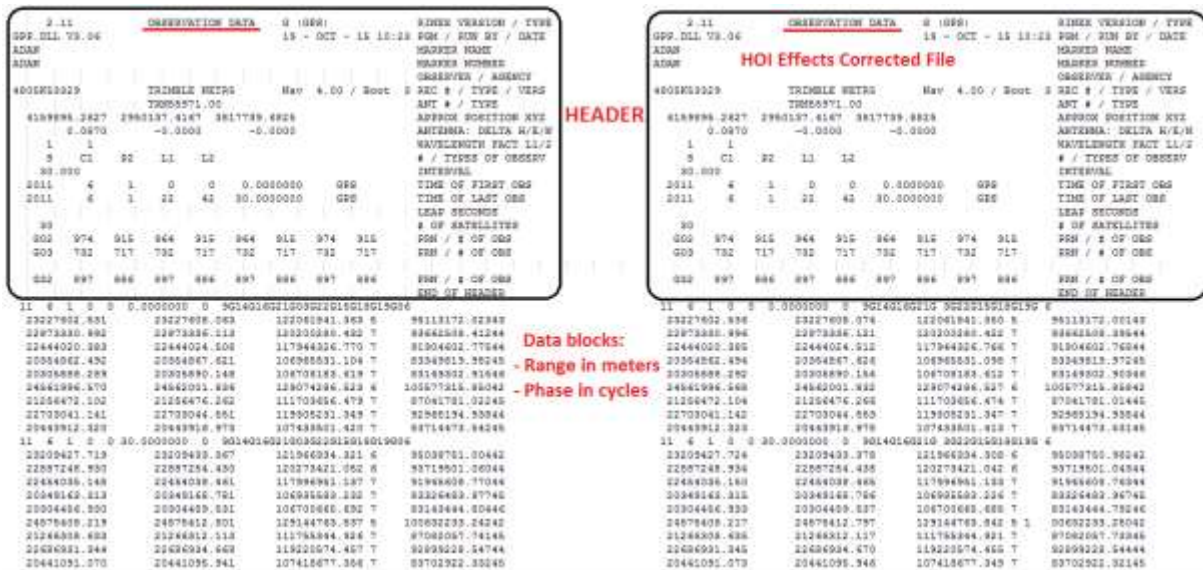


Figure 2.2 HOI Effects Correction

2.4 GEOMAGNETIC AND SOLAR CONDITIONS

The main reasons of HOI effects are solar activity, geomagnetic and ionospheric conditions. When the geomagnetic field is defined more accurately, the more accurate observations will give the more precise data to be obtained.

2.4.1 Geomagnetic Field Model

The International Geomagnetic Reference Field (IGRF) is an internationally agreed upon mathematical model of the Earth's magnetic field. The International Geomagnetism and Aviation Association (IGA) Working Group V-MOD has produced and maintained the Earth's magnetic field by a team of geomagnetic field modellers. These data has been derived from observations gathered from satellites, magnetic observatories and magnetic surveys. These data are used by scientists, business organizations and private individuals.

The almost completely core-generated geomagnetic field changes slowly but noticeable over the years. As a result, the IGRF should be revised to be up to date, usually every five years. Table 2.4 summarizes the detailed IGRF generations. IGRF generations consist of each five years intervals models which are determined definitive or non-definitive. When a model determined as definitive, it is called as Definitive Geomagnetic Reference Field (DGRF) which has been produced beginning from 1945 and it cannot be revised in the next generations of

IGRF. The non-definitive models are called as IGRF and the more detailed information about IGRF history especially 11th generation can be reached from Maus et. al. (2005), Barton (1997) or Macmillan and Finlay (2010). All versions of IGRF from past to nowadays can be reached from (URL-1 2017).

Table 2.4 Summary of IGRF generations, their intervals of validity, and related references

| Full name | Short name | Valid for | Definitive for | Reference |
|----------------|------------|---------------|----------------|-----------------------------|
| IGRF 12th gen. | IGRF-12 | 1900.0-2020.0 | 1945.0-2010.0 | Thébault et al. (2015) |
| IGRF 11th gen. | IGRF-11 | 1900.0-2015.0 | 1945.0-2005.0 | Finlay et al. (2010) |
| IGRF 10th gen. | IGRF-10 | 1900.0-2010.0 | 1945.0-2000.0 | Maus et al. (2005) |
| IGRF 9th gen. | IGRF-9 | 1900.0-2005.0 | 1945.0-2000.0 | Macmillan et al. (2003) |
| IGRF 8th gen. | IGRF-8 | 1900.0-2005.0 | 1945.0-1990.0 | Mandea and Macmillan (2000) |
| IGRF 7th gen. | IGRF-7 | 1900.0-2000.0 | 1945.0-1990.0 | Barton (1997) |
| IGRF 6th gen. | IGRF-6 | 1945.0-1995.0 | 1945.0-1985.0 | Langel (1992) |
| IGRF 5th gen. | IGRF-5 | 1945.0-1990.0 | 1945.0-1980.0 | Langel et al. (1988) |
| IGRF 4th gen. | IGRF-4 | 1945.0-1990.0 | 1965.0-1980.0 | Barracough (1987) |
| IGRF 3rd gen. | IGRF-3 | 1965.0-1985.0 | 1965.0-1975.0 | Peddie (1982) |
| IGRF 2nd gen. | IGRF-2 | 1955.0-1980.0 | - | IAGA (1975) |
| IGRF 1st gen. | IGRF-1 | 1955.0-1975.0 | - | Zmuda (1971) |

The new generation IGRF data is derived from the older versions. And this data has an importance in terms of presenting the original data to the user in the case of a new revision requirement.

The higher-order ionospheric effects are mostly related to the geomagnetic field, whose components in northward, eastward and vertically downward directions are provided by international Geomagnetic Reference Field (IGRF) model (Mandea and Macmillan 2000). Geomagnetic field is not same along the signal path, so IGRF model data are transformed into a generalized coordinate system using vector representation (Arfken 1985).

2.4.2 Solar Activity

The ionosphere consists of different layers. Ionization is present throughout the ionosphere, but it is available in different concentrations in different layers. As the radio waves pass through the ionosphere, they are refracted due to ion density and deviate in the signal path.

Ionization which varies in different layers of the ionosphere causes the effects on the high frequency bands to vary. Particularly solar radiation causes ions to ionize and convert into free ions of the upper ionosphere. Free electrons affect the radio waves by disturbing the dynamic balance in the ionosphere. Then, these electrons combine with positive ions to gain a new form. When the ionization level increases, the bending of the radio waves of the ionosphere is further gone up.

The amount of ionization depends on a number of parameters such as time of day, season and sunspot cycle. The amount of radiation emitted from the sun to the atmosphere is directly proportional to the number of sunspot cycles. This radiation reaches its peak at the top of the sunspot called plaga.



Figure 2.3 Solar Radiation (from URL-2 2017)

At the peak of sunspot, not only radiation increase, but also level of geomagnetic activity increases. The increase in geomagnetic activity occurs when the sun releases particles in large quantities. Normally, these particles have a steady flow, but this emission level is greatly increased when occasionally solar flares are present. This situation, which causes the earth's magnetic field to change, can also lead to the formation of magnetic storms and ionospheric storms after ruin that the ionosphere can produce.


A variety of indicators are used to determine the activities that take place on the sun, and the basic one of them is solar flux, which records data since 1945. This index is used to determine the level or amount of solar radiation. This index value determines the amount of radio noise or flux at the frequency of 2800 MHz (10.7 cm) in the solar flux unit (SFU).

2.4.3 F10.7 Flux

HOI effects depend on solar activity, geomagnetic and ionospheric conditions. Solar storms occurred on the sun are the major disturbance of Earth's magnetosphere with the efficient exchange of energy from the sun to Earth atmosphere. These disturbances are critical for atmospheric studies and recorded in a different type of indexes. Occurred energy currents in the magnetosphere follow a magnetic field and connect to dense currents in the auroral ionosphere. F10.7 flux is the most reliable solar activity indicator.

This index is managed by The Penticton Radio Observatory and the obtained data is shared daily. Since the solar flux is closely related to the amount of ionization, it is also related to the electron density in the upper layers of the ionosphere.

This data can be reached from the (URL-3 2017). When the data interval is entered and solar index F10.7 is selected and submitted, results can be obtained in the chosen format.


OMNIWeb


[About](#) [Browse](#) [FTP](#) [Input Data](#) [News](#) [Feedback](#)

Interface to produce plots, listings or output files from OMNI 2

[How to get data from command line](#)

For specification of Y scale ranges for data plots click [HERE](#)

Plot data List data Create file (file?)

***Select resolution**

Hourly averaged Daily averaged 27-day averaged

Click [HERE](#) to get time spans for individual parameters.

***Enter start and stop dates** (Use yyyyddd or yyyyymmdd)

Start: 20110001 Stop: 20110630

*** Select variables**

Batches Rotation Number # Fine Scale Points in IMF Avgs
 IMF Spacecraft ID # Fine Scale Points in Plasma Avgs
 Plasma Spacecraft ID

Magnetic field

IMF Magnitude Avg, nT By, GSM, nT
 Magnitude, Avg IMF Vr, nT Bz, GSM, nT
 Lat. of Avg. IMF, deg. Sigma in IMF Magnitude Avg.
 Long. of Avg. IMF, deg. Sigma in IMF Vector Avg
 Bx, GSE/GSM, nT Sigma Bx, nT
 By, GSE, nT Sigma By, nT
 Bz, GSE, nT Sigma Bz, nT

Plasma

Proton Temperature, K Sigma-T
 Proton Density, n/cc Sigma-Np
 Flow Speed, km/sec Sigma-V
 Flow Longitude, deg. Sigma-Flow-Longitude
 Flow Latitude, deg. Sigma-Flow-Latitude
 Alpha/Proton Density Ratio Sigma-Alpha/Proton Ratio
 Flow Pressure, nPa

Derived Parameters

Ey - Electric Field, mV/m Alfvén Mach Number
 Plasma Beta Magnetosonic Mach Number

Indices

Kp*10 Index AE Index, nT
 R Sunspot Number (new version) AL Index, nT
 Dst Index, nT AU Index, nT
 ap index, nT Polar Cap (PCN) index from Thule
 Solar index F10.7
 (sfu = 10⁻²² m⁻² Hz⁻¹) Lyman Alpha Solar Index
 (1e11 photons/cm²/sec)

Particles

Proton Flux* > 1 MeV Proton Flux* >30 MeV
 Proton Flux* > 2 MeV Proton Flux* >60 MeV
 Proton Flux* > 4 MeV Magnetospheric Flux Flag
 Proton Flux* >10 MeV * 1/(cm²-sec-ster)

***Advanced plot selections (optional)**

Y-axis Scale: Y scale range (for only one selected parameter):
 min value: max value:

Character size(0.5-2.0): Symbol Size(0.1-4.0):

Plot Symbol: Image size (pixels) X: Y:

[SPDF > OMNIWeb](#)

If you have any questions/comments about OMNIWEB system, contact:
[Dr. Nandini Papamashvili](mailto:Dr.Nandini.Papamashvili@nasa.gov), Space Physics Data Facility, Mail Code 672, NASA/Goddard Space Flight Center, Greenbelt, MD 20771

NASA Official: Dr. Robert McCombs, Head of the Space Physics Data Facility

Figure 2.4 Solar index F10.7 cm (from URL-3 2017)

CHAPTER 3

HIGH-ORDER IONOSPHERIC EFFECTS ON TROPOSPHERIC PARAMETERS

The tropospheric delay and gradient can be estimated from dual-frequency GPS observations with removing the ionospheric delay, which has been widely used for atmospheric study and weather forecasting. However, high-order ionospheric (HOI) delays are generally ignored in tropospheric estimation. In this paper, high-order ionospheric effects on GPS-estimated tropospheric delay and gradients are investigated from two weeks of GPS data in June 2011 at 8 GPS stations in Turkey. Firstly, the second and third-order effects on GPS data are corrected in RINEX using IGRF11 (International Geomagnetic Reference Field: 11th generation) model, and then tropospheric delay and gradient values are obtained from raw and corrected RINEX data using the GAMIT software. Results show that high-order ionospheric effects are up to 6 mm on zenith tropospheric delay (ZTD), 4 mm on North-South (NS) gradient and 12 mm on East-West (EW) gradient during this period, but can reach over 30 mm in slant tropospheric delay. Furthermore, the high-order effects on tropospheric delay and gradient are larger in the day time than in the night time. Also, solar activity effects on high-order ionospheric delay corrections are further investigated. The high-order ionospheric effects on GPS estimated tropospheric delay and gradient in high solar activity days are much larger than those in low solar activity days. While RMS values are 0.40 mm, 0.86 mm, 0.69 mm in low solar activity days, they can increase up to 0.81 mm, 2.74 mm, 2.20 mm on ZTD, North-South, and East-West gradients, respectively.

3.1 HOI EFFECTS ON GPS ESTIMATED ZTD

TUSAGA GPS Stations data in Turkey (ADAN, ANRK, DIYB, ERZR, ISPT, ISTN, IZMI, and SAMN) on days 152-181 2011 were processed using the RINEX-HO software and corrected observation files for high order ionospheric effects were obtained. During the process, geomagnetic field coefficients needed for HOI corrections was taken from IGRF11 model. And, another parameter total electron content in the ionosphere was used from GIM.

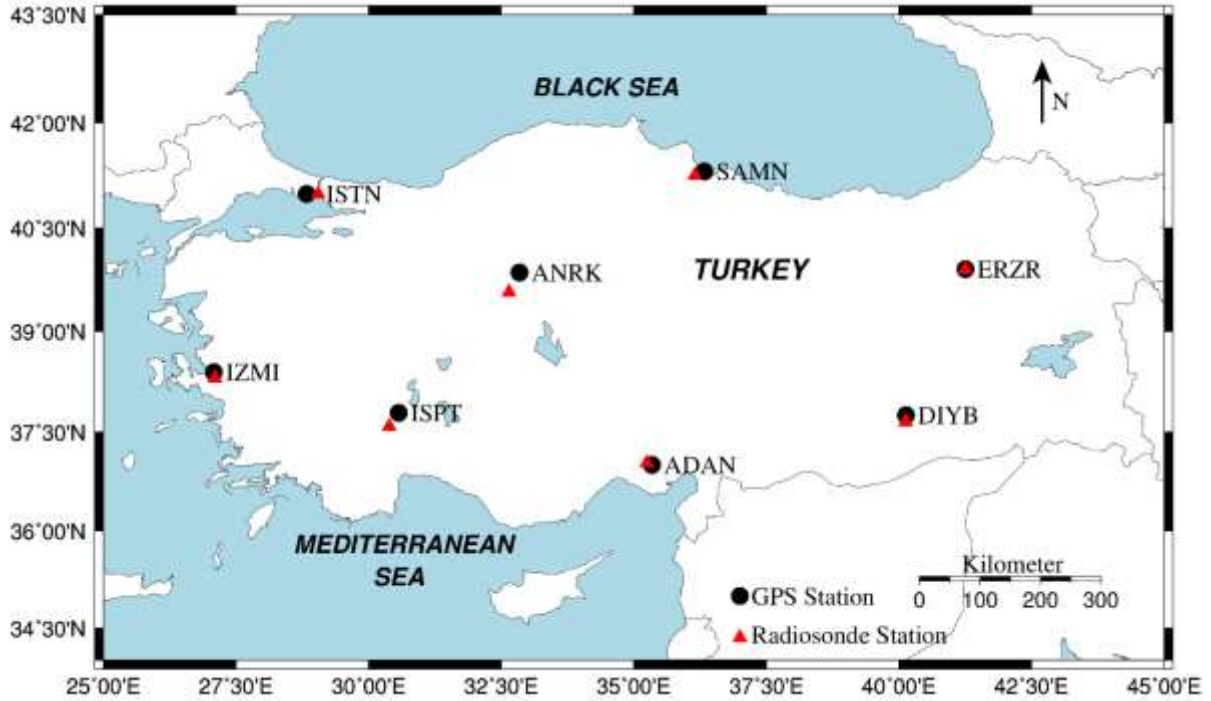


Figure 3.1 GPS and Radiosonde Stations

Then, raw and corrected observation files were processed by GAMIT software using Vienna Mapping Function, and zenith tropospheric delay (ZTD) was estimated for each station to investigate HOI effects on GPS estimated ZTD values. After the HOI effects are corrected, the residuals mean differences and RMSs of 30-minute ZTD estimations are shown in Table 3.1.

Table 3.1 Residuals mean differences and RMS on ZTD.

| Stations | Mean diff. (mm) | Residuals RMS (mm) |
|-------------|-----------------|--------------------|
| ADAN | 0.27 | 0.49 |
| ANRK | 0.25 | 0.48 |
| DIYB | 0.29 | 0.65 |
| ERZR | 0.25 | 0.53 |
| ISPT | 0.26 | 0.45 |
| ISTN | 0.23 | 0.44 |
| IZMI | 0.24 | 0.46 |
| SAMN | 0.25 | 0.45 |

The mean difference and mean RMS are about 0.25 mm and 0.50 mm, respectively, while the large one is found with RMS of 0.65 mm at DIYB station with the mean HOI effects on ZTD are not big. However, the HOI effects on ZTD time series can reach up to 6 mm, which should

be corrected for precise ZTD applications. ZTD time series and residuals for all stations are shown in Fig. 3.2 to Fig. 3.9. And, residuals of ZTD time series by RMS is shown in Fig. 3.10.

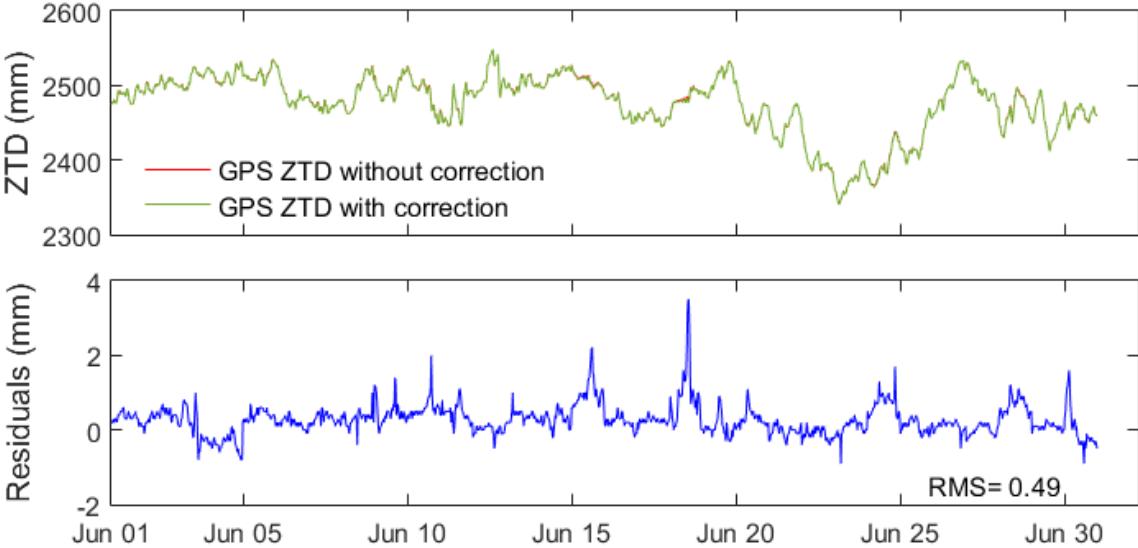


Figure 3.2 ADAN Station GPS ZTD Time Series and Residuals

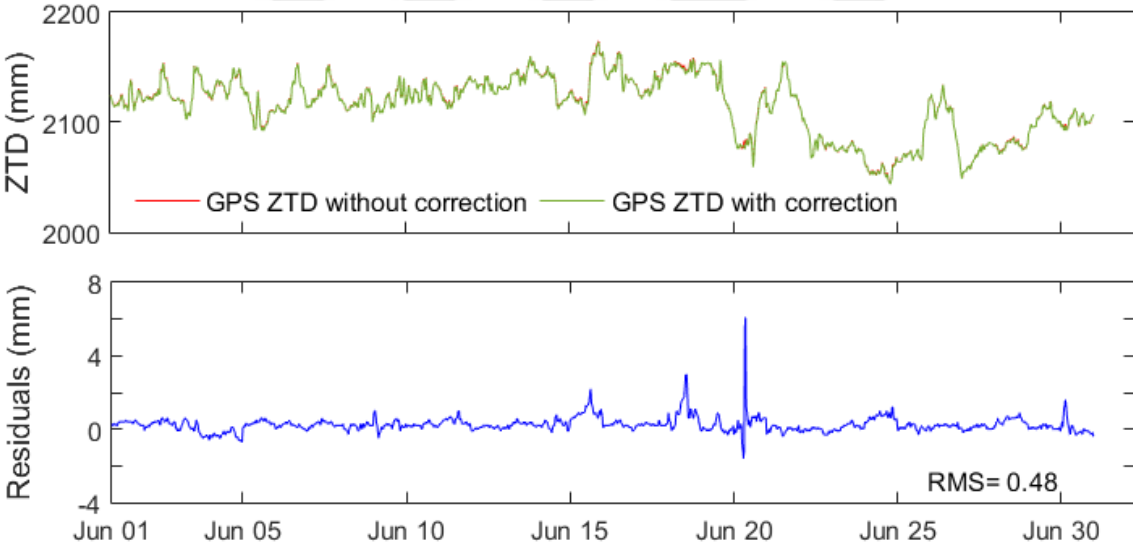


Figure 3.3 ANRK Station GPS ZTD Time Series and Residuals

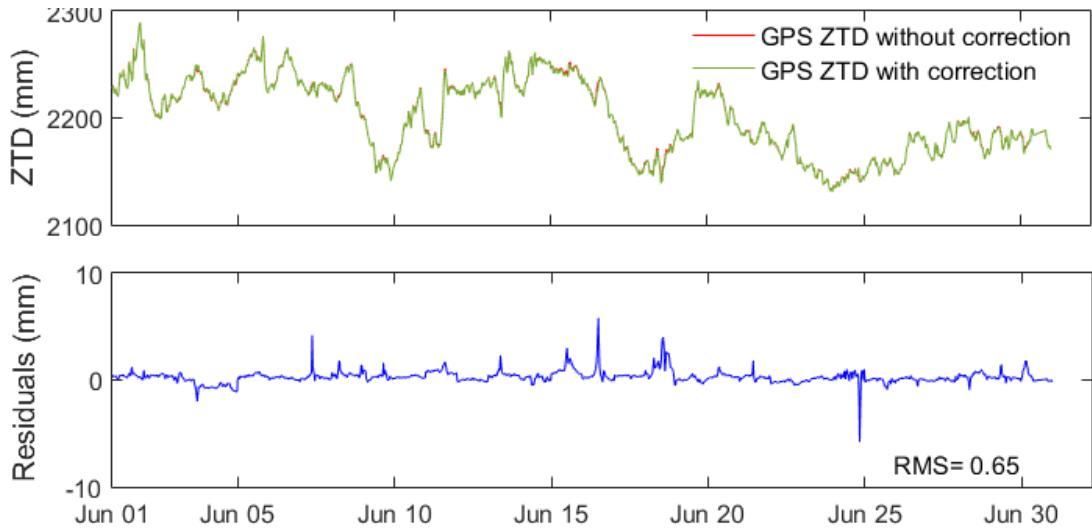


Figure 3.4 DIYB Station GPS ZTD Time Series and Residuals

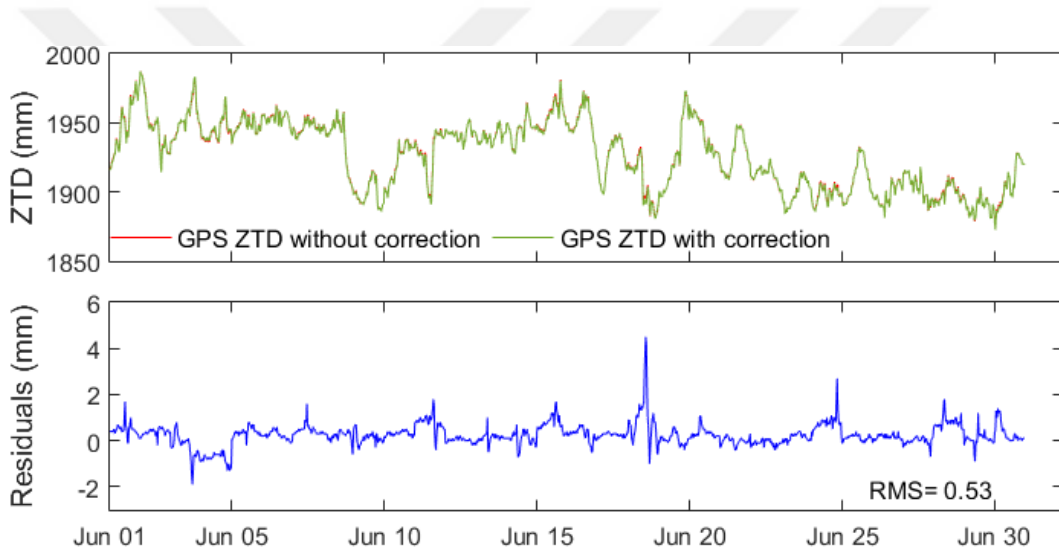


Figure 3.5 ERZR Station GPS ZTD Time Series and Residuals

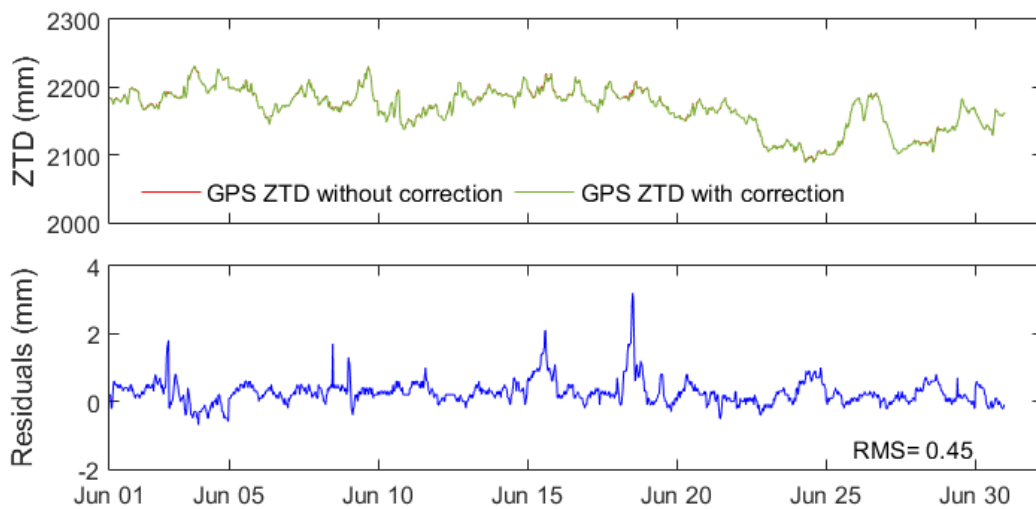


Figure 3.6 ISPT Station GPS ZTD Time Series and Residuals

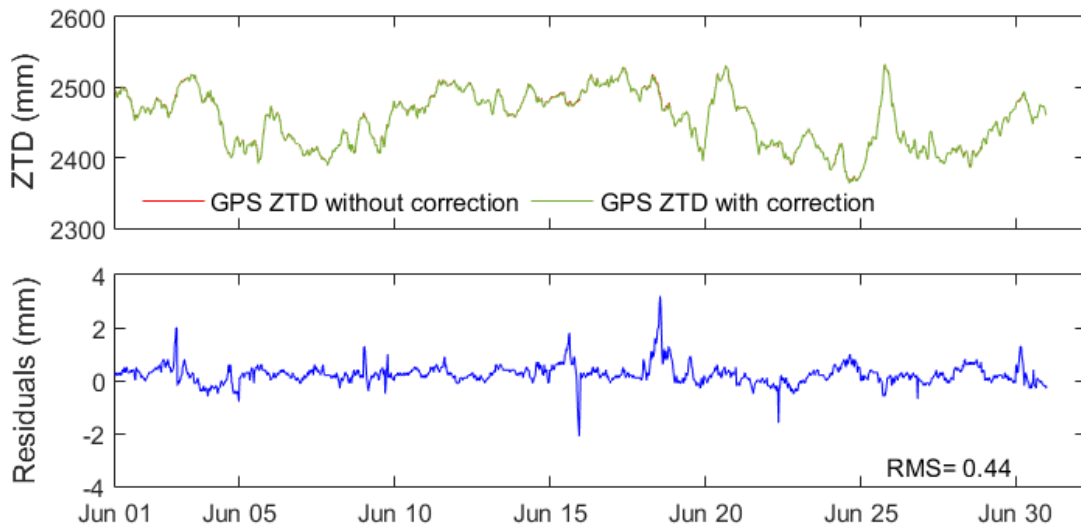


Figure 3.7 ISTN Station GPS ZTD Time Series and Residuals

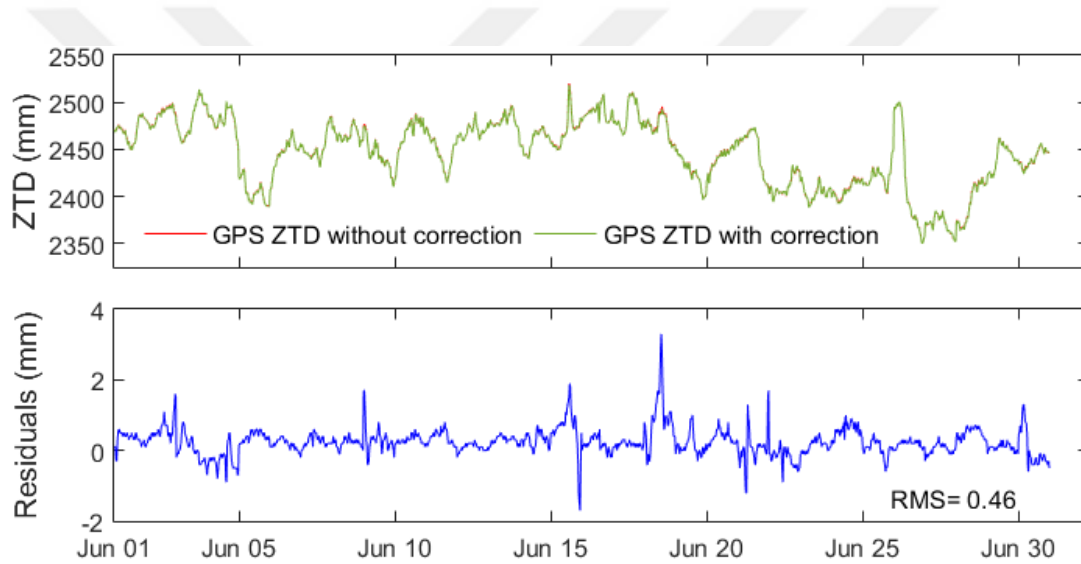


Figure 3.8 IZMI Station GPS ZTD Time Series and Residuals

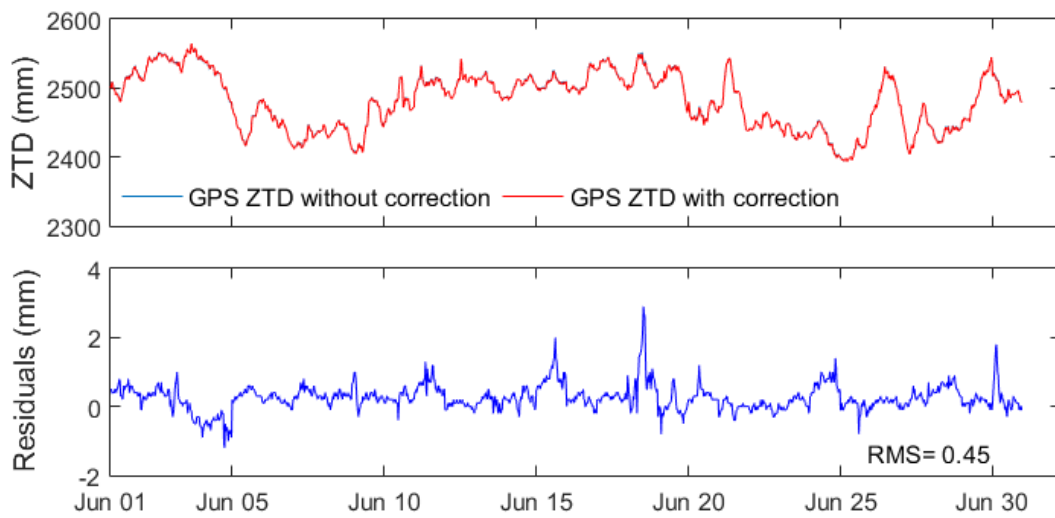


Figure 3.9 SAMN Station GPS ZTD Time Series and Residuals

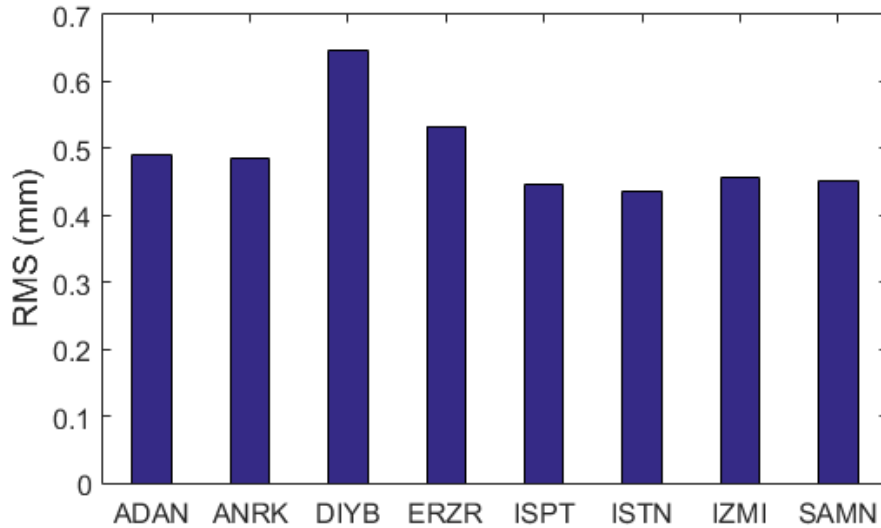


Figure 3.10 GPS Stations ZTD RMS

3.1.1 HOI effects on GPS estimated ZTD during the day and night time

HOI effects are related to the solar activity and ionospheric conditions. Total electron content is the main parameter of ionospheric delay. When the TEC values are increased from night time to daytime, HOI effects on GPS estimated ZTD also increases, e.g., Ankara station (Fig. 3.11).

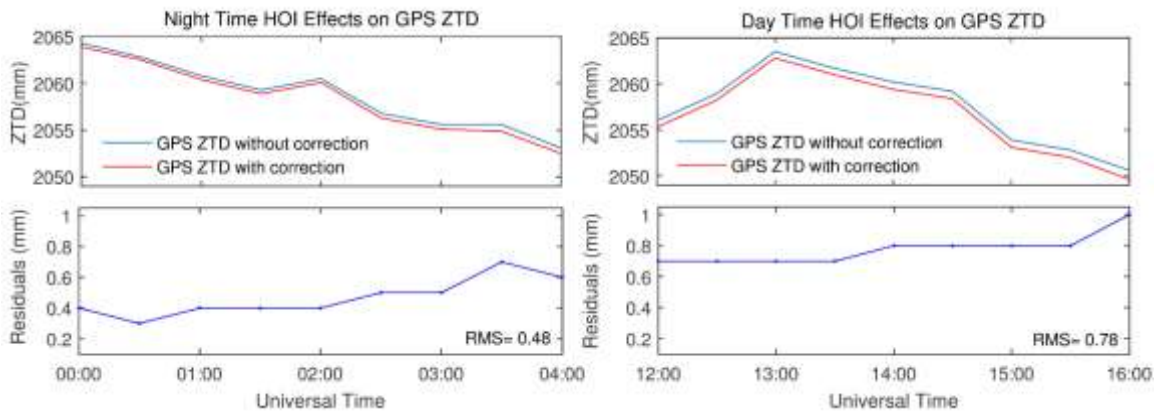


Figure 3.11 ZTD differences with HOI effects at ANRK Station during the night and the day time

The high-order effects on ZTD estimation are higher at daytime (12:00-16:00 UT) than night time (00:00-04:00 UT) at ANRK GPS station. The RMS increases from 0.48 mm at night to 0.78 mm at day time. This effect is significant for not only ANRK station but also other seven stations.

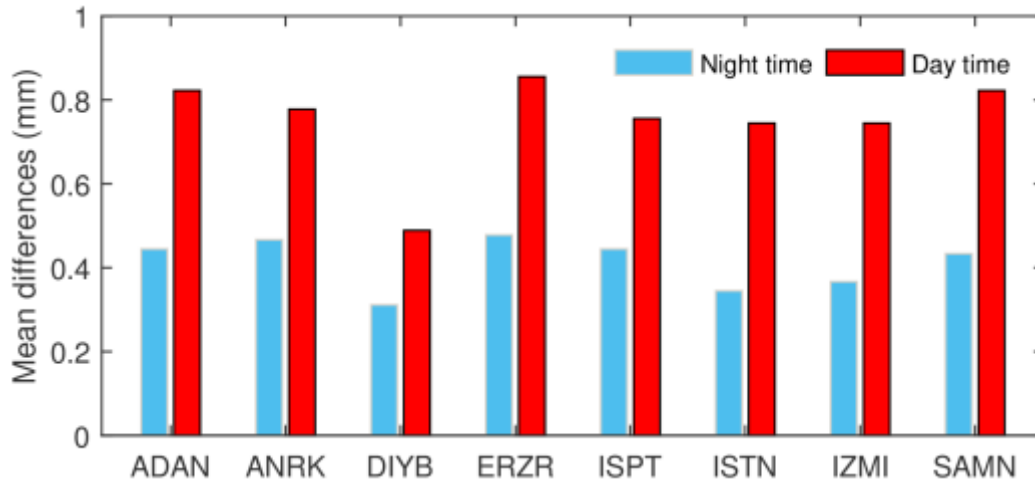


Figure 3.12 Daytime and night time HOI effects on GPS ZTD On day 167, 2011

The high-order ionospheric effect is related to the total electron content, while TEC in the ionosphere increases from night time to daytime. Therefore, HOI effects on GPS estimated ZTD is increasing from night time to daytime. Mean differences between two data sets with and without HOI correction are also plotted in a bar diagram to show change from night time to daytime (Fig. 3.12), and conclusions are the same. Mean differences are nearly 0.4 mm in the night time and 0.8 mm in the day time for each station.

3.1.2 HOI effects on GPS estimated ZTD during the high and low solar activities

HOI effects depend on solar activity, geomagnetic and ionospheric conditions. Solar storms occurred on the sun are the major disturbance of Earth's magnetosphere with the efficient exchange of energy from the sun to Earth atmosphere. These disturbances are critical for atmospheric studies and recorded in a different type of indexes. Occurred energy currents in the magnetosphere follow a magnetic field and connect to dense currents in the auroral ionosphere. F10.7 flux is the most reliable solar activity indicator. Daily averages of solar activity for 2011 are plotted (Fig. 3.13).

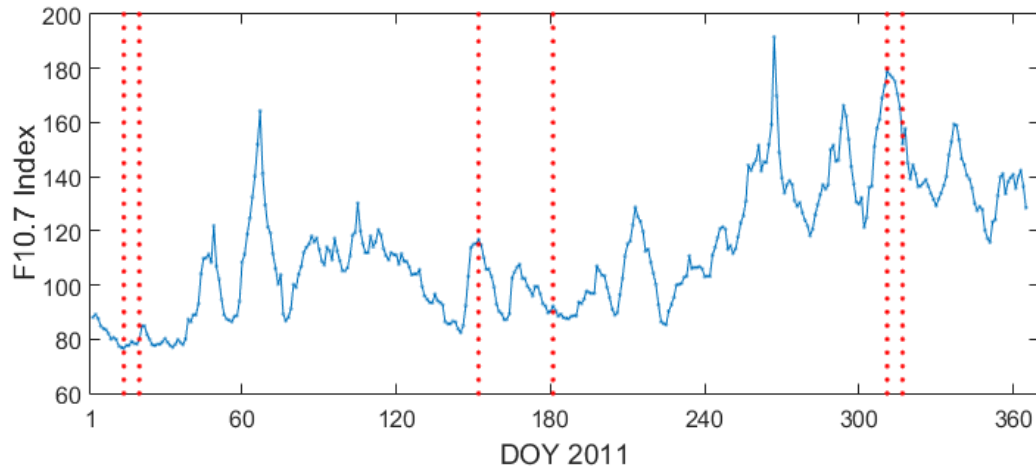


Figure 3.13 Daily averages of Solar 10.7 cm flux

The high-order ionospheric effects on ZTD estimations are investigated during high and low solar activities. Here one week GPS data on days 18-24 2011 with low solar activity and 317-323 2011 with high solar activity are processed, respectively. Results show that large HOI effects during high solar activity (Fig. 3.14), while HOI effects are much smaller on low solar activity days.

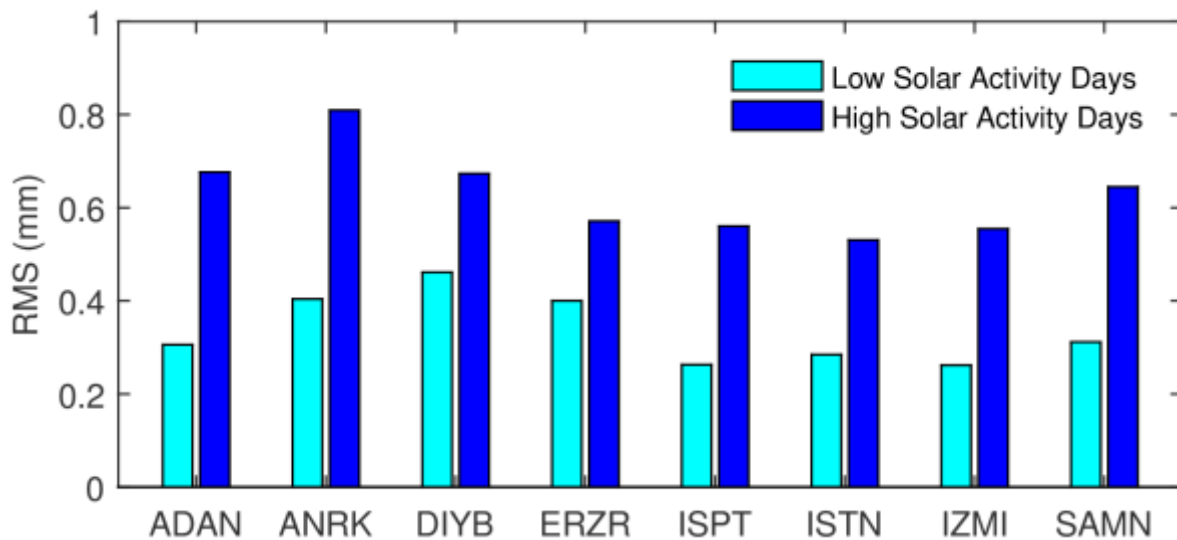


Figure 3.14 RMS of Low and High Solar Activity Days ZTD Residuals

As it mentioned in early paragraphs, HOI effects depend on solar activity and ionospheric conditions. The averaged TEC interpolation map from day 152 to 181 in 2011 was created to show regionally ionospheric conditions and interpret associated HOI effects over Turkey. The interpolation map prepared by taking the TEC values from GIM is as shown in Fig 3.15.

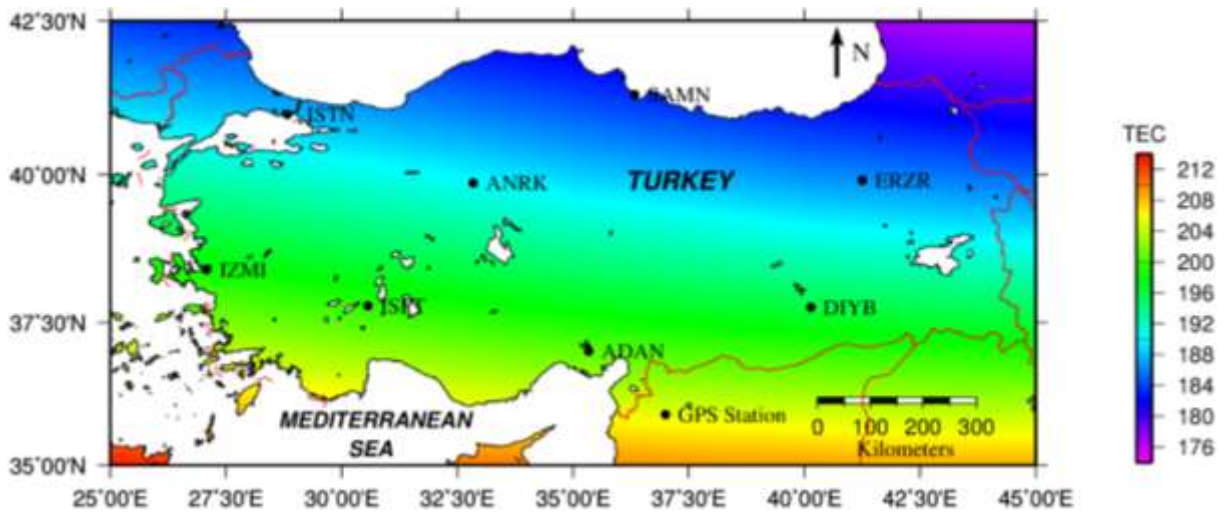


Figure 3.15 TEC distribution in Turkey during the days 152-181 2011

Here, TEC values increased from the north to the south, while there were not relative big changes of HOI effects on ZTD estimations.

3.1.3 HOI effects on slant tropospheric delay

When the GPS satellite angle is low, the more tropospheric delay will be induced. Here the HOI effects on slant tropospheric delay are further investigated. In this case, slant tropospheric delay (STD) is also estimated with and without HOI effects correction. For example, during the four hours, satellite PRN 7 on ANRK station starts to be seen with 293.13 azimuths and 71.79 elevation angles at 8:00 UT, then arrives at the 104.80 azimuths and 11.03 elevation angle at 12:00 UT (Fig. 3.16).

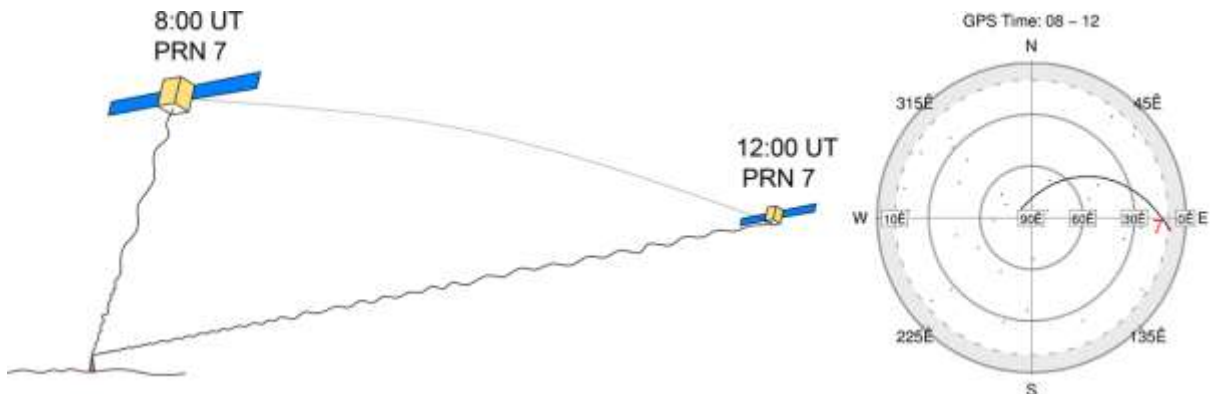


Figure 3.16 GPS PRN 7 visibility on DOY 167, 2011 at ANRK station

As it is seen in Figure 11, the satellite elevation has been increasing for the satellite PRN 7 from 8:00 UT to 12:00 UT. When the satellite position becomes closer to the zenith direction of that station, the tropospheric delay will be lowest with the minimum effect. If GPS signals come with lower elevation angle, the HOI effects are bigger. For example, Figure 12 shows HOI effects on GPS STD for PRN7 on Day 167 2011 at ANRK station. The HOI effects on the STD were reaching about 33 mm including some uncertainties when the GPS satellite elevation angle decrease to 11.03 degrees. Other stations have similar effects. Therefore, the high-order ionospheric delay has a large effect on slant tropospheric delay estimation with about a few centimeters.

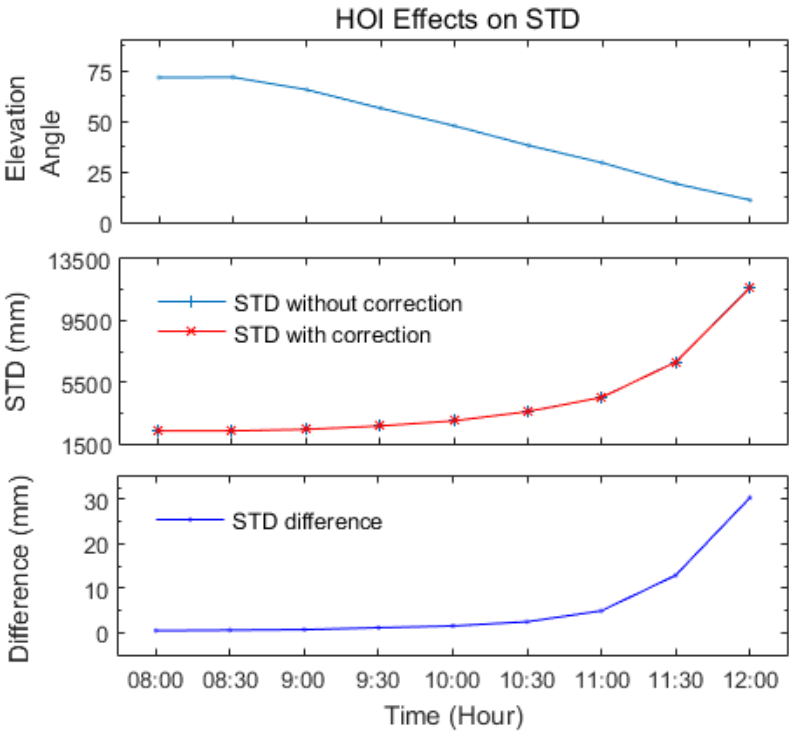


Figure 3.17 HOI effects on GPS STD for PRN7 on Day 167 2011 at ANRK station

3.2 HOI EFFECTS ON GPS GRADIENTS

Azimuthally asymmetric delays are described as troposphere gradients. Tropospheric delay gradients are continuously variable and affecting the baseline lengths and positioning (Davis et. al. 1993, Teke et. al. 2011). Here we further investigate HOI effect on tropospheric gradients. Residuals mean difference and RMS values with HOI effects on gradients are shown in Table 3.2.

Table 3.2 Residuals mean differences and RMS on Gradients.

| Stations | NS Gradient (mm) | | EW Gradient (mm) | |
|-------------|------------------|-------------|------------------|-------------|
| | Mean Diff. | RMS | Mean Diff. | RMS |
| ADAN | 1.00 | 1.09 | 0.43 | 1.39 |
| ANRK | 0.78 | 1.17 | 0.02 | 1.58 |
| DIYB | 1.02 | 1.29 | -0.03 | 2.12 |
| ERZR | 0.82 | 1.01 | 0.86 | 1.83 |
| ISPT | 0.99 | 1.11 | 0.14 | 0.70 |
| ISTN | 0.92 | 1.06 | -0.02 | 0.52 |
| IZMI | 0.83 | 1.09 | 0.13 | 0.77 |
| SAMN | 0.99 | 1.04 | 0.55 | 1.41 |

When the station has the highest RMS, NS and EW gradients are variable between -30 to 30 mm. Figure 3.20 shows tropospheric gradients on the NS and EW directions at DIYB GPS station. Residuals RMS with north-south and south-west gradients are 1.29 and 2.12 mm, respectively. Therefore, HOI effects can result in up to 4 and 12 mm change in north-south (NS) and east-west (EW) gradients respectively. These effects cannot be modeled in traditional estimation, which should be eliminated in precise GNSS applications.

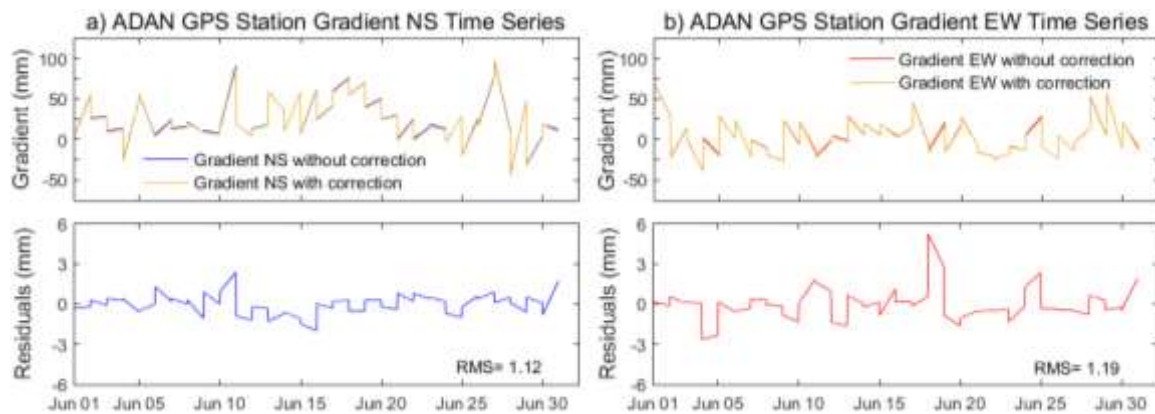


Figure 3.18 ADAN Station Gradient Time Series and Residuals

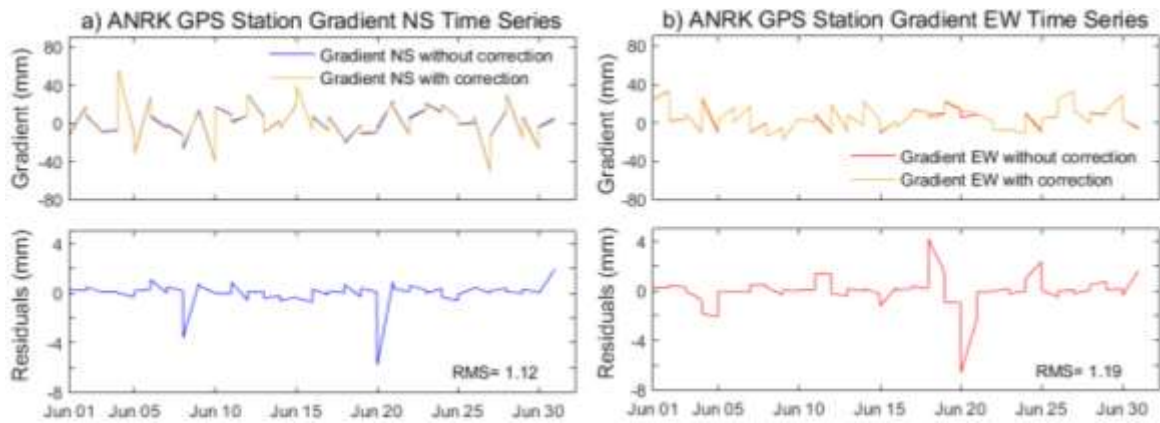


Figure 3.19 ANRK Station Gradient Time Series and Residuals

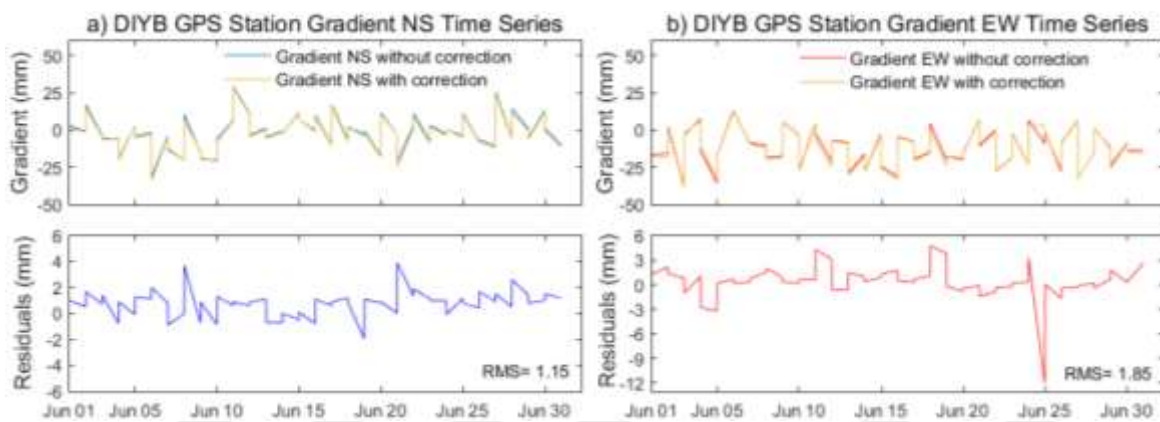


Figure 3.20 DIYB Station Gradient Time Series and Residuals

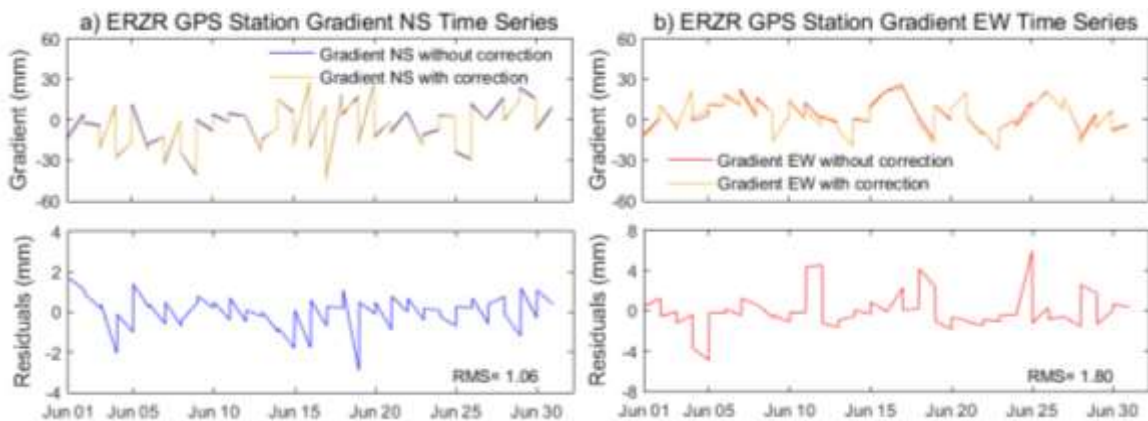


Figure 3.21 ERZR Station Gradient Time Series and Residuals

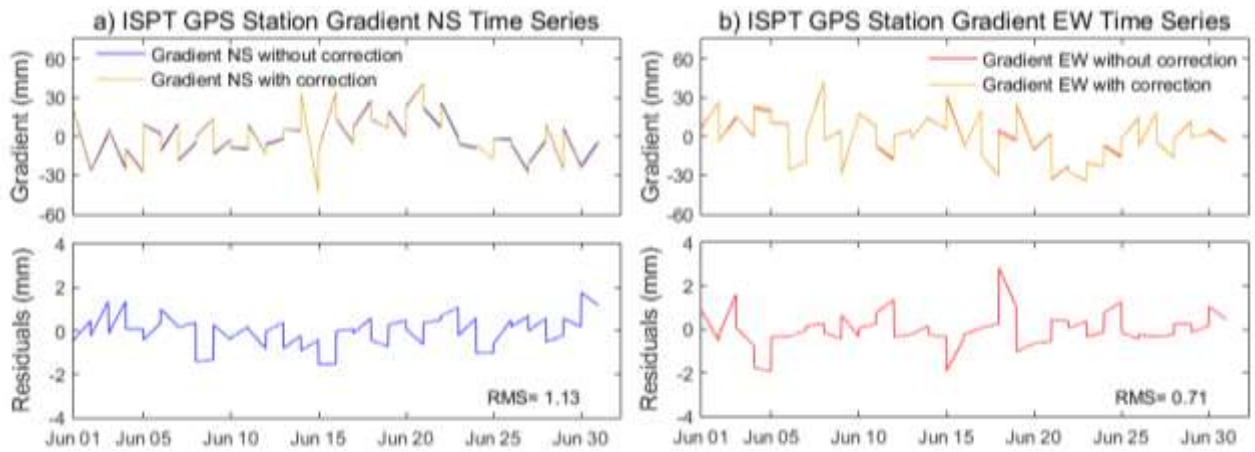


Figure 3.22 ISPT Station Gradient Time Series and Residuals

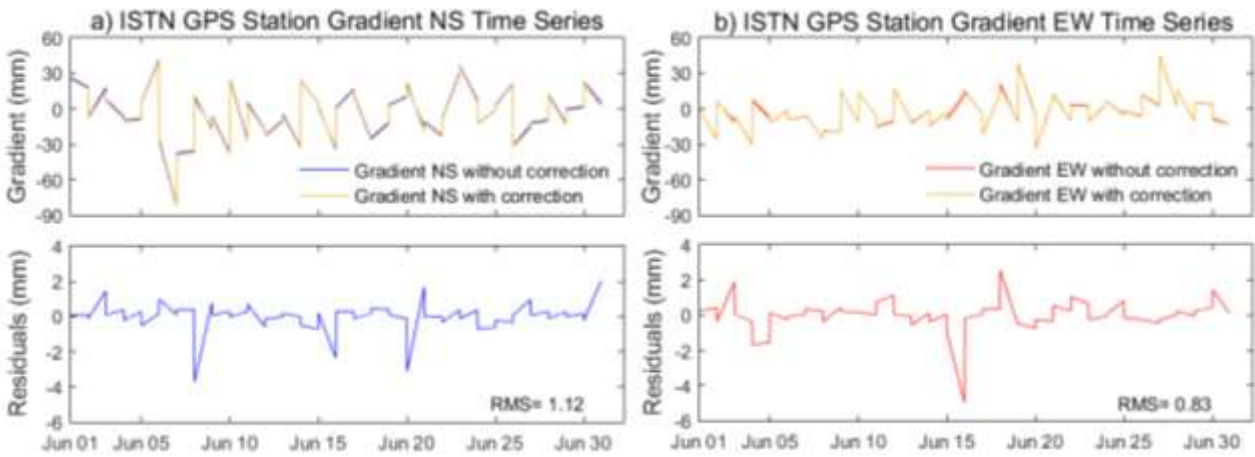


Figure 3.23 ISTN Station Gradient Time Series and Residuals

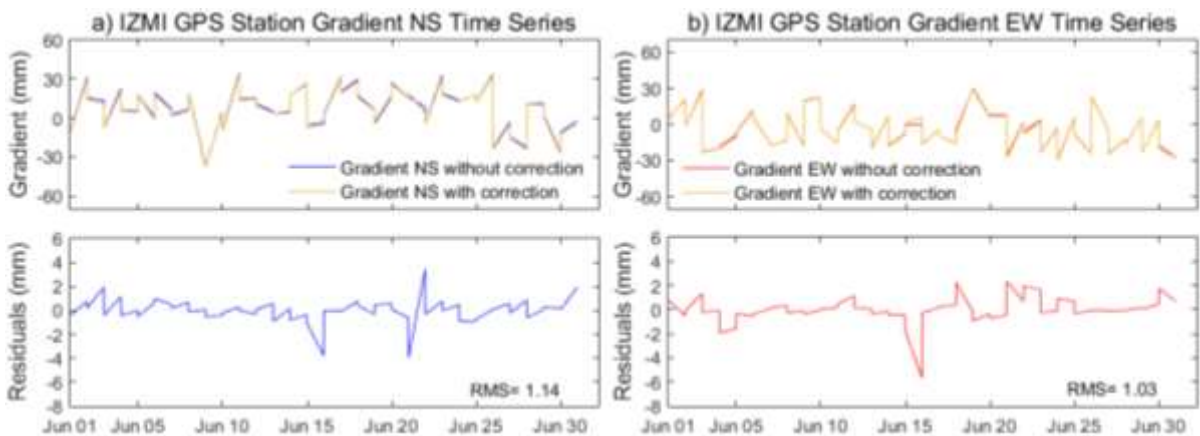


Figure 3.24 IZMI Station Gradient Time Series and Residuals

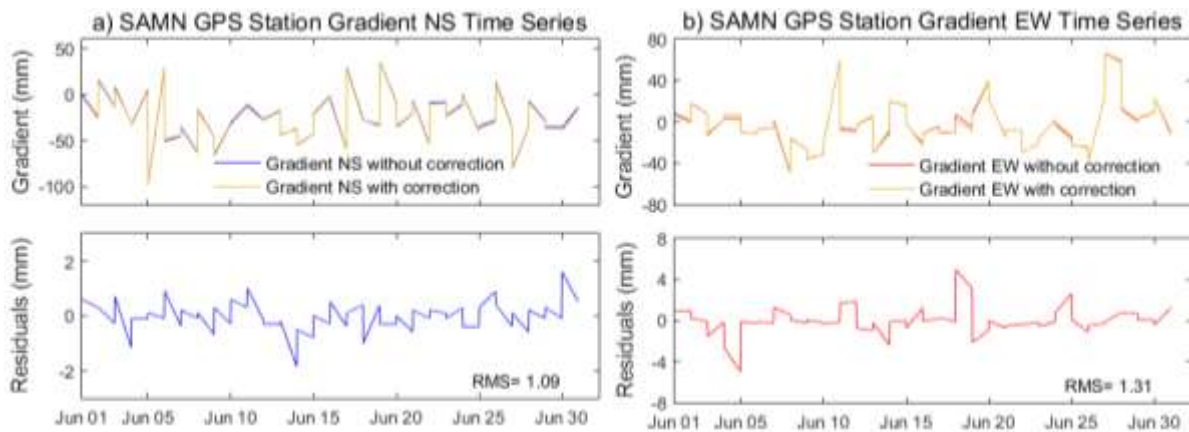


Figure 3.25 SAMN Station Gradient Time Series and Residuals

3.2.1 HOI effects on North-South Gradients With Solar Activities

High-order ionospheric effects on tropospheric gradients are further investigated during low and high solar activity days.

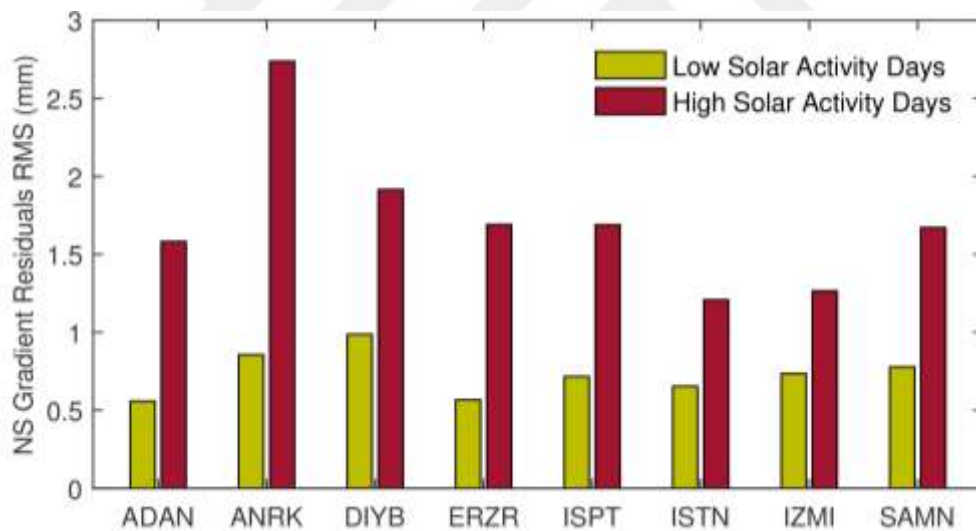


Figure 3.26 Low and High Solar Activity Days RMS of NS Gradient Residuals

The NS gradient residuals RMSs are bigger on high solar activity days than ones on low solar activity days (Figures 3.26). For example, North-South gradient residuals RMS at ANRK station is 0.86 mm on low solar activity days and reaches up to 2.74 mm on high solar activity days in 2011.

3.2.2 HOI effects on East-West Gradients With Solar Activities

When the HOI effects are investigated for East-West gradients with RMSs, the increase of RMSs are clearly seen from low solar activity days to high solar activity days (Figure 3.27).

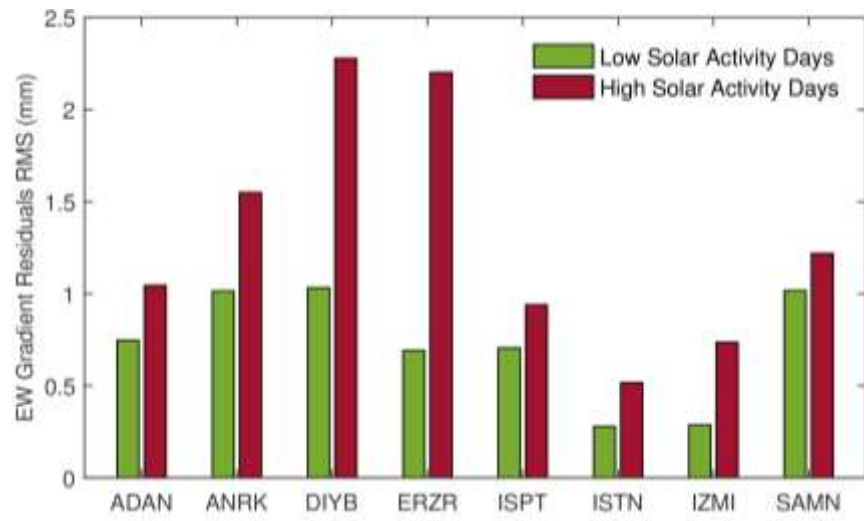


Figure 3.27 Low and High Solar Activity Days RMS of EW Gradient Residuals

ERZR station has maximum effect in east-west gradient residuals RMS. While it is 0.69 mm on low solar activity days, it reaches up to 2.20 mm on high solar activity days in 2011. When the solar activity increased, effects on ZTD and gradients are also increasing relatively. Therefore, HOI effects on ZTD and tropospheric gradients should be corrected to improve the precision of GPS tropospheric parameters estimations.

3.3 HOI EFFECTS ON GPS ESTIMATED PWV

The high-order ionospheric effects on GPS estimated tropospheric delay and gradient are investigated using with IGRF11 model, and results show that high-order effects can reach 6 mm on ZTD, 12 mm on gradient estimations change. HOI effects depend on solar activity, geomagnetic and ionospheric conditions. These effects are much smaller when compared to the first order ionospheric effects, so HOI effects are generally ignored in GPS applications. However, in high precision GPS applications, HOI effects should be corrected from GPS observations. Furthermore, the GPS estimated PWV with and without HOI corrections were compared with radiosonde observations and the HOI corrected results are closer to radiosonde observations.

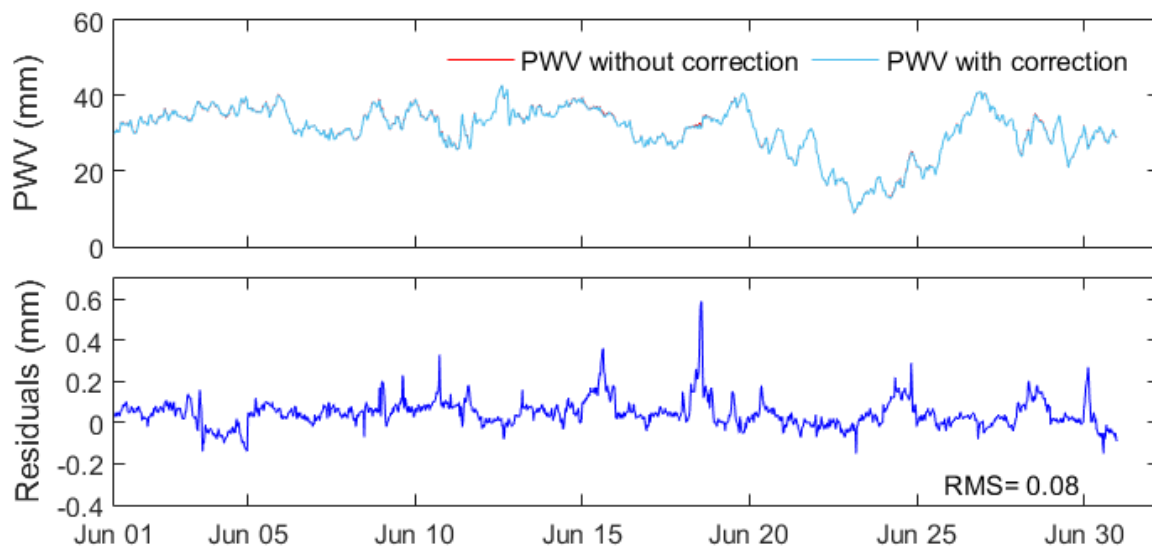


Figure 3.28 ADAN Station GPS PWV Time Series and Residuals

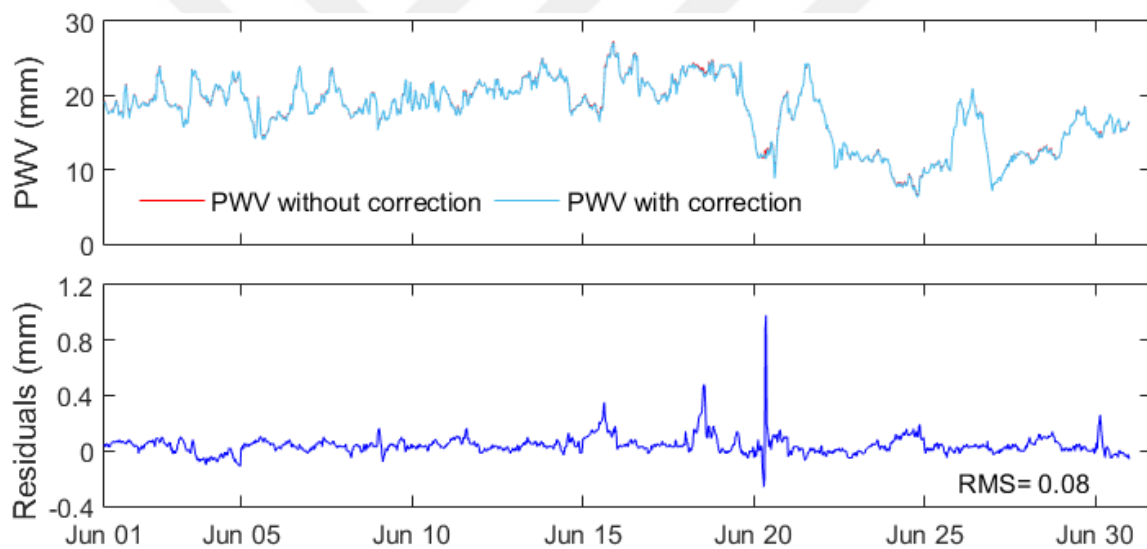


Figure 3.29 ANRK Station GPS PWV Time Series and Residuals

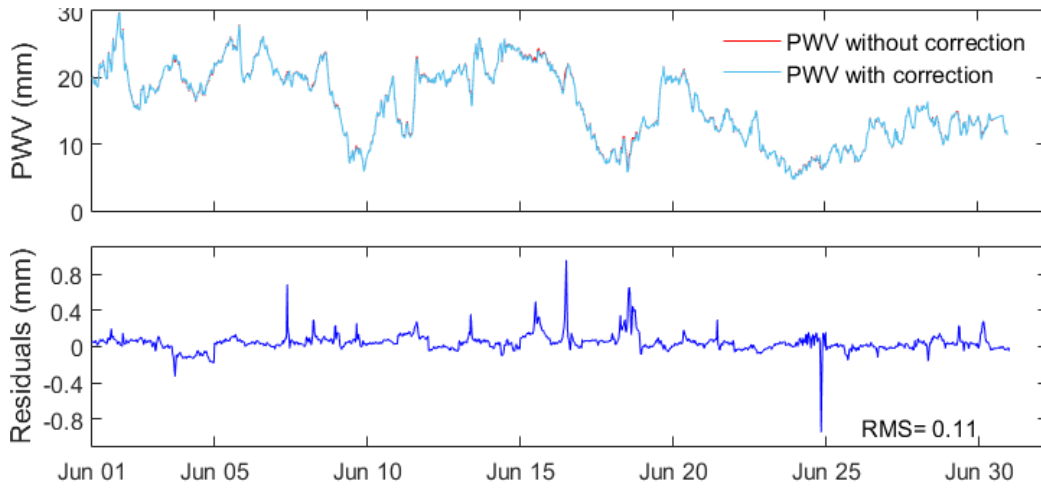


Figure 3.30 DIYB Station GPS PWV Time Series and Residuals

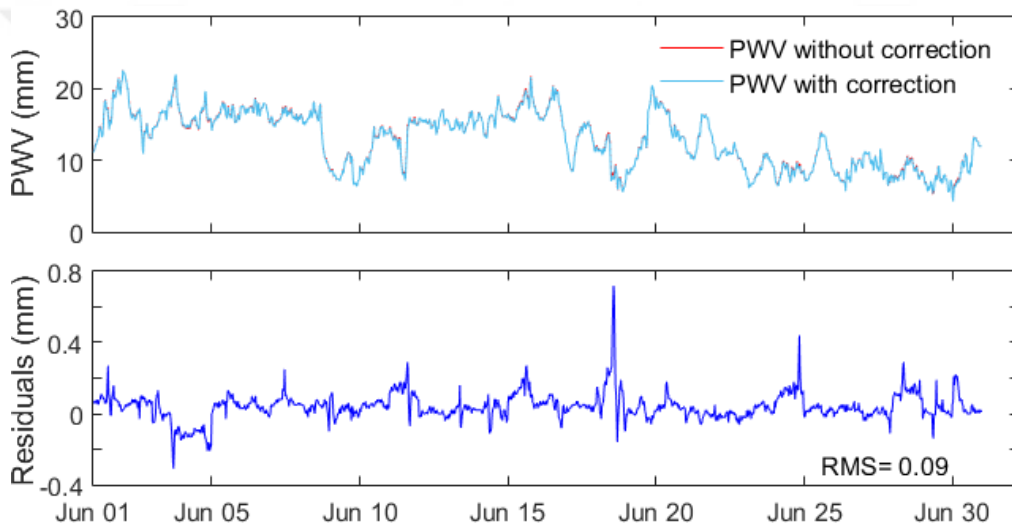


Figure 3.31 ERZR Station GPS PWV Time Series and Residuals

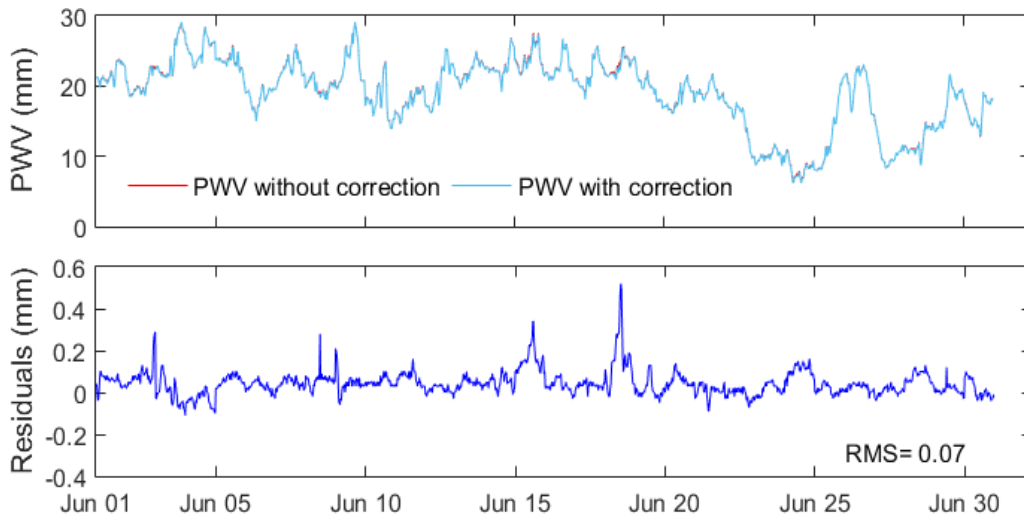


Figure 3.32 ISPT Station GPS PWV Time Series and Residuals

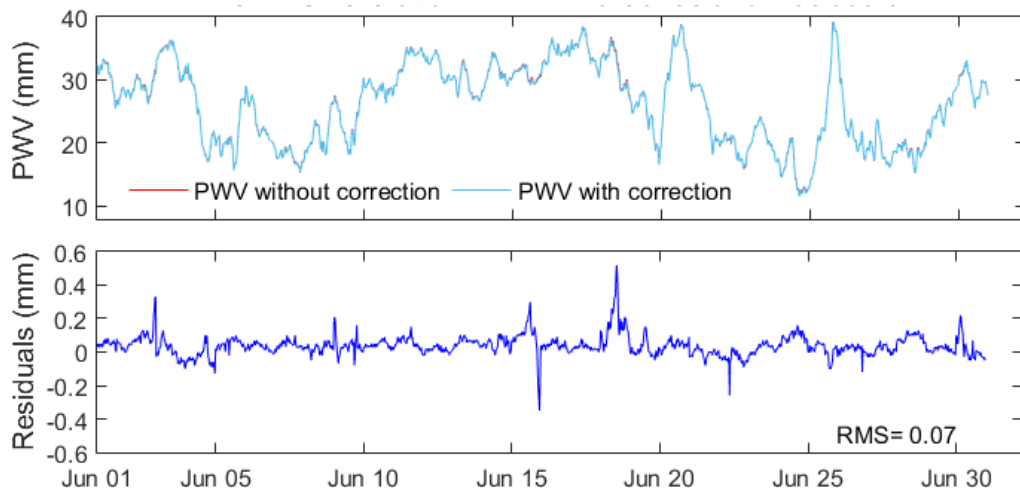


Figure 3.33 ISTN Station GPS PWV Time Series and Residuals

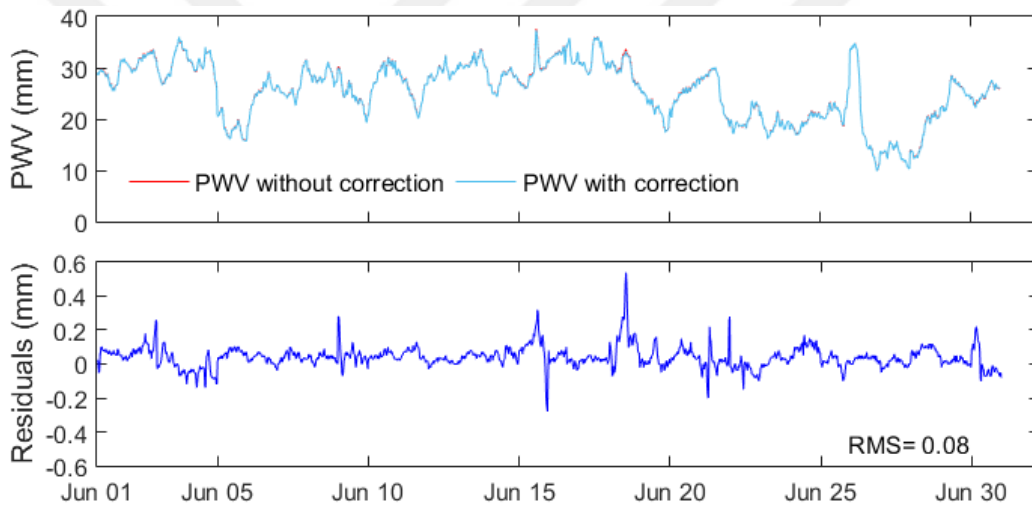


Figure 3.34 IZMI Station GPS PWV Time Series and Residuals

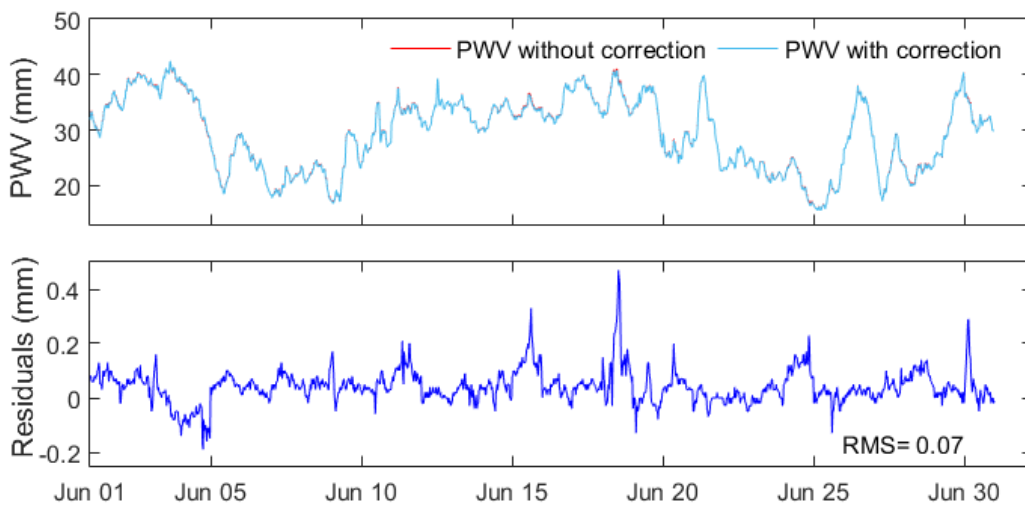


Figure 3.35 SAMN Station GPS PWV Time Series and Residuals

3.3.1 HOI Effects on GPS PWV During the High and Low Solar Activities

Furthermore, high-order ionospheric effects on GPS estimated PWV are further investigated during low and high solar activity days (Fig. 3.36). The PWV residuals RMSs are bigger on high solar activity days than ones on low solar activity days (Fig. 3.37).

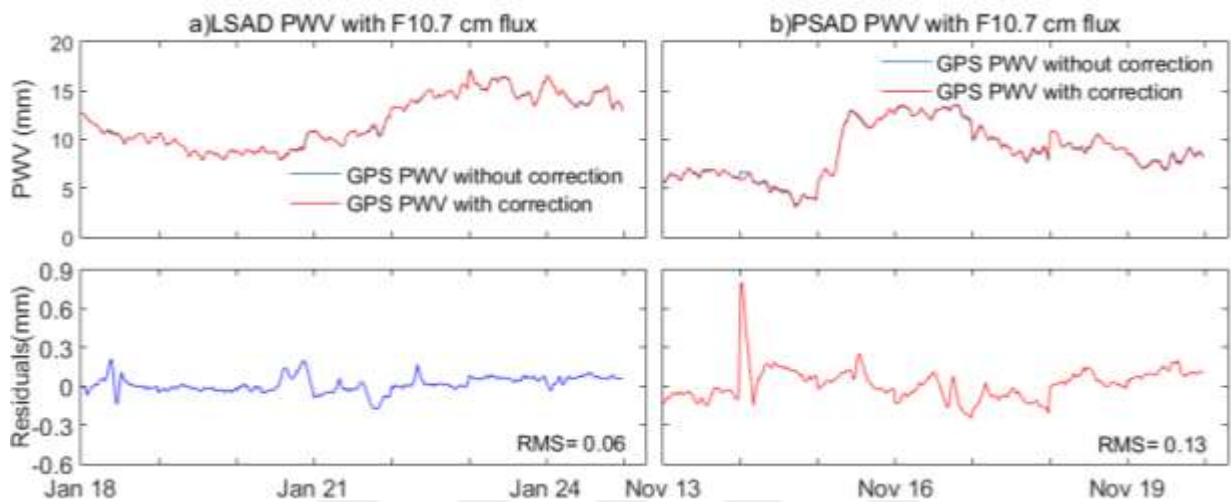


Figure 3.36 ANRK Station GPS PWV Time Series and Residuals on Solar Activity Days

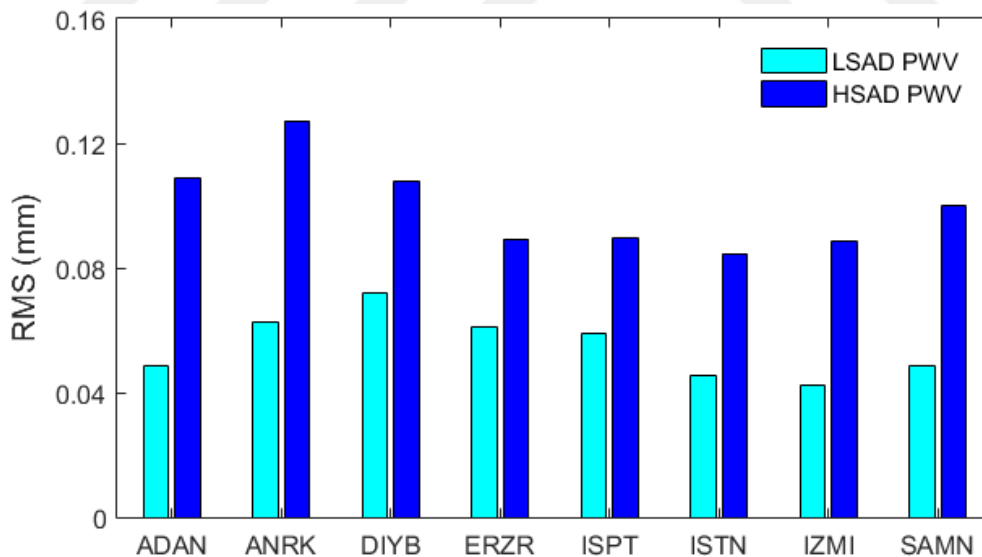


Figure 3.37 RMS of PWV during low and high solar activity days

ANKR station has maximum effect in PWV residuals RMS. While it is 0.06 mm on low solar activity days, it reaches up to 0.13 mm on high solar activity days in 2011. When the solar activity increased, effects on PWV are also increasing relatively. Therefore, HOI effects on PWV should be corrected to improve the precision of GPS tropospheric parameters estimations.

In the past time, the second- and third-order ionospheric effects are ignored in PWV estimation. In this study, the high-order ionospheric effects on PWV are investigated at 8 continuous GPS stations. Results show that high-order ionospheric effects are up to 1 millimeter on PWV during this period. Furthermore, the high-order ionospheric effects on PWV are bigger during the peak solar activity days, while, much smaller during low solar activity days.

3.3.2 Radiosonde and GPS PWV Comparison

The high-order ionospheric effects on GPS estimated tropospheric delay and gradient are investigated using with IGRF11 model, and results show that high-order effects can reach 6 mm on ZTD, 12 mm on gradient estimations change. HOI effects depend on solar activity, geomagnetic and ionospheric conditions. These effects are much smaller when compared to the first order ionospheric effects, so HOI effects are generally ignored in GPS applications. However, in high precision GPS applications, HOI effects should be corrected from GPS observations. Furthermore, the GPS estimated PWV with and without HOI corrections were compared with radiosonde observations and the HOI corrected results are closer to radiosonde observations.

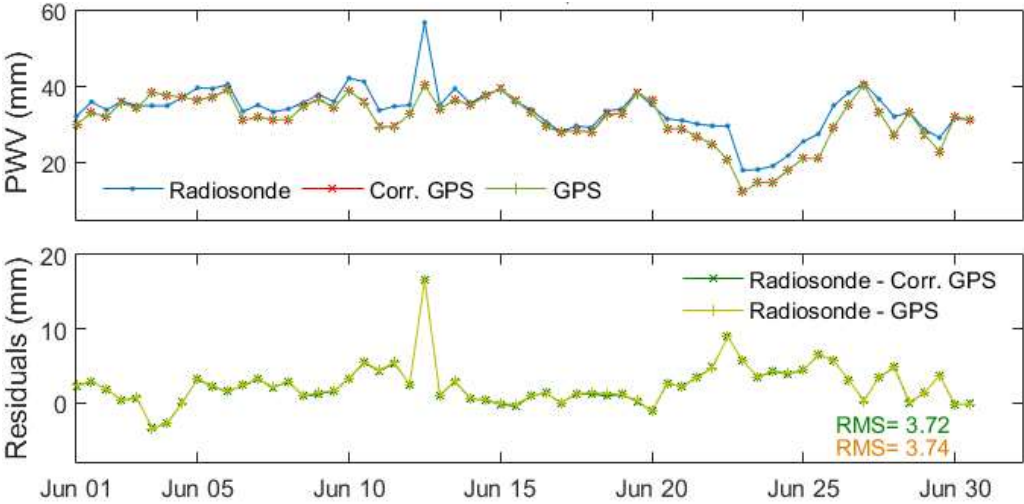


Figure 3.38 ADAN Station PWV Time Series Comparison and Residuals

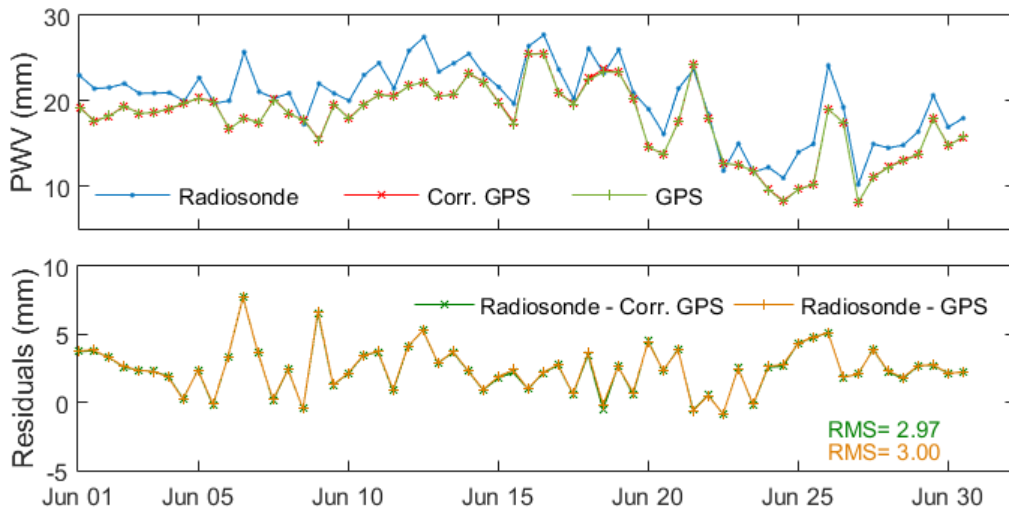


Figure 3.39 ANRK Station PWV Time Series Comparison and Residuals

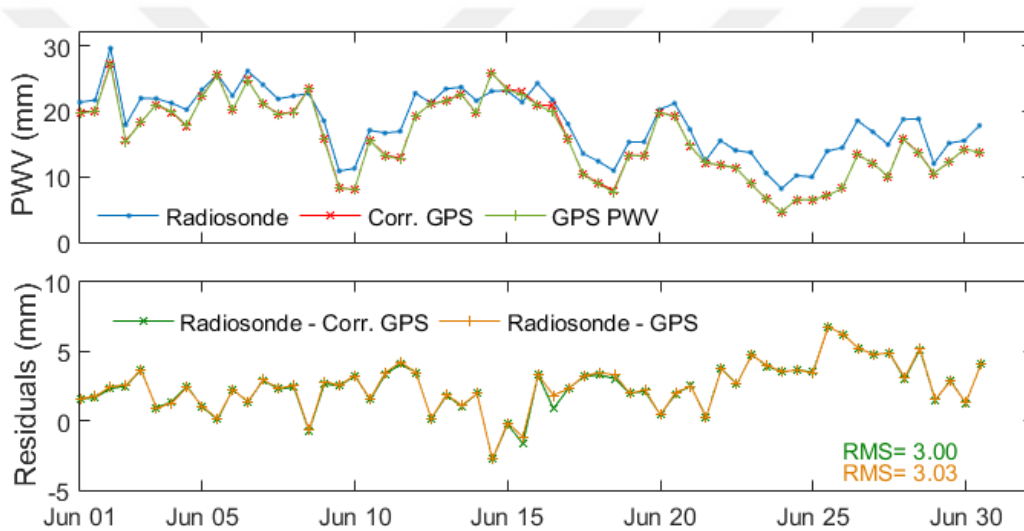


Figure 3.40 DIYB Station PWV Time Series Comparison and Residuals

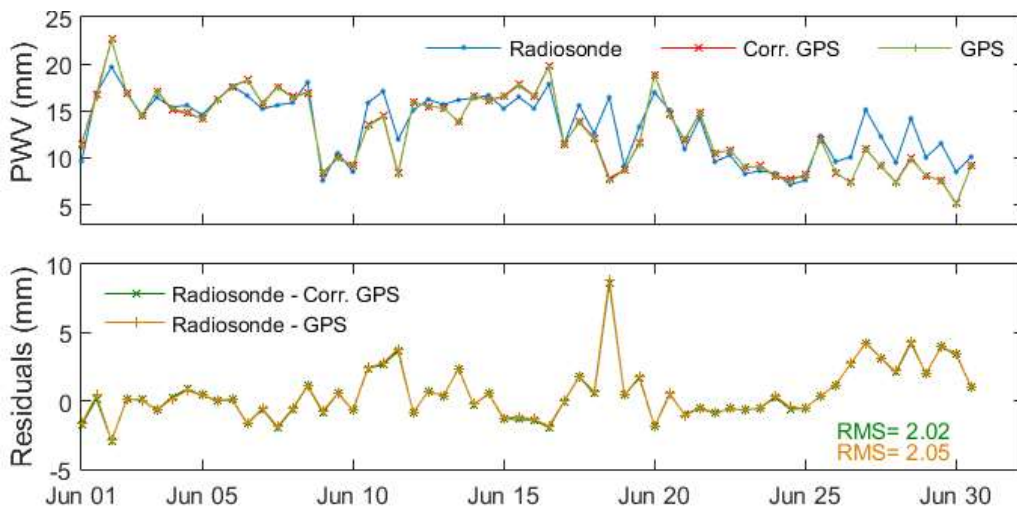


Figure 3.41 ERZR Station PWV Time Series Comparison and Residuals

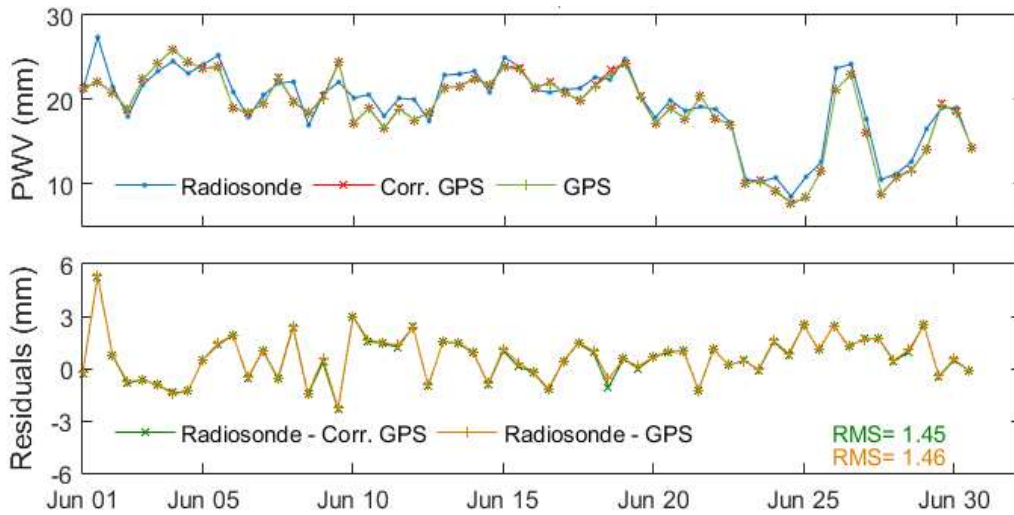


Figure 3.42 ISPT Station PWV Time Series Comparison and Residuals

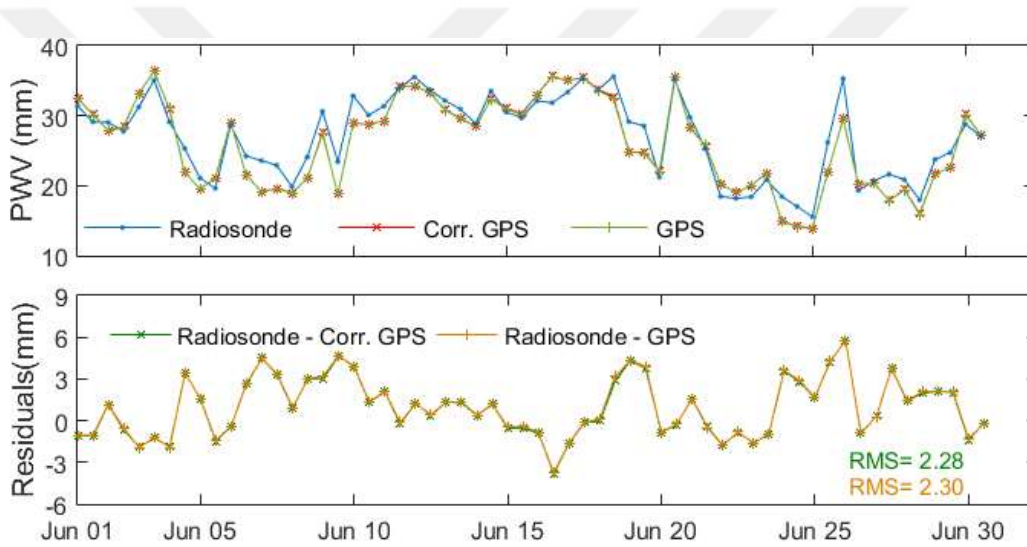


Figure 3.43 ISTN Station PWV Time Series Comparison and Residuals

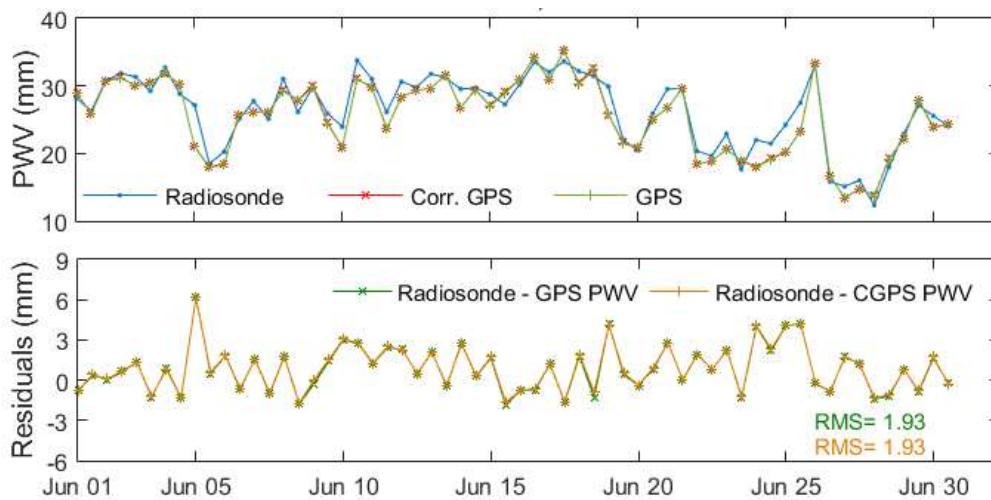


Figure 3.44 IZMI Station PWV Time Series Comparison and Residuals

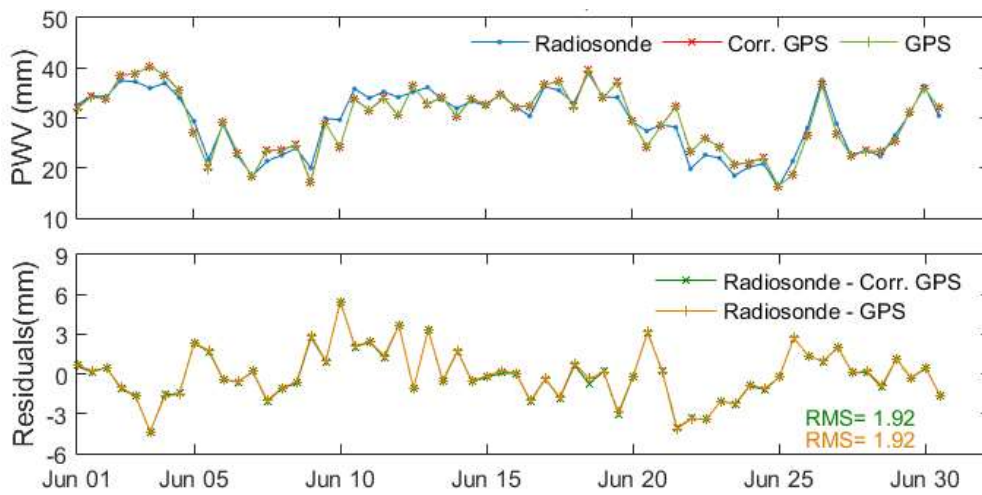


Figure 3.45 SAMN Station PWV Time Series Comparison and Residuals





CHAPTER 4

HIGH-ORDER IONOSPHERIC EFFECTS ON COORDINATES

Global Positioning System (GPS) gives a chance for users to obtain high precision positioning information with the real time applications. GPS signals are effected in the ionosphere and have a delay. First order ionospheric effects are eliminated using with the double frequency receivers. High-order ionospheric effects are very smaller than first order effects, therefore generally ignored in studies. Its effect can be low but, high order ionospheric effects should be eliminated in precise GPS applications also. Precise positioning components can be obtained using observation files evaluated on GAMIT software with post processing applications. In this case, high-order ionospheric effects on coordinates are investigated from GPS data in June 2011 at 8 TUSAGA-Active GPS stations in Turkey. High order ionospheric effects on coordinate components are observed for same stations with peak solar activity days data also. Firstly, the second and third-order effects on GPS data are corrected in RINEX observation files using IGRF11 (International Geomagnetic Reference Field) model. Then two different coordinates are separately obtained for these stations from raw and corrected RINEX data with GAMIT/GlobK software. Results show that, 10, 7 and 24 millimeters changes occurred in order of north, east and up components by high-order ionospheric effects. When data during the peak solar activity days observation files are used for same stations in 2011, it is observed that, high-order ionospheric effects on north, east and up components can be reached in order of 18, 11 and 43 millimeters change.

Although the high-order ionospheric effects on major or by-products obtained as a result of GPS assessments is considered small, it is needed to be handled in order to increase precision and accuracy in positioning and atmospheric parameter estimation. In this study, GPS observation data of 8 TUSAGA-Active stations were used. The distribution of the GPS stations used in the evaluations is as shown in Figure 3.1.

Firstly, second and third order ionospheric effects were corrected in RINEX observation files using with RINEX-HO software. Then, raw and corrected observation files evaluated by GAMIT / GLOBK academic GPS evaluation software and coordinate components of stations were obtained from both data types.

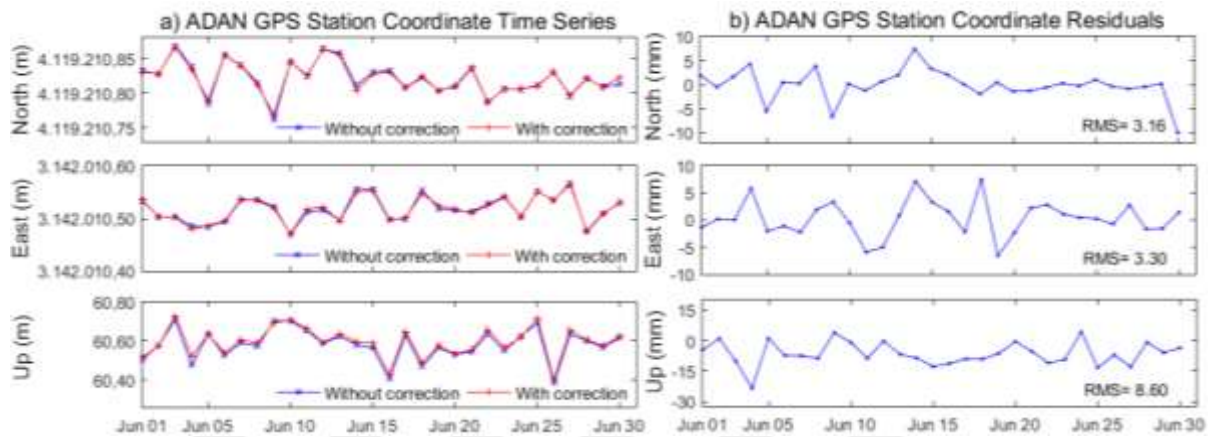


Figure 4.1 ADAN GPS Station Coordinate Time Series and Residuals

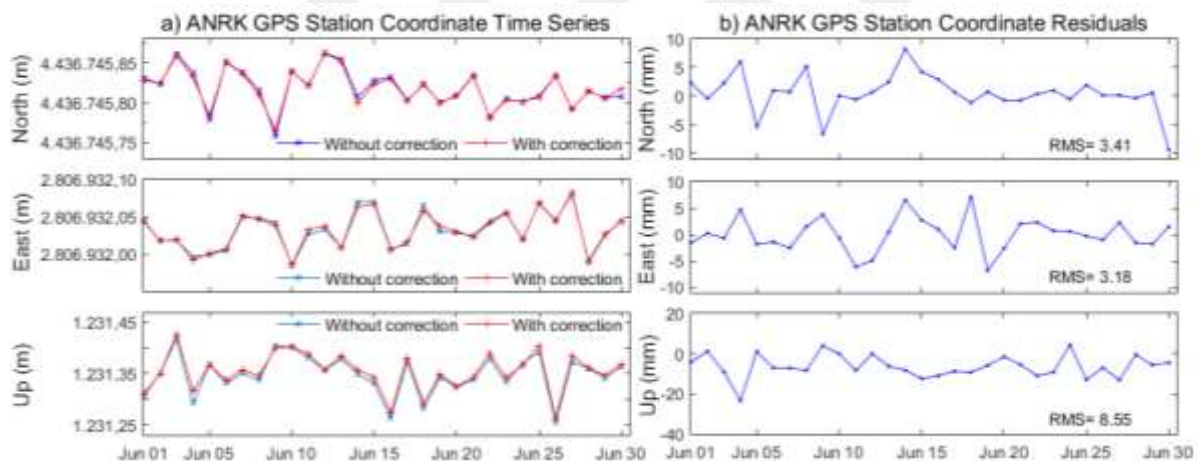


Figure 4.2 ANRK GPS Station Coordinate Time Series and Residuals

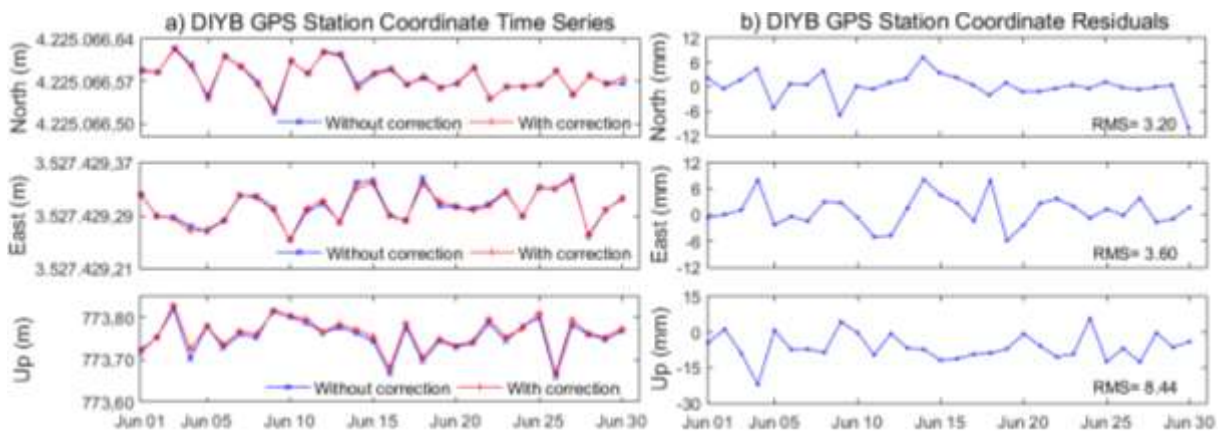


Figure 4.3 DIYB GPS Station Coordinate Time Series and Residuals

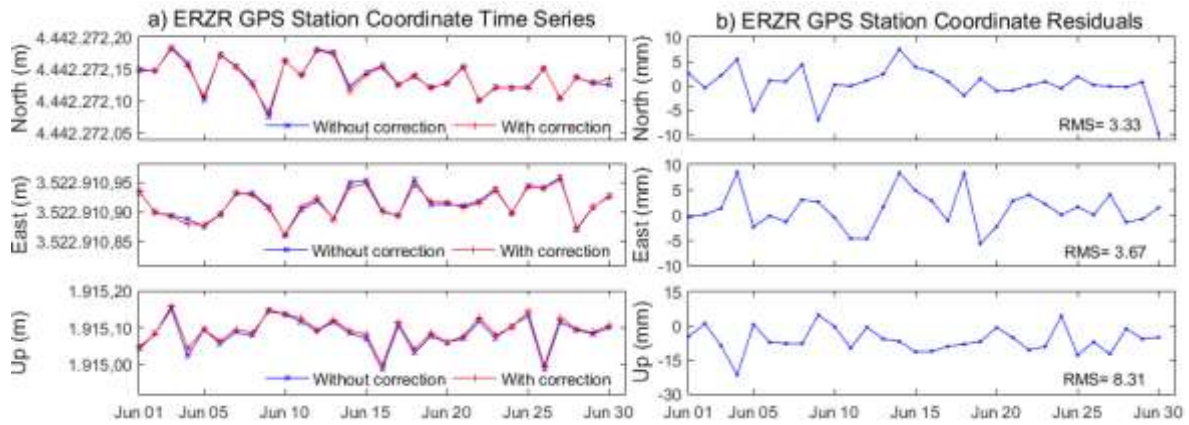


Figure 4.4 ERZR GPS Station Coordinate Time Series and Residuals

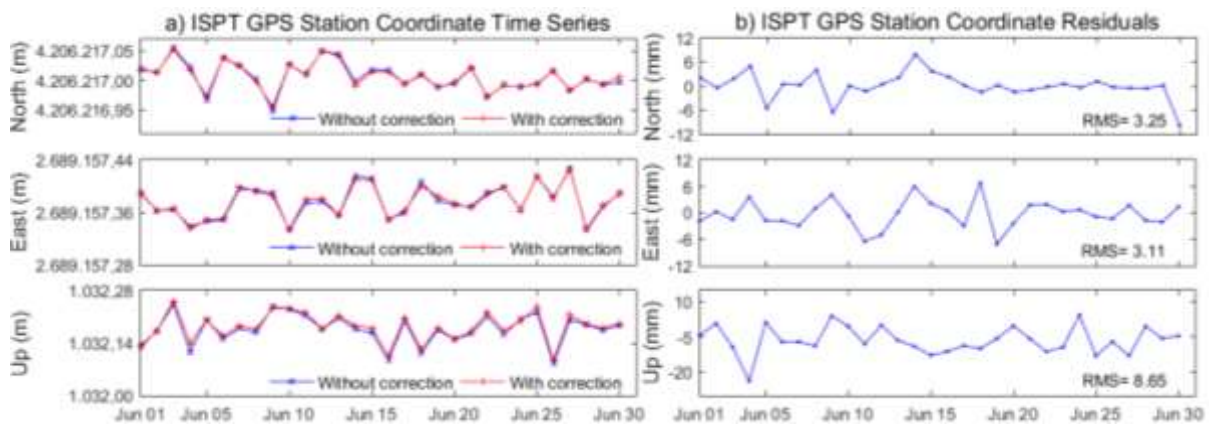


Figure 4.5 ISPT GPS Station Coordinate Time Series and Residuals

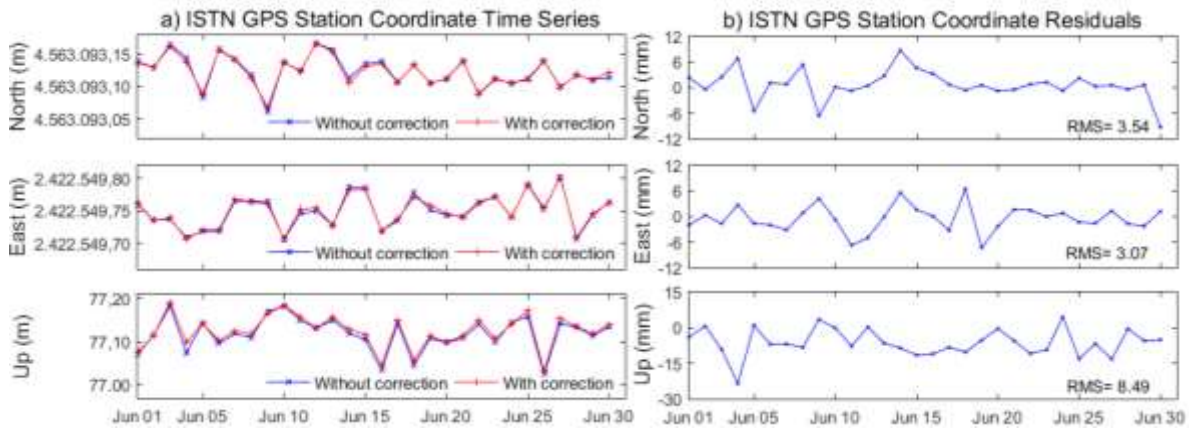


Figure 4.6 ISTN GPS Station Coordinate Time Series and Residuals

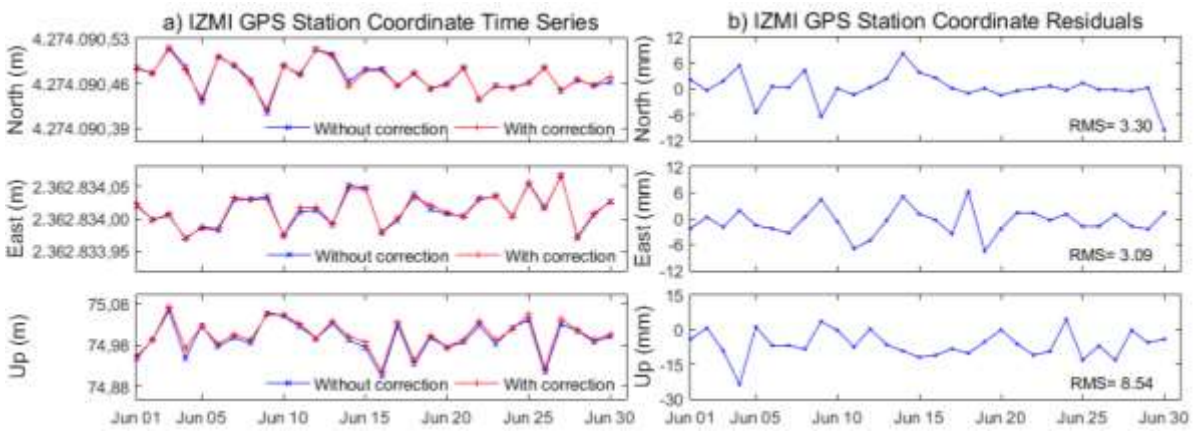


Figure 4.7 IZMI GPS Station Coordinate Time Series and Residuals

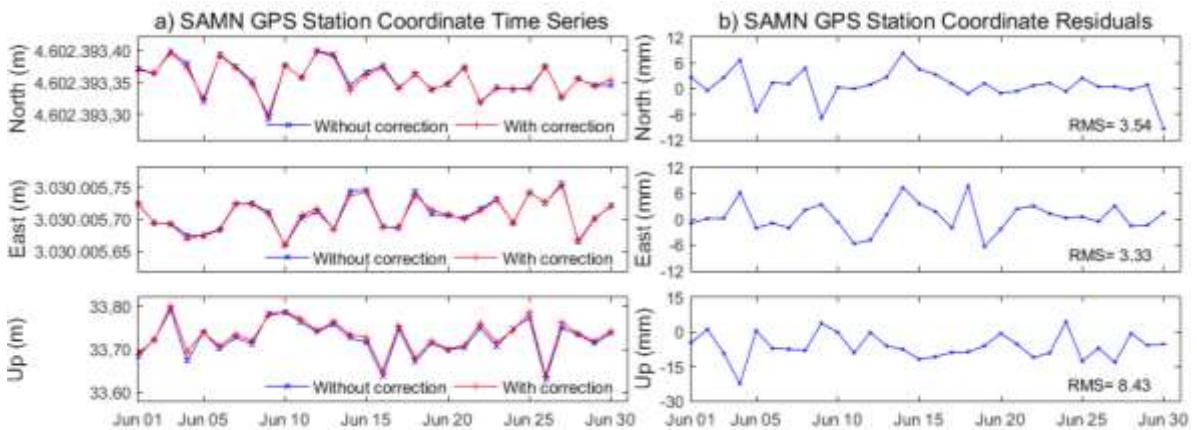


Figure 4.8 SAMN GPS Station Coordinate Time Series and Residuals

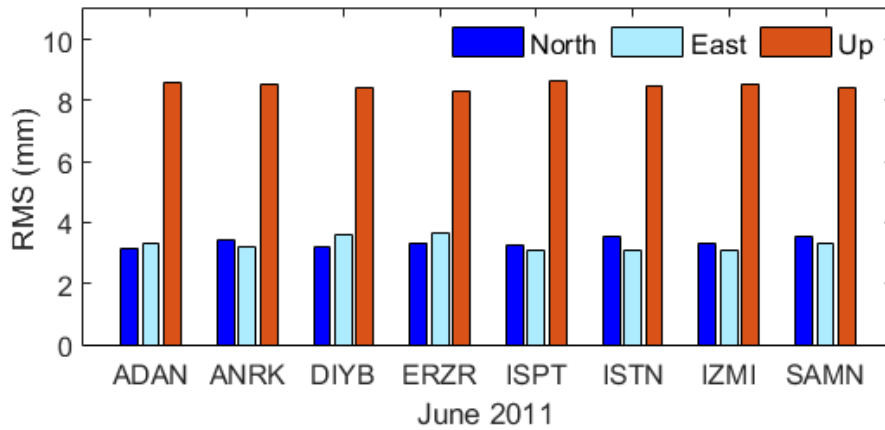


Figure 4.9 Each Stations North, East and Up Components RMS

4.1 COORDINATE CHANGES ON LOW SOLAR ACTIVITY DAYS

Suddenly happened flares in the sun causes magnetic energy in the form of electromagnetic radiation. This magnetic energy affects the earth atmosphere with solar storms. Solar activities can be recorded in varies indices. The F10.7 flux index is the most important index available online since 1947, in which solar activity values are recorded. In this study, high order ionospheric effects depend on low solar activity days were also investigated (Figure 4.10).

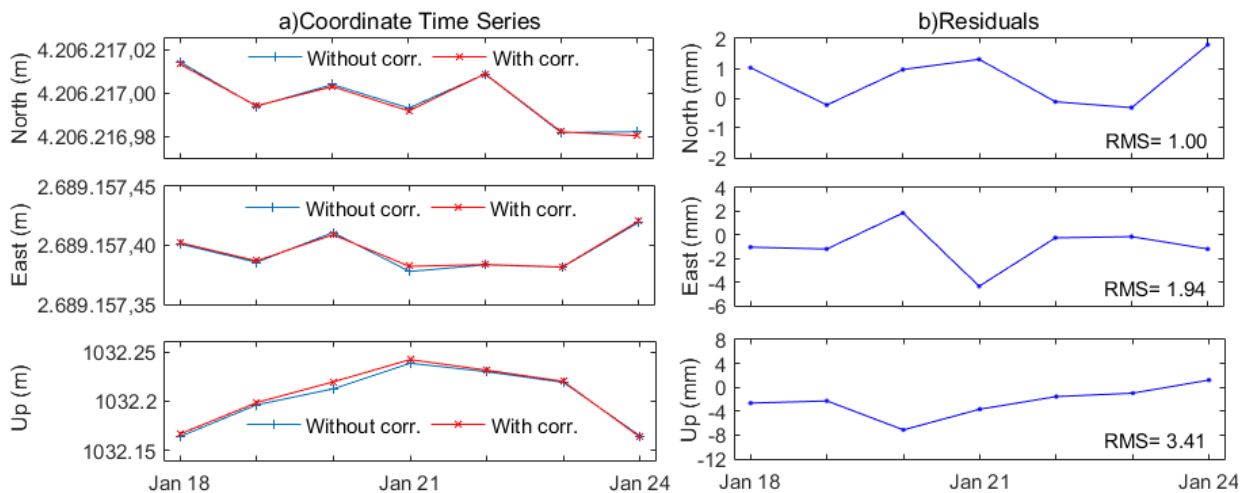


Figure 4.10 ISPT Station North, East and Up Time Series and Residuals on Low Solar Activity Days, 2011

HOI effects over the coordinate components with low solar activity were found that 2, 4 and 9 mm on north, east and up components of ISPT station, respectively. On the days when the solar activity is low, the HOI effect on the coordinate components is low enough to be neglected.

4.2 COORDINATE CHANGES ON HIGH SOLAR ACTIVITY DAYS

When the same process was applied for coordinate estimations of ISPT station on high solar activity days, results show that HOI effects on coordinates are also increasing with solar activities. As a result of the assessments, high-order ionospheric effects causes about differences of 10 mm, 7 mm, 24 mm in East, North and Up coordinate components respectively.

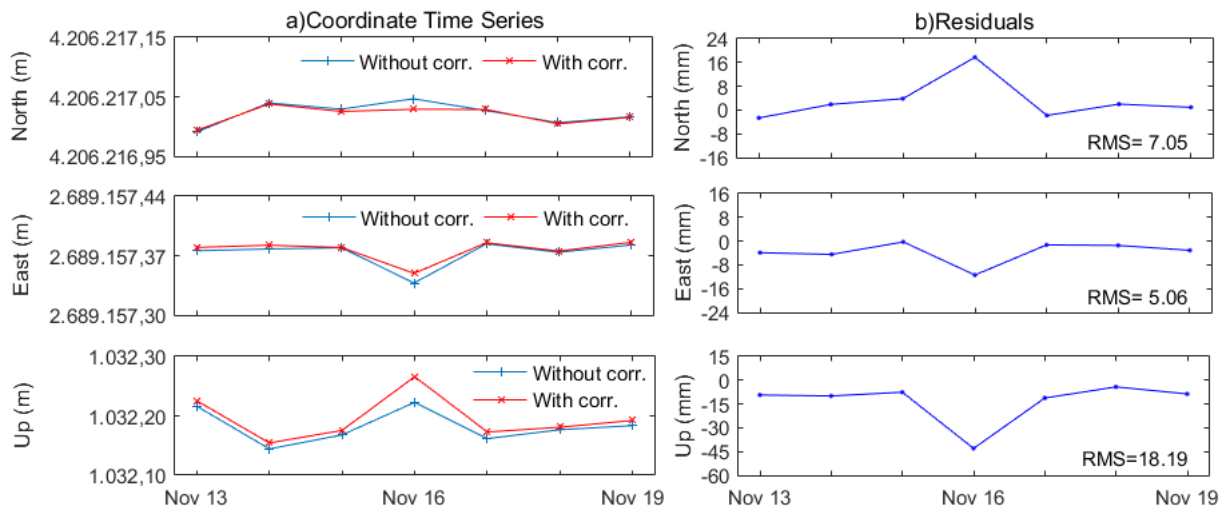


Figure 4.11 ISPT Station North, East and Up Time Series and Residuals on High Solar Activity Days, 2011

The effect of high-order ionospheric effects on the receiver's coordinate components also varies, depending on the increase in solar activity, as seen in the results from two different data sets used.

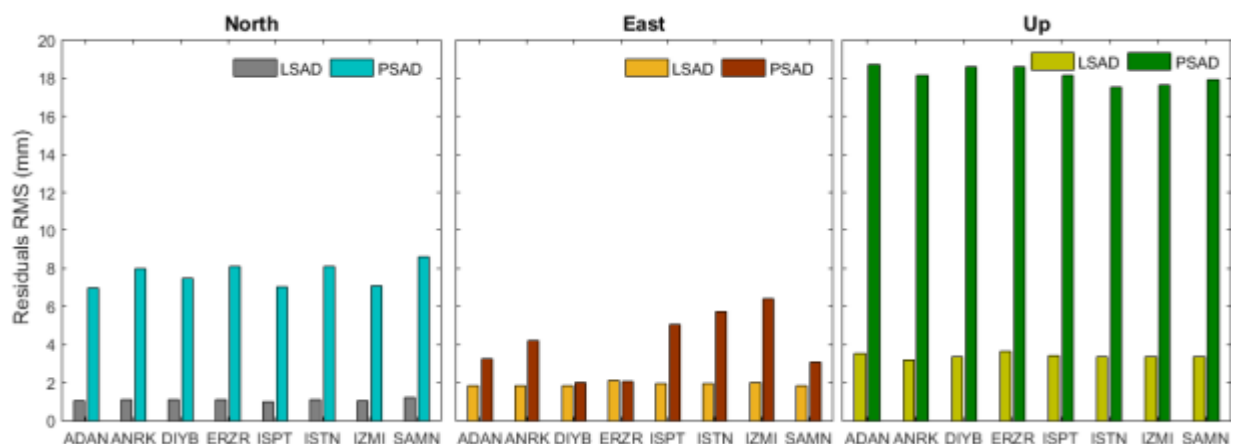


Figure 4.12 North, East and Up Components RMS on Solar Activity Days

It was observed that in the days when the solar activity was at the highest level in 2011, when the observation data belonging to the same stations were used, these differences were reached 18 mm, 11 mm and 43 mm in the East, North and Up coordinate components respectively.





CHAPTER 5

CONCLUSION

A significant part of the ionospheric delay is first order ionospheric effects and this error is corrected by using dual frequency GPS receivers. High order ionospheric delays also must be eliminated in high precision positioning and atmospheric estimation studies.

In this study, high-order ionospheric effects on GPS tropospheric and coordinate estimations are investigated. IGRF11 model for geomagnetic field coefficients and GIM for total electron content are used in HOI correction process. As a result of the evaluations, high-order effects can reach 6 mm on ZTD, 12 mm on gradient estimations change.

HOI effects depend on solar activity, geomagnetic and ionospheric conditions. These effects are much smaller when compared to the first order ionospheric effects, so HOI effects are generally ignored in GPS applications. However, in high precision GPS applications, HOI effects should be corrected from GPS observations. In addition, the GPS estimated PWV with and without HOI corrections were compared with radiosonde observations and the HOI corrected results are closer to radiosonde observations.

From night time to day time, its effects on tropospheric delay are nearly doubled. The increase in RMS of ZTD residuals is seen from low solar activity days to high solar activity day. Also, HOI effects on slant tropospheric delay are big in low elevations and can reach over 30 mm. Therefore the high-order ionospheric delay has a large effect on tropospheric delay and gradient estimation, which should be considered for high precision GPS meteorological applications.

HOI effects on coordinates were also handled and, high-order ionospheric effects caused differences in 10 mm, 7 mm, 24 mm on north, east and up components, respectively. When the same stations observation data were used for high solar activity days in 2011, those effects were

reached to 18 mm, 11 mm and 43 mm in the north, east and up coordinate components. These results cannot be ignored, and it is necessary to eliminate these effects in precise positioning.

Sustainable and developable location determination can be achieved with high-order ionospheric corrections. These effects depend on solar activity and geomagnetic effects. When the geomagnetic field is defined more accurately, the more accurate observations will give the more accurate data to be obtained.



REFERENCES

- Arfken G B** (1985) *Mathematical methods for physicists*. 3rd edition, ISBN: 978-0-12-059820-5, Academic Press, Orlando, 985 pp/s.
- Barraclough D R** (1987) International Geomagnetic Reference Field: the fourth generation. *Phys Earth planet Int*, 48: 279-292.
- Barton C E** (1997) International Geomagnetic Reference Field: The Seventh Generation, *J. Geomag. Geoelect.*, 49: 123–148.
- Bassiri S and Hajj G A** (1993) Higher-order ionospheric effects on the global positioning system observables and means of modeling them. *Manuscripta geodaetica*, 18: 280-289.
- Bevis M, Businger S, Chiswell S, Herring T A, Anthes R A, Rocken C and Ware R H** (1994) GPS Meteorology: Mapping Zenith Wet Delays onto Precipitable Water. *Journal of Applied Meteorology*, 33: 379-386.
- Bevis M, Businger S, Herring T A, Rocken C, Anthes R A and Ware R H** (1992) GPS meteorology: Remote sensing of atmospheric water vapor using the global positioning system. *Journal of Geophysical Research: Atmospheres*, 97: 15787-15801.
- Blewitt G** (1990) An Automatic Editing Algorithm for GPS data. *Geophysical Research Letters*, 17: 199-202.
- Brunner F K and Gu M** (1991) An improved model for the dual frequency ionospheric correction of GPS 260 observations. *Manuscripta Geodaetica*, 16(3): 205–214.
- Davis J L, Elgered G, Niell A E and Kuehn C E** (1993) Ground-based measurements of gradients in the “wet” radio refractivity of air. *Radio Science*, 28(6): 1003–1018.
- Davis J L, Herring T A, Shapiro I I, Rogers A E E and Elgered G** (1985) Geodesy by radio interferometry: Effects of atmospheric modeling errors on estimates of baseline length. *Radio Science*, 20: 1593-1607.
- Duan J, Bevis M, Fang P, Bock Y, Chiswell S, Businger S, Rocken C, Solheim F, Hove T v, Ware R, McClusky S, Herring T A and King R W** (1996) GPS Meteorology: Direct Estimation of the Absolute Value of Precipitable Water. *Journal of Applied Meteorology*, 35: 830-838.
- Elmas Z G, Aquino M, Marques H and Monico J F** (2011) Higher order ionospheric effects in GNSS positioning in the European region. *Annales Geophysicae*, 29: 1383-1399.

REFERENCES (continued)

- Emardson T R, Elgered G and Johansson J M** (1998) Three months of continuous monitoring of atmospheric water vapor with a network of Global Positioning System receivers. *Journal of Geophysical Research: Atmospheres*, 103: 1807-1820.
- Finlay C C, Maus S, Beggan C D, Bondar T N, Chambodut A, Chernova T A, Chulliat A, Golovkov V P, Hamilton B, Hamoudi M, Holme R, Hulot G, Kuang W, Langlais B, Lesur V, Lowes F J, Lühr H, Macmillan S, Manda M, McLean S, Manoj C, Menvielle M, Michaelis I, Olsen N, Rauberg J, Rother M, Sabaka T J, Tangborn A, Tøffner-Clausen L and Thébault E** (2010) International Geomagnetic Reference Field: the eleventh generation. *Geophys J Int*, 183.
- Fritsche M, Dietrich R, Knöfel C, Rülke A, Vey S, Rothacher M and Steigenberger P** (2005) Impact of higher-order ionospheric terms on GPS estimates. *Geophysical Research Letters*, 32: L23311.
- Hartmann G K and Leitinger R** (1984) Range errors due to ionospheric and tropospheric effects for signal frequencies above 100 MHz. *Bulletin géodésique*, 58: 109-136.
- Hawarey M, Hobiger T and Schuh H** (2005) Effects of the 2nd order ionospheric terms on VLBI measurements. *Geophys Res Lett*, 32: No. 11, L11304.
- Hernández-Pajares M, Juan J M, Sanz J, Colombo O L and van der Marel H** (2001) A new strategy for real-time integrated water vapor determination in WADGPS Networks. *Geophysical Research Letters*, 28: 3267-3270.
- Hernández-Pajares M, Juan J M, Sanz J and Orús R** (2007) Second-order ionospheric term in GPS: Implementation and impact on geodetic estimates. *Journal of Geophysical Research: Solid Earth*, 112: B08417.
- Hofmann-Wellenhof B, Lichtenegger H and Collins J** (1993) *Global positioning system: theory and practice*, 3rd ed, ISBN: 978-3-211-82591-4, Springer-Verlag, Wien, 355 pp/s.
- Hofmann-Wellenhof B, Lichtenegger H and Wasle E** (2008) *GNSS--global navigation satellite systems GPS, GLONASS, Galileo, and more*, ISBN: 978-3-211-73012-6, Springer, Wien; New York 516 pp/s.
- Hoque M M and Jakowski N** (2008) Estimate of higher order ionospheric errors in GNSS positioning. *Radio Science*, 43: RS5008.
- IAGA Division 1 Study Group on Geomagnetic Reference Field** (1975) International Magnetic Reference Field 1975, *J. Geomag. Geoelectr.*, 27: 437– 439.
- Jin S, Li Z and Cho J** (2008a) Integrated Water Vapor Field and Multiscale Variations over China from GPS Measurements. *Journal of Applied Meteorology and Climatology*, 47: 3008-3015.
- Jin S and Luo O** (2009) Variability and climatology of PWV from global 13-year GPS observations. *IEEE Transactions on Geoscience and Remote Sensing*, 47: 1918-1924.

REFERENCES (continued)

- Jin S, Luo O F and Cho J** (2009a) Systematic errors between VLBI and GPS precipitable water vapor estimations from 5-year co-located measurements. *Journal of Atmospheric and Solar-Terrestrial Physics*, 71: 264-272.
- Jin S, Luo O F and Gleason S** (2009b) Characterization of diurnal cycles in ZTD from a decade of global GPS observations. *Journal of Geodesy*, 83: 537-545.
- Jin S, Wu Y, Heinkelmann R and Park J** (2008b) Diurnal and semidiurnal atmospheric tides observed by co-located GPS and VLBI measurements. *Journal of Atmospheric and Solar-Terrestrial Physics*, 70: 1366-1372.
- Jin S G and Park P H** (2005) A new precision improvement in zenith tropospheric delay estimation by GPS. *Current Science*, 89: 997-1000.
- Kedar S, Hajj G A, Wilson B D and Heflin M B** (2003) The effect of the second order GPS ionospheric correction on receiver positions. *Geophysical Research Letters*, 30(16): 1829.
- Kim B C and Tinin M V** (2007) Contribution of ionospheric irregularities to the error of dual-frequency GNSS positioning. *Journal of Geodesy*, 81: 189-199.
- Klobuchar J K** (1991) Ionospheric effects on GPS. *GPS World*, 2: 48-51.
- Klobuchar, J A** (1996) Ionospheric Effects on GPS. *Global Positioning System: Theory and Applications*, Parkinson B W and Spilker J J (Ed.), ISBN: 156347106X, American Institute of Aeronautics & Astronautics, 485-515.
- Langel R A** (1992) International Geomagnetic Reference Field: the sixth generation. *J Geomag Geoelect*, 44: 679-707.
- Langel R A, Barraclough D R, Kerridge D J, Golovkov V P, Sabaka T J and Estes R H** (1988) Definitive IGRF models for 1945, 1950, 1955, and 1960. *J. Geomag. Geoelectr.*, 40: 645-702.
- Macmillan S and Finlay C** (2010) The International Geomagnetic Reference Field. *Geomagnetic Observations and Models*. Manda M and Korte M (Ed.), ISBN: 978-90-481-9857-3, Springer Netherlands, Dordrecht, 265-276.
- Macmillan S, Maus S, Bondar T, Chambodut A, Golovkov V, Holme R, Langlais B, Lesur V, Lowes F J, Lühr H, Mai W, Manda M, Olsen N, Rother M, Sabaka T J, Thomson A and Wardinski I** (2003) The 9th-Generation International Geomagnetic Reference Field. *Geophys J Int*, 155: 1051-1056.
- Manda M and Macmillan S** (2000) International Geomagnetic Reference Field - the eighth generation. *Earth Planets Space*, 52: 1119-1124.

REFERENCES (continued)

- Maus S, Macmillan S, Chernova T, Choi S, Dater D, Golovkov V, Lesur V, Lowes F, Lühr H, Mai W, McLean S, Olsen N, Rother M, Sabaka T J, Thomson A and Zvereva T** (2005) The 10th-Generation International Geomagnetic Reference Field. *Geophys. J. Int.*, 161: 561–565.
- Niell A E** (1996) Global mapping functions for the atmosphere delay at radio wavelengths. *Journal of Geophysical Research: Solid Earth*, 101: 3227-3246.
- Odijk D** (2002) *Fast precise GPS positioning in the presence of ionospheric delays*. ISBN: 90-804147-2-7, Optima Grafische Communicatie, The Netherlands, 242 pp/s.
- Özlüdemir M T** (2004) The Stochastic Modelling of GPS Observations. *Turkish J. Eng. Env. Sci, Tubitak*, 28: 223 – 231.
- Peddie N W** (1982) International Geomagnetic Reference Field: the third generation. *J Geomagn Geoelect*, 34: 309-326.
- Petrie E J, King M A, Moore P and Lavallée D A** (2010) Higher-order ionospheric effects on the GPS reference frame and velocities. *Journal of Geophysical Research: Solid Earth*, 115: B03417.
- Reinisch B W, Haines D M, Benson R F, Green J L, Sales G S and Taylor W W L** (2001) Radio sounding in space: magnetosphere and topside ionosphere. *Journal of Atmospheric and Solar-Terrestrial Physics*, 63: 87-98.
- Rocken C, Anthes R, Exner M, Hunt D, Sokolovskiy S, Ware R, Gorbunov M, Schreiner W, Feng D, Herman B, Kuo Y H and Zou X** (1997) Analysis and validation of GPS/MET data in the neutral atmosphere. *Journal of Geophysical Research: Atmospheres*, 102: 29849-29866.
- Rocken C, Hove T V, Johnson J, Solheim F, Ware R, Bevis M, Chiswell S and Businger S** (1995) GPS/STORM—GPS Sensing of Atmospheric Water Vapor for Meteorology. *Journal of Atmospheric and Oceanic Technology*, 12: 468-478.
- Saastamoinen J** (1972) *Atmospheric Correction for the Troposphere and Stratosphere in Radio Ranging Satellites*, The Use of Artificial Satellites for Geodesy. American Geophysical Union, 247-251.
- Seeber G** (2003) *Satellite Geodesy: Foundations, Methods, and Applications*. ISBN: 9783110200089, De Gruyter Berlin, New York, 589 pp/s.
- Strangeways H J and Ioannides R T** (2002) Rigorous calculation of ionospheric effects on GPS Earth-Satellite paths using a precise path determination methods. *Acta Geod Geoph Hung*, Vol. 37: No. 2-3, 281-292.
- Syndergaard S** (2000) On the ionosphere calibration in GPS radio occultation measurements. *Radio Science*, 35: 865-883.

REFERENCES (continued)

- Teke K, Böhm J, Nilsson T, Schuh H, Steigenberger P, Dach R, Heinkelmann R, Willis P, Haas R, Espada S G, Hobiger T, Ichikawa R and Shimizu S** (2011) Multi-technique comparison of troposphere zenith delays and gradients during CONT08. *Journal of Geodesy*, 85(7): 395-413.
- Thébault E, Finlay C C, Beggan C D, Alken P, Aubert J, Barrois O, Bertrand F, Bondar T, Boness A, Brocco L, Canet E, Chambodut A, Chulliat A, Coïsson P, Civet F, Du A, Fournier A, Fratter I, Gillet N, Hamilton B, Hamoudi M, Hulot G, Jager T, Korte M, Kuang W, Lalanne X, Langlais B, Léger J-M, Lesur V, Lowes F J, Macmillan S, Manda M, Manoj C, Maus S, Olsen N, Petrov V, Ridley V, Rother M, Sabaka T J, Saturnino D, Schachtschneider R, Sirol O, Tangborn A, Thomson A, Tøffner-Clausen L, Vigneron P, Wardinski I and Zvereva T** (2015). International Geomagnetic Reference Field: the 12th generation. *Earth, Planets and Space*, 67: 79.
- Tregoning P, Boers R, O'Brien D and Hendy M** (1998) Accuracy of absolute precipitable water vapor estimates from GPS observations. *Journal of Geophysical Research: Atmospheres*, 103: 28701-28710.
- Troller M** (2004) GPS based determination of the integrated and spatially distributed water vapor in the troposphere. *PhD. Thesis*, Swiss Federal Institute of Technology, Zurich.
- Tsunoda R T** (1988) High-latitude F region irregularities: A review and synthesis. *Reviews of Geophysics*, 26: 719-760.
- URL-1** <https://www.ngdc.noaa.gov/IAGA/vmod/igrf_old_models.html>, Last Visit: 15.12.2017.
- URL-2** <<https://phys.org/news/2016-03-powerful-geomagnetic-storms-solar.html>>, Last Visit: 01.12.2017.
- URL-3** <<https://omniweb.gsfc.nasa.gov/form/dx1.html>>, Last Visit: 09.11.2017.
- Zmuda A J** (1971) The International Geomagnetic Reference Field: introduction. *Bull Int Assoc Geomag Aeronomy*, 28: 148-152.



CURRICULUM VITAE

Volkan AKGÜL was born in 1988 in Elbistan. After than completing his primary and secondary education in Elbistan, he has received bachelor's degree from the Department of Geomatics Engineering at Istanbul Technical University in 2011. After four years of private companies experience, he has started to work as a research assistant in Engineering Faculty of Bulent Ecevit University. At the same time, he has started master education in Graduate School of Natural and Applied Sciences, Department of Geomatics Engineering in 2015.

ADDRESS:

Address: Bulent Ecevit University
Engineering Faculty
Department of Geomatics

Phone: (+90) 372 291 25 77

E-mail: akgulvo@gmail.com